NASA CR-165556

R82 AEB198

National Aeronautics and
Space Administration

CF6 JET ENGINE PERFORMANCE IMPROVEMENT: HIGH PRESSURE TURBINE ACTIVE CLEARANCE CONTROL

by

S.E. Rich and W.A. Fasching

GENERAL ELECTRIC COMPANY

June 1982

Prepared for

National Aeronautics and Space Administration

NASA Lewis Research Center
Contract NAS3-20629

1. Report No.	2. Government Accession No.	3. Recipient's Catalog No.
NASA CR-165556		

4. Title and Subtitle	5. Report Date
CF6 Jet Engine Performance Improvement Program - High Pressure Turbine Active Clearance Control	May 1982
	6. Performing Organization Code

7. Author(s)	8. Performing Organization Report No.
S.E. Rich, W.A. Fasching	R82AEB198
	10. Work Unit No.

9. Performing Organization Name and Address	11. Contract or Grant No.
General Electric Company Aircraft Engine Group Cincinnati, OH 45215	NAS3-20629
	13. Type of Report and Period Covered
12. Sponsoring Agency Name and Address	Contractor Report
National Aeronautics and Space Administration Washington, D.C. 20546	14. Sponsoring Agency Code

15. Supplementary Notes

Project Manager - J. McAulay, Project Engineer - R. Antl
NASA-Lewis Research Center, Cleveland, Ohio

16. Abstract

As part of the NASA-Sponsored Engine Component Improvement Program an Active Clearance Control System was developed which reduces fuel consumption and performance degradation. This system utilizes compressor discharge air during takeoff and fan discharge air during cruise to impinge on the shroud support structure to improve the thermal response. The system was evaluated in component and engine tests. The test results demonstrated a performance improvement of 0.7 percent in cruise SFC.

17. Key Words (Suggested by Author(s))	18. Distribution Statement
Jet Engine High Pressure Turbine Turbofan Engine Active Clearance Control Performance	Unclassified - Unlimited

19. Security Classif. (of this report)	20. Security Classif. (of this page)	21. No. of Pages	22. Price*
Unclassified	Unclassified	136	

* For sale by the National Technical Information Service, Springfield, Virginia 22161

FOREWORD

The work was performed by the CF6 Engineering Department of General Electric's Aircraft Engine Business Group, Aircraft Engine Engineering Division, Cincinnati, Ohio. The program was conducted for the National Aeronautics and Space Administration, Lewis Research Center, Cleveland, Ohio, under Subtask 2.6 of the CF6 Jet Engine Performance Improvement Program, Contract Number NAS3-20629. The Performance Improvement Program is part of the Engine Component Improvement (ECI) Project, which is part of the NASA Aircraft Energy Efficiency (ACEE) Program. The NASA Project Engineer for this program was R. Antl. The program was initiated in October 1978 and completed in September 1981.

The report was prepared by S. Rich, Project Engineer and W.A. Fasching, General Electric Program Manager.

TABLE OF CONTENTS

Section		Page
1.0	SUMMARY	1
2.0	INTRODUCTION	2
3.0	TECHNICAL APPROACH	4
	3.1 Introduction	4
	3.1.1 Design Approach	4
	3.2 Design Description	6
	3.3 Analysis	9
	3.3.1 Stress Analysis	9
	3.1.1.1 Forward Hook Analysis	9
	3.1.1.2 Shroud Hanger Analysis	9
	3.1.1.3 First Stage Outer Screen Analysis	12
	3.1.1.4 Compressor Rear Frame/High Pressure Turbine Case Flange Analysis	12
	3.3.2 Performance	12
	3.3.2.1 Thermal Analysis	12
	3.3.2.2 Transient Analysis and Clearances	19
	3.3.2.3 Performance Estimates	23
	3.3.3 Engine Testing	23
4.0	CONTROL COMPONENT AND SYSTEM BENCH TEST	28
	4.1 Test Objectives	28
	4.2 Instrumentation and Test Setup	28
	4.2.1 Test Procedure	29
	4.2.2 Test Results	31
5.0	VIBRATION TESTING	33
	5.1 Test Objectives	33
	5.2 Instrumentation and Test Procedure	33
	5.3 Test Facility and Test Setup	38

TABLE OF CONTENTS (CONTINUED)

Section			Page
	5.4	Test Results	38
		5.4.1 Vibratory Frequencies	40
		5.4.1.1 Frequency Response of Accelerometer #116	40
		5.4.1.2 Frequency Response of Accelerometer #111	42
	5.5	Discussion	41
6.0		HIGH ENERGY X-RAY TRANSIENT/ENDURANCE TESTING	45
	6.1	Test Objectives	45
	6.2	Test Facility	45
	6.3	Instrumentation	46
		6.3.1 Active Clearance Control Instrumentation	46
		6.3.2 Engine Instrumentation	49
	6.4	Active Clearance Control Piping Flow Calibration	54
		6.4.1 Test Objectives	54
		6.4.2 Test Hardware	54
		6.4.3 Instrumentation	54
		6.4.4 Test Procedure	54
		6.4.5 Test Results	54
	6.5	Temperature Data	59
		6.5.1 Introduction	59
		6.5.2 Test Objectives	59
		6.5.3 Transient Temperature Data	59
		6.5.3.1 Engine Throttle Bursts and Chop Temperature Data	66
		6.5.3.2 Cyclic Endurance Testing	66
		6.5.3.3 HPT Rotor Throttle Reburst Testing	66
		6.5.3.4 Steady State Cruise Testing	66

TABLE OF CONTENTS (CONCLUDED)

Section		Page
	6.6 HEX Data	88
	6.6.1 Test Procedure	88
	6.6.2 Analysis Procedure	88
	6.6.3 Test Results	94
	6.7 Data Comparisons	102
	6.7.1 Transient Clearance Change	102
	6.7.2 Steady State Clearance Change	102
7.0	PERFORMANCE TESTING	105
	7.1 Test Objectives	105
	7.2 Test Facility	105
	7.3 Instrumentation	106
	7.4 Performance Test	106
	7.4.1 Sea Level Test Results	106
	7.4.2 Altitude Cruise Performance Estimates	111
	7.5 Accel Testing	118
	7.5.1 Test Results	118
8.0	ECONOMIC ASSESSMENT	119
9.0	SUMMARY OF RESULTS	121
APPENDIX A	QUALITY ASSURANCE	123
APPENDIX B	NOMENCLATURE	125
APPENDIX C	REFERENCES	126

LIST OF ILLUSTRATIONS

Figure		Page
1.	Active Clearance Control High Pressure Turbine.	7
2.	External Piping Configuration Schematic.	8
3.	Analytical Model - Forward Shroud Support.	10
4.	Effective Stress - Forward Shroud Support.	10
5.	Effective Stress - Shroud Hanger.	11
6.	Analytical Model - HPT Nozzle and Screen.	13
7.	Effective Stress Summary - HPT Nozzle Outer Screen.	14
8.	Analytical Model - Compressor Rear Frame/HPT Case Flange.	15
9.	Effective Stress Summary.	16
10.	Heat Transfer Model - HPT ACC Structure.	17
11.	Structural Analysis Model - HPT ACC Structure.	18
12.	Internal Flange Flow.	20
13.	First Stage HPT Clearance Comparison.	24
14.	Performance Comparisons HPT ACC.	25
15.	Engine Testing Procedure.	27
16.	Room Temperature Test Setup.	30
17.	Valve Flow Versus Valve Pressure Ratio.	32
18.	Fourier Analysis System.	34
19.	ACC Ducting Assembly - Accelerometer Location and Number.	35
20.	Impingement Assembly - Accelerometer Location and Number	36
21.	Typical Fast Fourier Transform Output.	37

LIST OF ILLUSTRATIONS (CONTINUED)

Figure		Page
22.	Impingement Tube Vibratory Scan.	39
23.	Accelerometer No. 116 Direction Radial.	41
24.	Accelerometer No. 111 Direction Radial.	43
25.	Cooling Supply Instrumentation.	47
26.	Impingement System Instrumentation.	48
27.	HPT Case and Internal Structure Instrumentation.	50
28.	Engine Instrumentation.	51
29.	HPT Active Clearance Control Hardware.	55
30.	Flow Calibration Instrumentation - Cooling Supply.	56
31.	Flow Function Versus Pressure Ratio for the HPT Active Clearance Control Piping System.	58
32.	Throttle Burst and Chop Test Cycle.	60
33.	Takeoff to Intermediate Power Level Test Cycle.	61
34.	Ground Idle to Intermediate Power Thermal Test Cycle.	62
35.	CF6-6 Simulated Service "C" Cycle.	63
36.	Hot Rotor Reburst Test Cycle.	64
37.	Steady-State HPT Active Clearance Control Cruise Test Cycle.	65
38.	Temperature Match - Compressor Rear Frame Shallow Thermocouple.	67
39.	Temperature Match - Compressor Rear Frame Deep Thermocouple.	68
40.	Temperature Match - HPT Forward Flange Shallow Thermocouple.	69
41.	Temperature Match - HPT Forward Flange Deep Thermocouple.	70

LIST OF ILLUSTRATIONS (CONTINUED)

Figure		Page
42.	Temperature Match - HPT Mid Flange Shallow Thermocouple.	71
43.	Temperature Match - HPT Mid Flange Deep Thermocouple.	72
44.	Temperature Match - HPT Mid Flange Shallow Thermocouple.	73 73
45.	Temperature Match - HPT Mid Flange Deep Thermocouple.	74
46.	Temperature Match - HPT Rear Flange Shallow Thermocouple.	75
47.	Temperature Match - HPT Rear Flange Deep Thermocouple.	76
48.	Temperature Match - Compressor Rear Frame Shallow Thermocouple.	77
49.	Temperature Match - Compressor Rear Frame Deep Thermocouple.	78
50.	Temperature Match - HPT Forward Flange Shallow Thermocouple.	79
51.	Temperature Match - HPT Forward Flange Deep Thermocouple.	80
52.	Temperature Match - HPT Mid Flange Shallow Thermocouple.	81
53.	Temperature Match - HPT Mid Flange Deep Thermocouple.	82
54.	Temperature Match - HPT Mid Flange Shallow Thermocouple.	83
55.	Temperature Match - HPT Mid Flange Deep Thermocouple.	84
56.	Temperature Match - HPT Rear Flange Shallow Thermocouple.	85
57.	Temperature Match - HPT Rear Flange Deep Thermocouple.	86
58.	HEX Facility - Front View	89

LIST OF ILLUSTRATIONS (CONTINUED)

Figure		Page
59.	HEX Facility - Rear View.	90
60.	Stage 1 HEX Radiographs.	91
61.	Stage 2 HEX Radiographs.	92
62.	X-Ray Image and Density Contour.	93
63.	HEX Radiograph Stage 1 - Measurement.	95
64.	HEX Radiograph Stage 2 - Measurement.	96
65.	Stage 1 Position Change Following Throttle Burst from Ground Idle to Takeoff Power.	97
66.	Stage 1 Position Change Following Hot Rotor Reburst to Maximum Climb After 70 Second Dwell at Flight Idle.	98
67.	Stage 1 Position Change Following Hot Rotor Reburst to Maximum Climb after 130 Second Dwell at Flight Idle.	99
68.	Stage 2 Position Change Following Throttle Burst from Ground Idle to Takeoff.	100
69.	Stage 2 Position Change Following Throttle Chop from Takeoff to Ground Idle.	101
70.	Stage 1 Change in Clearance Following Throttle Burst from Ground Idle to Takeoff Power.	103
71.	Maximum Cruise Closure Versus Cooling Air.	104
72.	Measured SFC Improvement Versus W_{Cool} - Minimum Cruise.	107
73.	Measured SFC Improvement Versus W_{Cool} - Average Cruise.	108
74.	Measured SFC Improvement Versus W_{Cool} - Maximum Cruise.	109
75.	SFC Versus HPT ACC Cooling Flow - Engine 451-111/7 Sea Level Maximum Cruise.	110
76.	High Pressure Turbine Active Clearance Control.	112

LIST OF ILLUSTRATIONS (CONCLUDED)

Figure		Page
77.	Δ Turbine Efficiency (η_t) Versus Percent W_{Cool} - Predicted.	113
78.	Stage 1 Closure at Altitude Cruise Versus W_{Cool} Based on Match Temperature Data.	114
79.	Stage 2 Closure Versus Percent W_{Cool} Based on Match Temperature Data.	115
80.	η_T Versus W_{Cool}.	116
81.	Engine Performance Improvement Versus Percent W_{Cool}.	117

1.0 SUMMARY

As part of the NASA-sponsored Engine Component Improvement Program an active clearance control system for the CF6-6 HP Turbine was developed which reduces fuel consumption. The design utilizes compressor discharge air during the takeoff transient to improve the thermal response of the shroud support structure and, at cruise, allows fan discharge air to impinge on the shroud support structure. The fan discharge air cools the shroud support structure, thereby reducing turbine blade tip clearance and engine SFC.

The system demonstrated a repeatable test cell SFC reduction of 1.3 percent at the simulated maximum cruise power setting at sea level. This is equivalent to an altitude cruise SFC reduction of 0.7 percent. The system has the potential of a 0.9 percent reduction in cruise SFC provided that some minor design refinements are made. Throughout the engine testing sequence, including throttle burst, hot rotor reburst, cooling and revenue service endurance cycles, the high pressure turbine shrouds sustained very light rubbing, and the hardware adequately demonstrated its ability to retain the SFC reduction.

The HP turbine active clearance control performance improvement offers an annual fuel savings per DC-10-10 aircraft of 30,200 to 184,000 liters (8000 to 48600 gal.) depending on mission range.

2.0 INTRODUCTION

National energy demand has outpaced domestic supply creating an increased U.S. dependence on foreign oil. This increased dependence was dramatized by the OPEC oil embargo in the winter of 1973 to 1974. In addition, the embargo triggered a rapid rise in the cost of fuel which, along with the potential of further increases, brought about a changing economic circumstance with regard to the use of energy. These events, of course, were felt in the air transport industry as well as other forms of transportation. As a result of these experiences, the Government, with the support of the aviation industry, has initiated programs aimed at both the supply and demand aspects of the problem. The supply problem is being investigated by looking at increasing fuel availability from such sources as coal and oil shale. Efforts are currently underway to develop engine combustor and fuel systems that will accept fuels with broader specifications.

Reduced fuel consumption is the other approach to deal with the overall problem. A long-range effort to reduce fuel consumption is to evolve new technology which will permit development of a more energy efficient turbofan or use of a different propulsive cycle, such as a turboprop. Although studies have indicated large reductions in fuel usage are possible (e.g., 15 percent to 40 percent), any significant impact of the turboprop approach is about 15 years away. In the near term, the only practical propulsion approach is to improve the fuel efficiency of current engines. Examination of this approach has indicated that the 5 percent fuel reduction goal starting in the 1980 to 1982 time period is feasible for current commercial engines. These engines will continue to be significant fuel users for the next 15 to 20 years.

Accordingly, NASA is sponsoring the Aircraft Energy Efficient (ACEE) Program (based on a Congressional request) which is directed at providing reduced fuel consumption of commercial air transports. The Engine Component Improvement (ECI) Program is the element of the ACEE Program directed at reducing fuel consumption of current commercial aircraft engines. The ECI Program consists of two parts: engine diagnostics and performance improvement. The engine

diagnostics effort is to provide information to identify the sources and causes of engine deterioration. The performance improvement effort is directed at developing engine components having performance improvement and retention characteristics which can be incorporated into new production and existing engines.

The performance improvement effort was initiated with a feasibility analysis which identified performance improvement concepts and then assessed the technical and economic merits of these concepts. This assessment included a determination of airline acceptability, the probability of introducing the concepts into production by the 1980 to 1982 time period, and their retrofit potential. The study was conducted in cooperation with Boeing and Douglas aircraft companies and American and United Airlines, and is reported in Reference 1.

In the feasibility analysis, the high pressure (HP) turbine active clearance control performance improvement concept was selected for development and evaluation because of its fuel savings potential and reasonable airline payback period. The objective of the HP turbine active clearance control program was to develop technology and to verify the predicted fuel savings by engine ground tests. An improvement in cruise SFC of 0.6 percent was originally estimated for the HP turbine active clearance control concept.

The program was a 35-month effort which included design, analysis, hardware manufacture as well as component and full scale engine testing.

3.0 TECHNICAL APPROACH

3.1 INTRODUCTION

The objective of the HP Turbine Active Clearance Control (ACC) Program was to demonstrate a reduction in cruise specific fuel consumption (SFC) of approximately 0.6 percent, and a SFC retention capability better than that currently achievable on the CF6-6 engine. The system utilizes compressor discharge air during the takeoff transient to improve the thermal response of the shroud support structure, and uses fan discharge air at cruise to impinge on the shroud support structure. The fan air reduces the shroud support structure temperature and reduces the turbine blade tip-to-shroud clearances. The reduced tip clearance yields improved turbine efficiency and reduces engine specific fuel consumption.

3.1.1 Design Approach

The advantage of a HP Turbine active clearance control system for the CF6-6 engine is derived from the differences in the transient and steady state radial positions of the rotating and stationary components. Providing sufficient turbine blade tip clearance to prevent a rub during throttle burst to take-off power and during hot rotor rebursts results in the cruise clearance being greater than desirable. The characteristics of the turbine which result in more open cruise clearances are rotor/stator relative radial thermal response differences, and differences in the elastic mechanical loads-rotational growth and pressure loads.

As the engine is accelerated, the elastic stretching of the rotor, as well as the inward deflection of the stator from pressure forces, both combine to reduce the tip clearance before the stator structure can heat up sufficiently to establish an increased radial position. An acceleration, performed when the rotor mass is hot but the stator mass is cold, termed a "hot rotor reburst", results in the greatest blade tip to shroud transient closure because the thermal growth of the rotor results in additional closure to that provided by the rotor elastic stretch and stator inward pressure deflection. The level of tolerable rub for a hot rotor reburst, therefore, effectively establishes the

clearances for other operating points of interest. All of these other points, takeoff and cruise being the most significant in terms of fuel use, will operate at clearances that are less efficient than could be achieved if the hot rotor reburst condition did not require consideration.

There are two fundamental approaches to improve cruise clearance. One is to design the rotor and stator to respond transiently in as similar a manner as possible. Reducing the level of hot rotor reburst closure allows setting tighter clearances at cruise. This approach is called passive clearance control.

The other approach is to heat and cool structures, as appropriate, to open or close tip clearances such that efficient clearances can be achieved at cruise. This approach is called active clearance control.

This task encompasied the design and evaluation of an active system which incorporates aspects of passive response matching as well. The system incorporates the following features:

1. Segmented shroud hangers attached to a thermally stable mass.

   The shroud support structure consists of segments which have flanges that are isolated from the hot flowpath to promote roundness and uniformity of temperature. Also, the entire shroud support structure is contained in a separate high pressure turbine case whose thermal mass at the flanges is sized to control stator radial response.

2. The stator is not pressure sensitive.

   The shrouds are attached to the HPT case in a manner such that the application of pressure and mechanical loads will cause an outward radial deflection. This improves both transient and steady state clearances.

3. Match, as closely as practical, the thermal response of the HPT case to the rotor.

   The thermal response of the HPT case is matched to the rotor by the impingement of compressor discharge air on the outside of the HPT case during an acceleration to takeoff.

4. Cool HPT Casing at Cruise

The impingement of fan discharge air on the HPT casing reduces the HPT casing temperature and therefore the turbine blade tip-to-shroud clearance.

5. Control External Influences

As a further aid in controlling the HPT case temperatures, an impingement shield is placed around the HPT case. The impingement shield helps to control the flow of impingement air over the flanges and mitigates the effects of outside circumferential temperature variations.

3.2 DESIGN DESCRIPTION

The design configuration is depicted on Figures 1 and 2 which illustrate the HPT ACC system and the external piping configuration, respectively. The HPT ACC system utilizes two valves: a Compressor Discharge Pressure (CDP) valve and a high pressure turbine ACC valve.

The CDP valve opens at low engine core speeds and permits air, at compressor discharge conditions, to impinge on the HPT casing. This air increases the thermal response rate of the HPT case and thus allows tighter turbine blade tip-to-shroud clearances at assembly. The valve remains open for a period of 2 minutes after throttle motion.

The HPT ACC valve, providing fan discharge air,is opened after the engine is at a cruise power setting. This air cools the HPT case and consequently reduces the turbine blade tip-to-shroud operating clearance. This reduced clearance increases turbine efficiency and decreases specific fuel consumption. A controllable valve was employed for the testing so that engine performance vs cooling flow could be determined.

The impingement system consists of three impingement tubes covered by an impingement shield. The tubes are approximately 25 mm (1 inch) in diameter and contain 1100 impingement holes per tube. The impingement shield prevents external temperature gradients from adversely affecting the HPT casing temperature.

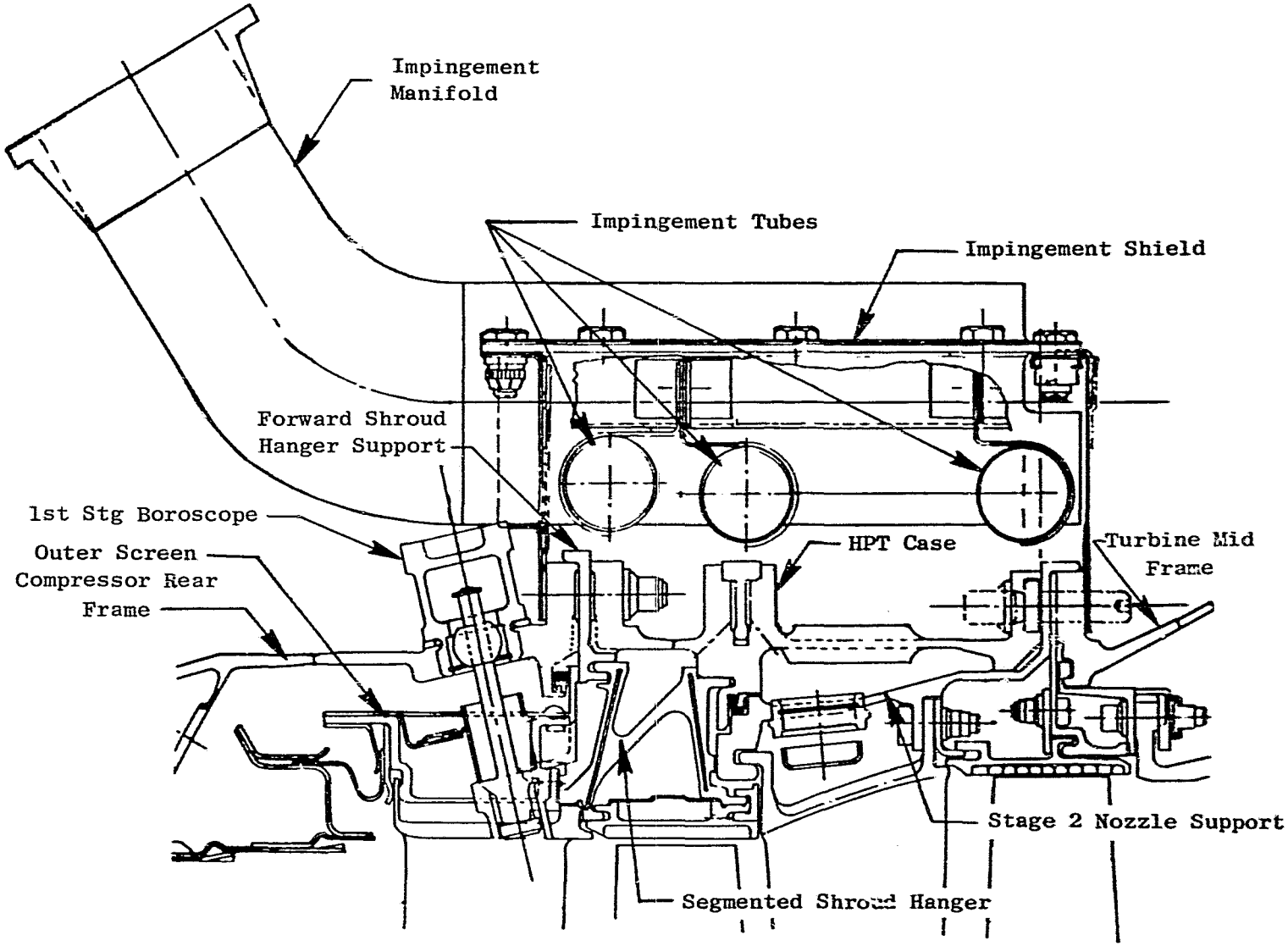

Figure 1. Active Clearance Control High Pressure Turbine.

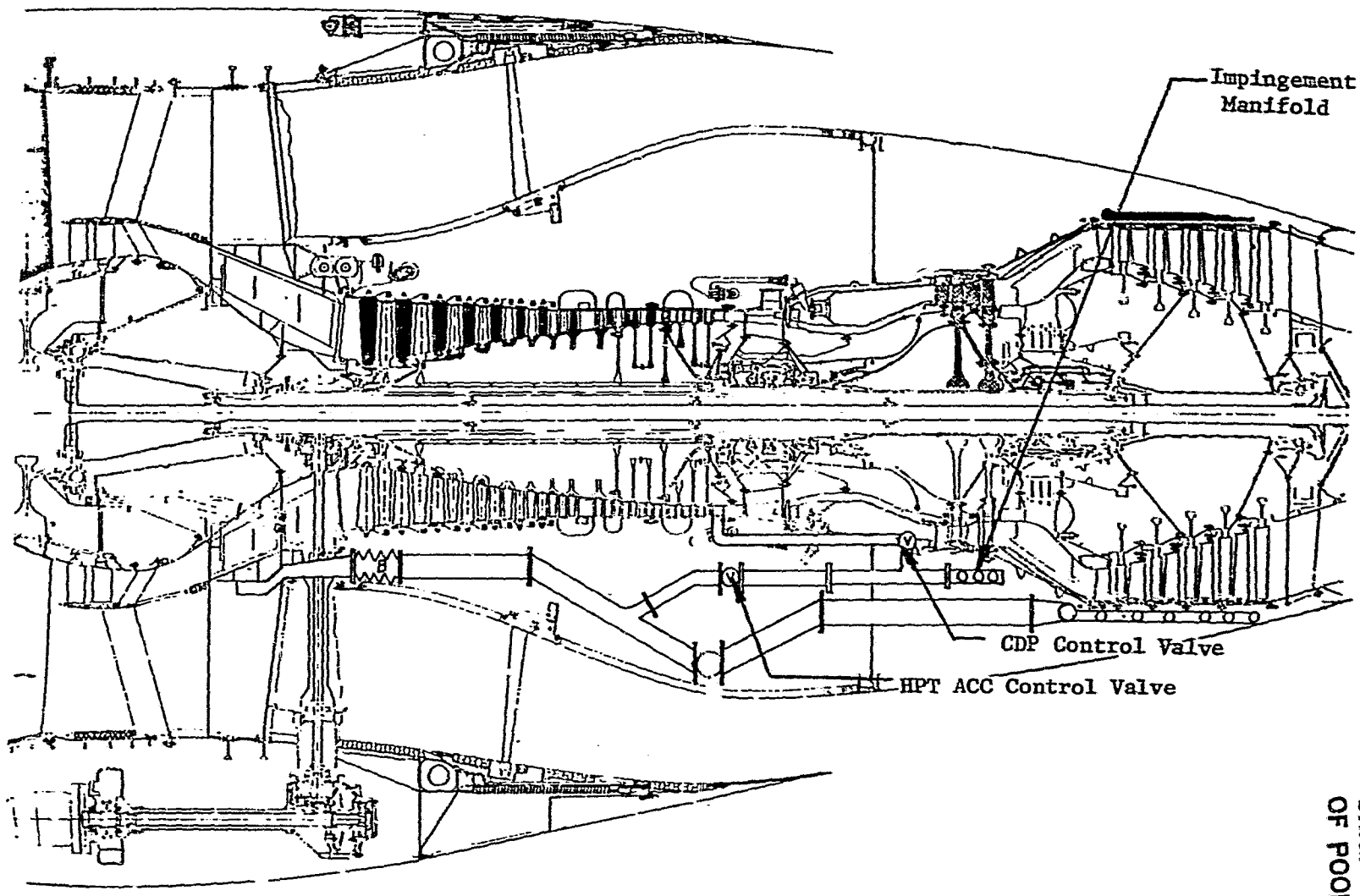

Figure 2. External Piping Configuration Schematic.

The impingement tubes are attached to the impingement shield by brackets that allow for the relative thermal expansion/contraction of the impingement tubes and case. The impingement shield is attached to the engine by the compressor rear frame/HPT case and HPT case/turbine midframe mount bolts. Installed in the impingement shield is an impingement manifold which acts as a plenum for the impingement air distribution system.

The HPT case performs the following function:

1. Provides a thermally stable mass.
2. Provides a means of supporting the internal structure.
3. Forms a portion of the structural casing of the engine.

The HPT case allows better control of buildup clearances. A segmented shroud hanger is used to support the first stage HPT shroud. It is rabbeted into the HPT case so that, as the HPT case expands or contracts, the shroud hanger moves with it.

3.3 ANALYSIS

Presented herein are the results of various stress, clearance and performance analyses conducted during the course of the design work. The information presented is mainly devoted to the analysis of the final design configuration.

3.3.1 Stress Analysis

3.3.1.1 Forward Hook Analysis

An analysis of the forward hook was conducted and the hot day takeoff condition was found to be the worst operating condition. The analytical results are shown on Figures 3 and 4. The stresses shown are concentrated surface stresses, and the material is INCO 718. No operating problems were expected at these stress levels.

3.3.1.2 Shroud Hanger Analysis

A finite element model of the shroud hanger was analyzed for transient and steady-state stresses. Figure 5 illustrates the model mesh and the hot day takeoff stress summary. The stresses shown are concentrated and no operating problems were expected.

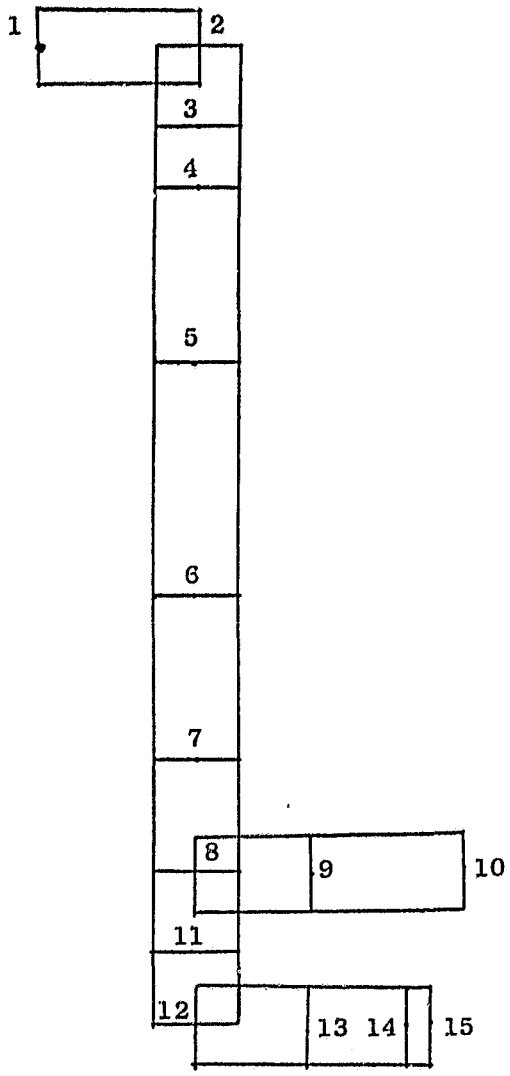

Figure 3. Analytical Model - Forward Shroud Support.

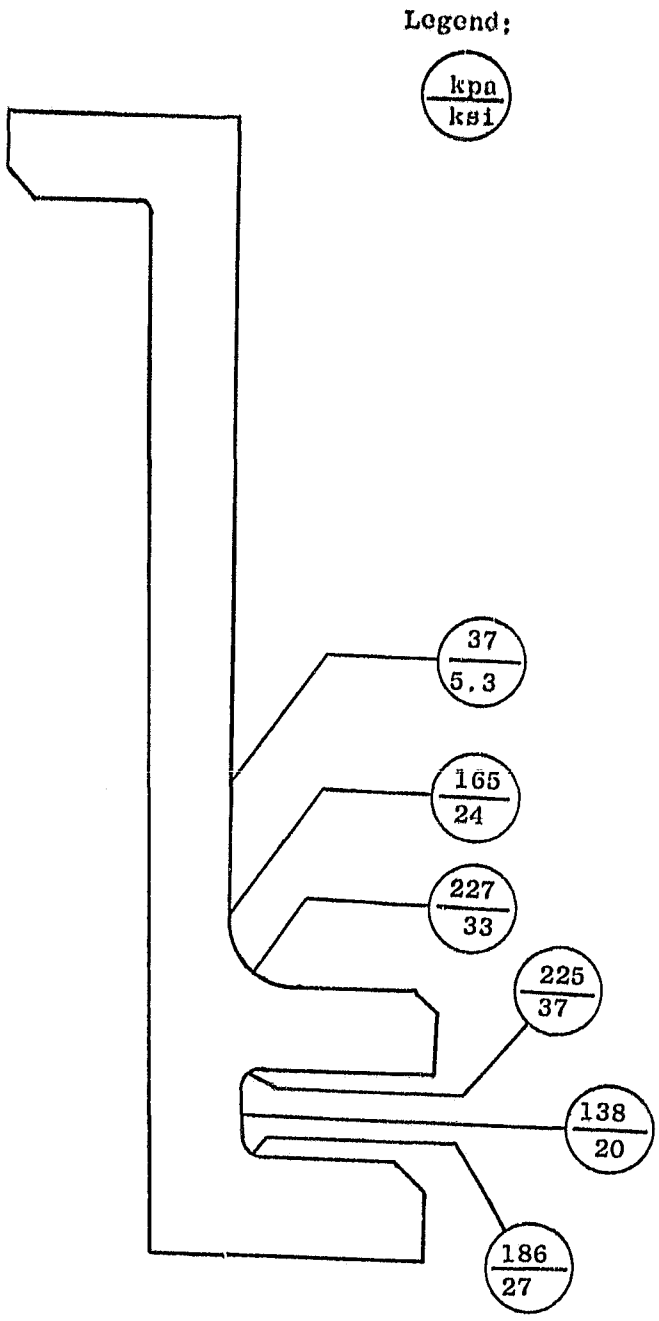

Figure 4. Effective Stress - Forward Shroud Support.

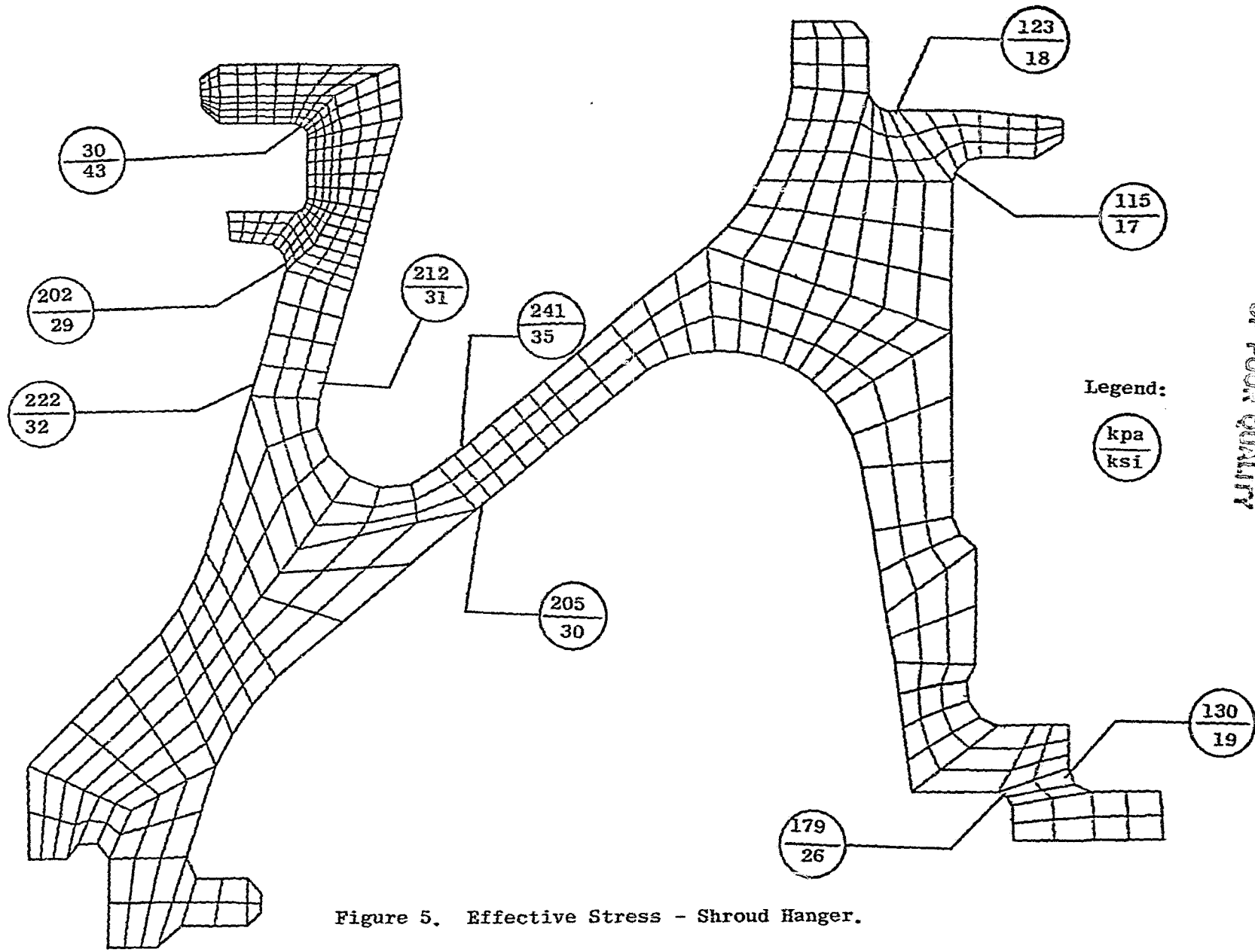

Figure 5. Effective Stress - Shroud Hanger.

3.3.1.3 First Stage Outer Screen Analysis

An analysis was conducted on the 1st stage high pressure turbine nozzle outer screen. This model included the effects of the 1st stage HPT nozzle support stiffeners, vane loads and the outer E-seal. The model and the stress levels are shown on Figures 6 and 7. The stresses shown are effective surface stresses and were not expected to cause operational problems.

3.3.1.4 Compressor Rear Frame/High Pressure Turbine Case Flange Analysis

A detailed analysis of the compressor rear frame (CRF) /High Pressure Turbine case flange joint was conducted. Preliminary analysis showed that this particular flange joint would experience higher mechanical loads and steeper thermal gradients than the other flange joint combinations in the HPT case. A detailed analysis was undertaken in order to better understand the stress levels. Figures 8 and 9 illustrate the model mesh generated and the stress levels in the joint. The model included the effects of thermal grandients, bolt preload, and mechanical and pressure loads. The highest stress occurred at cruise with cooled casing and maximum fan air flow. Although the maximum effective stress is in excess of 689.5 kpa (100 ksi), the material temperature at this location is low and no operational problems were anticipated.

3.3.2 Performance

Thermal, clearance and performance analyses were conducted during the design process. The thermal and clearance analyses deal with the subject of flanges with and without internal air flow. Also presented are the analytical results of the final design configuration.

3.3.2.1 Thermal Analysis

In order to assess the ability of a given design to adequately control the high pressure turbine clearance, an assessment of both transient and steady state temperatures, mechanical loads, and clearances was required. The temperatures were calculated by THTD, a second program (TITAN) was used to perform the thermal structural interface, and a third program (CLASS-MASS) was used for structural deflections. All of the above programs were written and are maintained by General Electric. Figures 10 and 11 depict the THTD and CLASS/MASS models respectively.

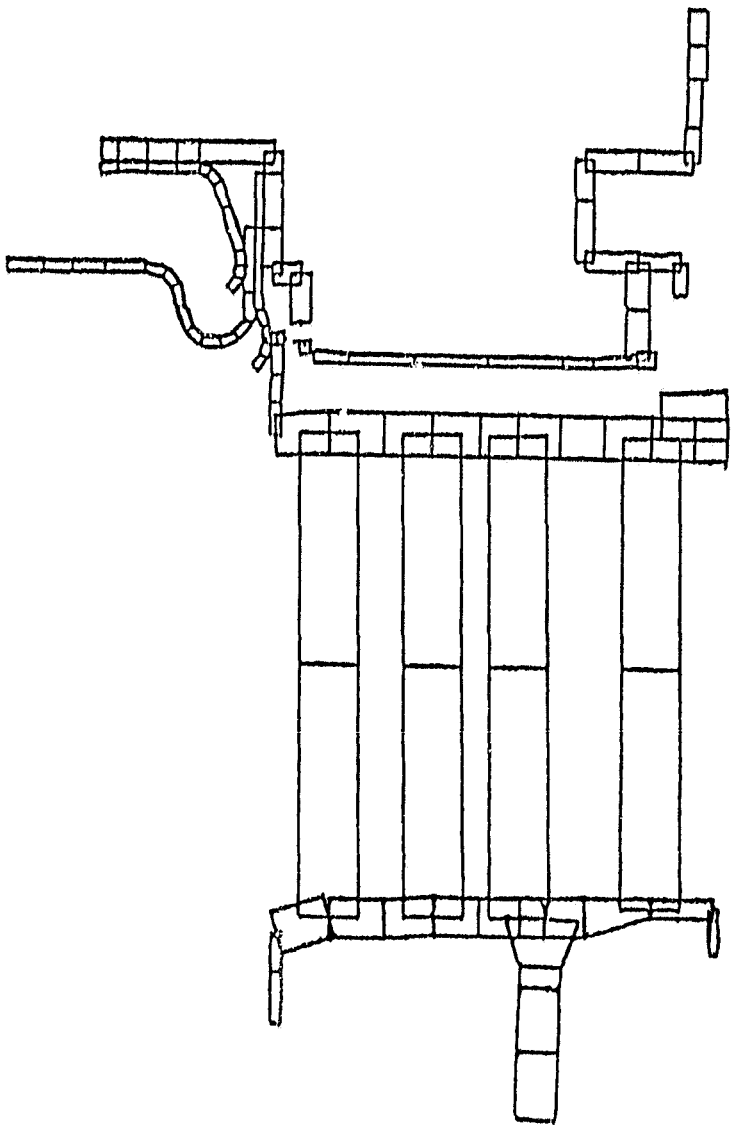

Figure 6. Analytical Model - HPT Nozzle and Screen.

Outer Stress

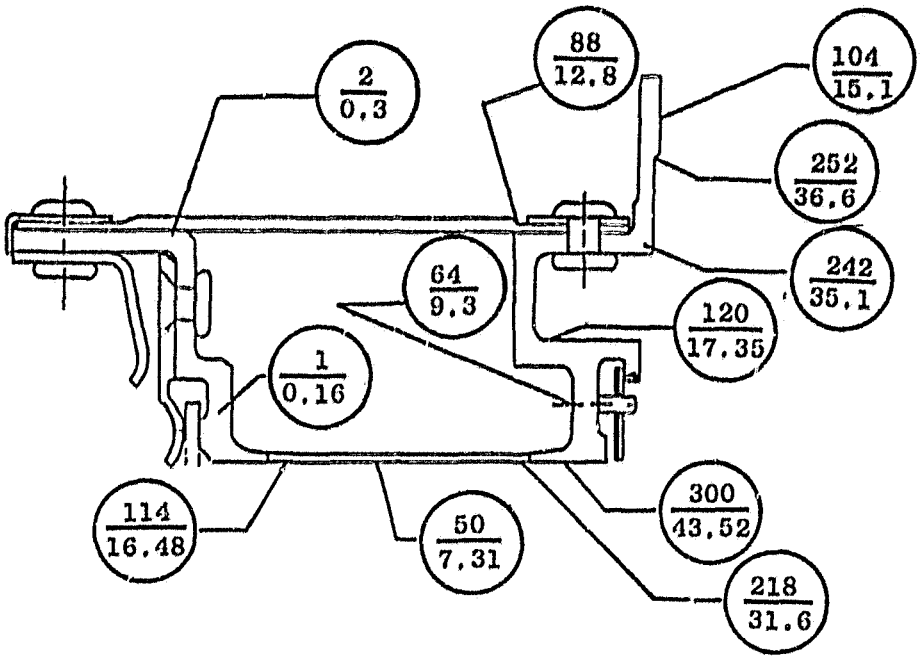

Legend:
kpa
ksi

Inner Stress

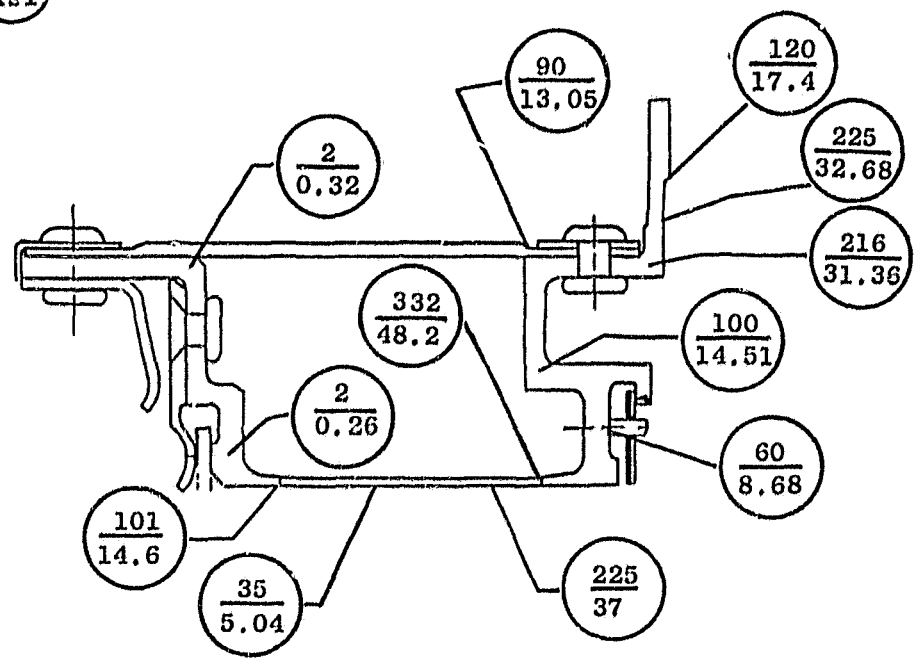

Figure 7. Effective Stress Summary - HPT Nozzle Outer Screen.

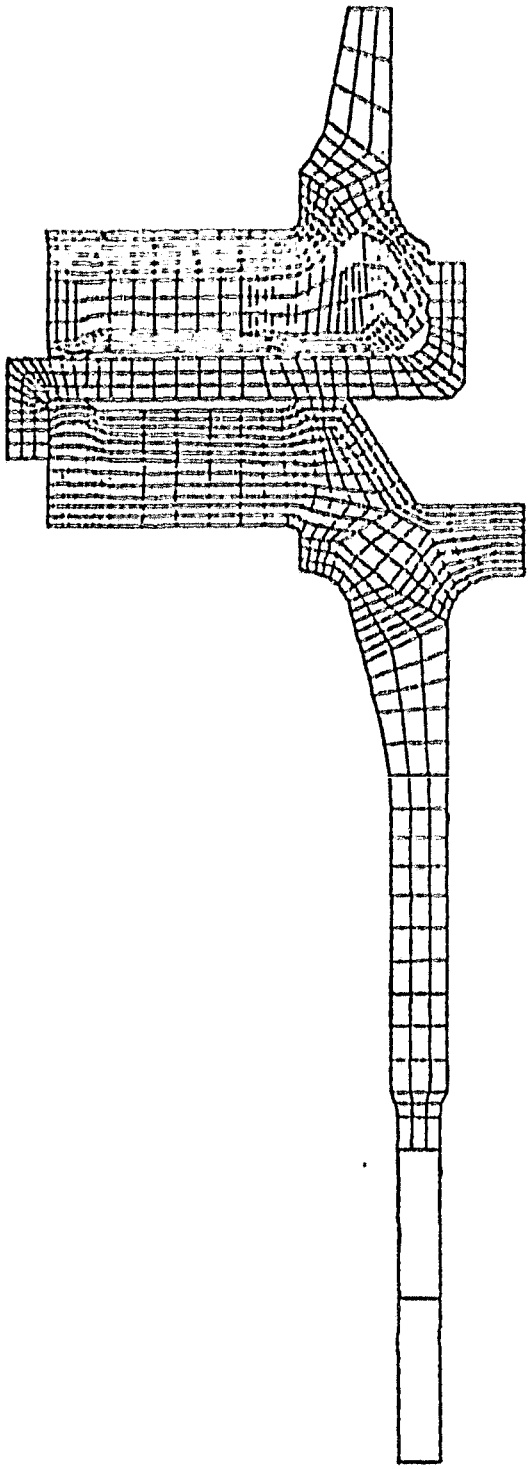

Figure 8. Analytical Model - Compressor Rear Frame/HPT Case Flange.

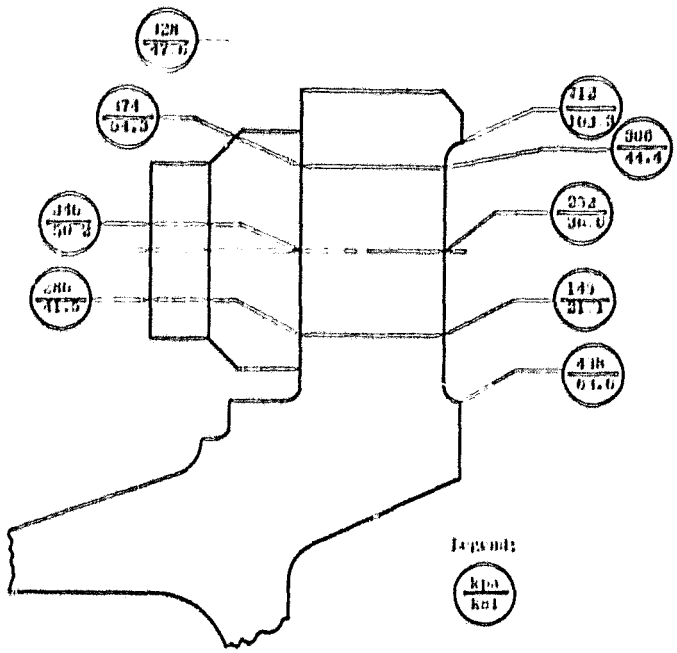

(a) Compressor Rear Frame Flange

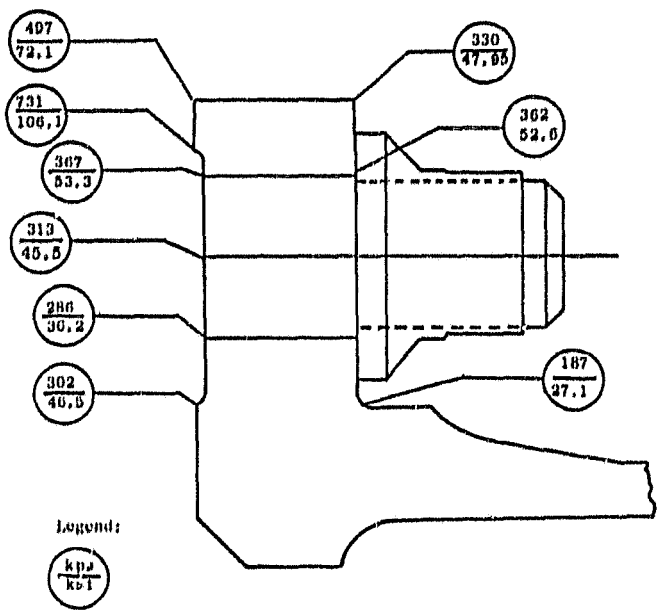

(b) High Pressure Turbine Case Flange

Figure 9. Effective Stress Summary.

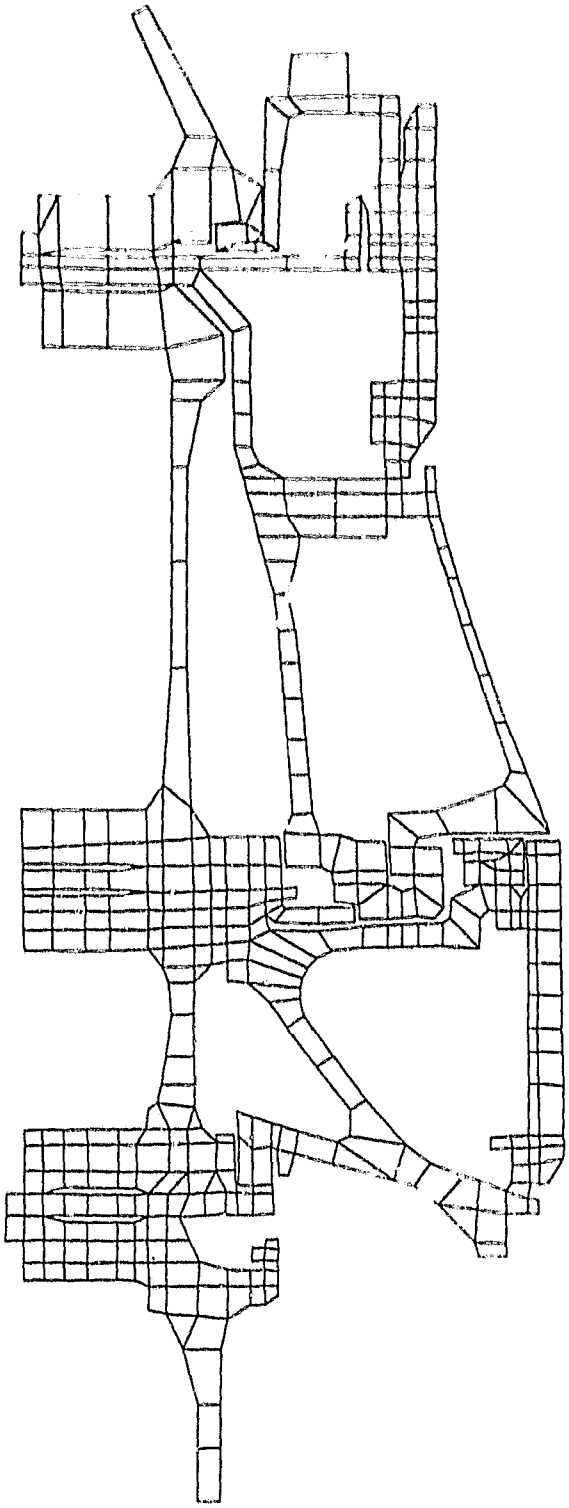

Figure 10. Heat Transfer Model - HPT ACC Structure.

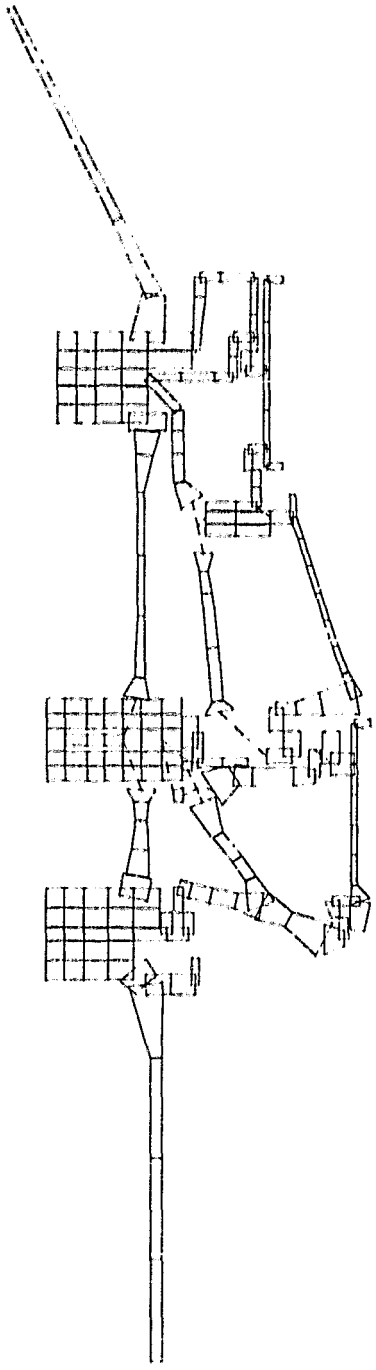

Figure 11. Structural Analysis Model - HPT ACC Structure.

After finalizing the design configuration of the High Pressure Turbine Active Clearance Control hardware, analysis was performed to determine both transient and steady state flange response. Of primary importance was an assessment of the amount of clearance reduction achievable for a given quantity of cooling air flow. In the initial design concept the flanges were to utilize compressor discharge air flowing inside of the flange as the means for increasing the thermal response of the flange as shown in Figure 12. However, performance stackups indicated that in order to achieve the design goal of 0.6 percent reduction in altitude cruise SFC, a clearance reduction of 0.50 to 0.75 mm (.020 to .030 in.) on the first stage and 0.25 to 0.50 mm (.010 to .020 in.) on the second stage would be required. The internally heated flange was analyzed with various amounts of fan air impingement, and the calculated cruise clearance reduction was found to be insufficient to achieve the performance improvement objective. See Table I for details.

An analysis was then conducted in which the internal flange air was deleted. The results, shown in Table II and compared with the internal flow in Table 1, indicated the objective could not be met with this approach.

3.3.2.2 Transient Analysis and Clearances

The transient analysis was performed in a fashion similar to the steady state analysis. The thermal analysis was performed at various points in time through the acceleration, and these temperatures were then imposed on the structural model to determine the radial growth vs time. The stator and rotor responses were then plotted to determine minimum throttle burst clearance and to establish build-up clearance. At this point in the design, the following assumptions were made:

1. This stator possesses the same out-of-roundness characteristics as the current design.
2. The ACC design must maintain the same minimum throttle burst clearance as the current design.

Based on the above assumptions rotor/stator clearances were determined for 0.2 percent internal flange air and for no internal flange air. The above cases were analyzed for a throttle burst from ground idle to hot day takeoff, steady

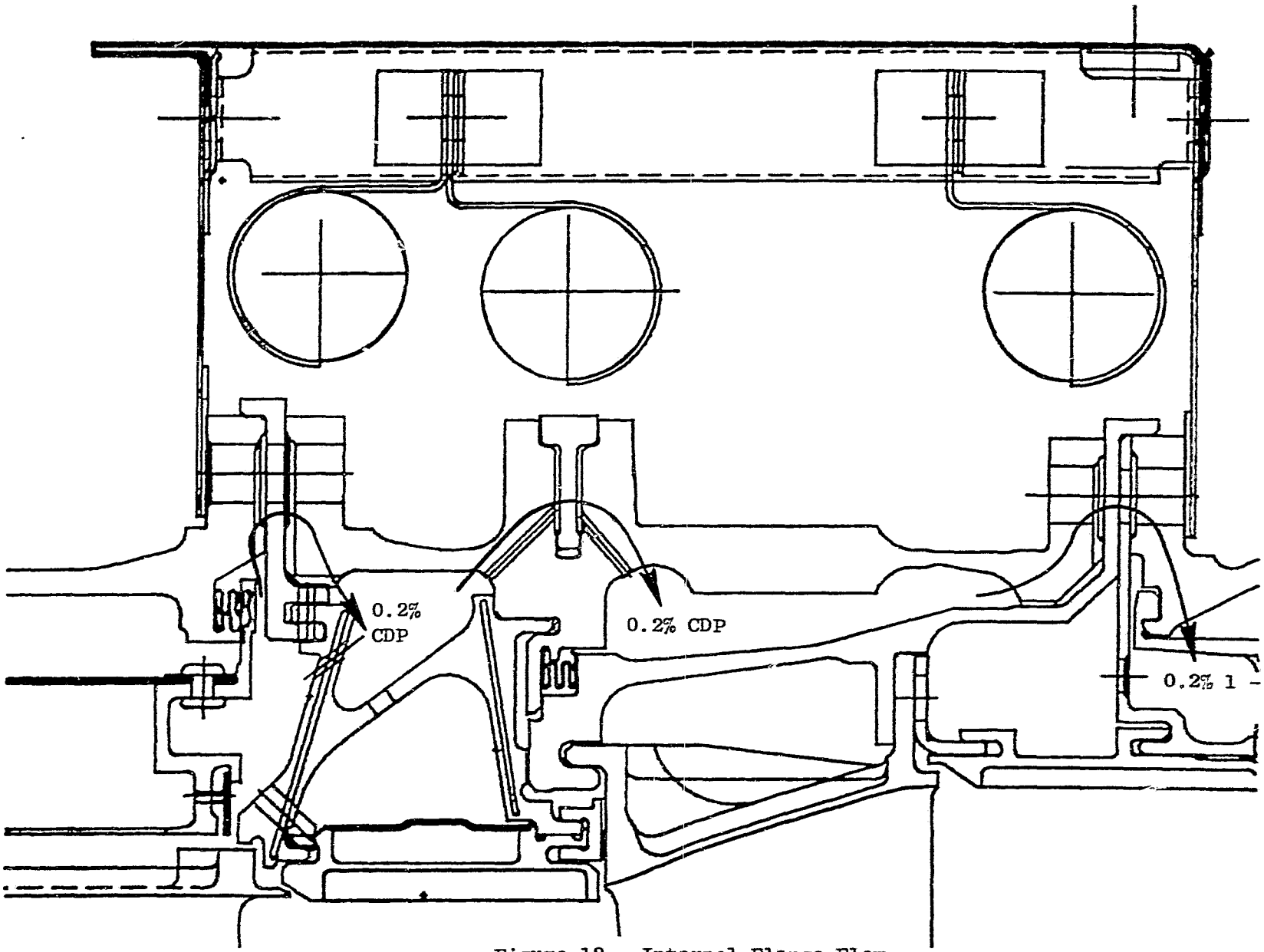

Figure 12. Internal Flange Flow.

Table I. Cruise Closure - Internal Flange Flow.

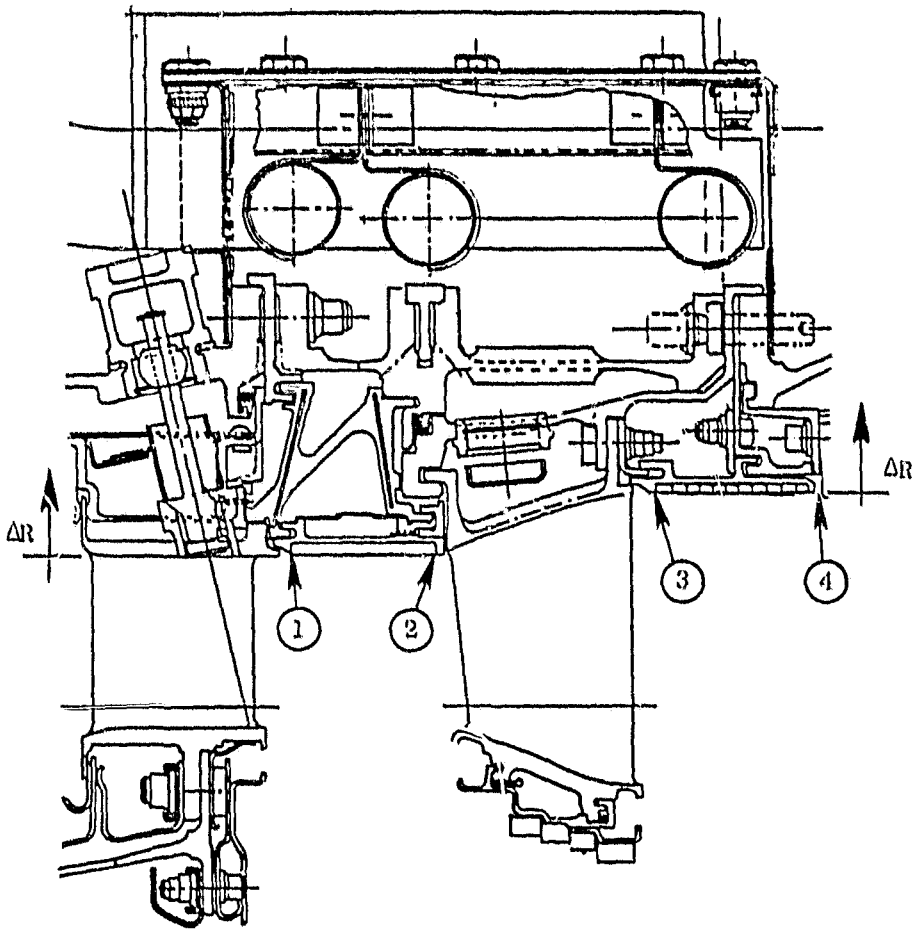

Clearances - mm (in.)

Condition 1 : 0.2% Internal Flange Air 0% External Fan Air	
ΔR_1 = 2.52 (0.099)	ΔR_3 = 2.27 (0.090)
ΔR_2 = 2.44 (0.096)	ΔR_4 = 2.44 (0.096)
Condition 2 : 0.2% Internal Flange Air 0.3% External Fan Air	
ΔR_1 = 2.16 (0.085)	ΔR_3 = 2.25 (0.089)
ΔR_2 = 2.11 (0.083)	ΔR_4 = 2.08 (0.082)
Closure = Condition 1 - Condition 2	
① = 0.36 (0.014)	③ = 0.03 (0.001)
② = 0.33 (0.013)	④ = 0.36 (0.014)

Table II. Cruise Closure - No Internal Flange Flow.

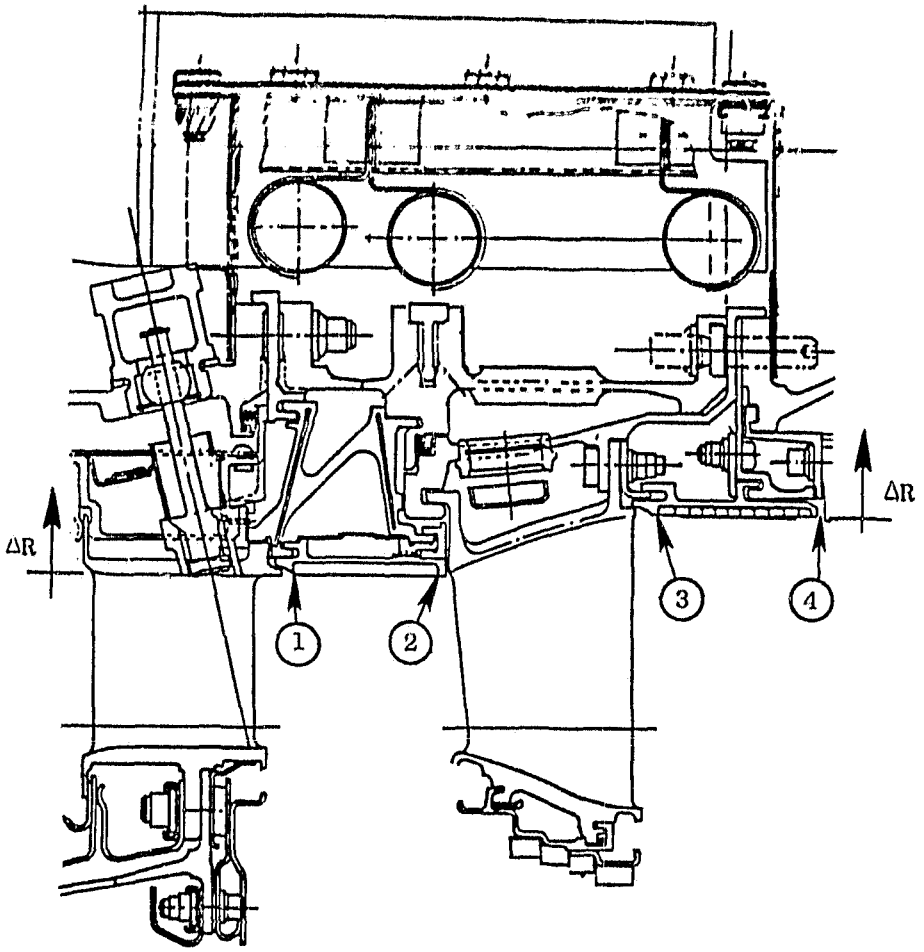

Clearances - mm (in.)

Condition 1 : 0% Internal Flange Flow 0% External Air	
ΔR_1 = 2.38 (0.094)	ΔR_3 = 2.32 (0.092)
ΔR_2 = 2.23 (0.088)	ΔR_4 = 2.26 (0.089)
Condition 2 : 0% Internal Flange Flow 0.3% External Air	
ΔR_1 = 1.63 (0.064)	ΔR_3 = 2.08 (0.082)
ΔR_2 = 1.70 (0.067)	ΔR_4 = 1.85 (0.073)
Closure = Condition 1 - Condition 2	
① = 0.75 (0.030)	③ = 0.24 (0.010)
② = 0.53 (0.021)	④ = 0.41 (0.016)

state maximum cruise and cooled maximum cruise. It became apparent that the response of the stator with no internal flange air was slow, and would have required a large build-up clearance to maintain the minimum required throttle burst clearance. In order to increase the thermal response of the stator during the accel transient, compressor discharge air was assumed to be impinged on the outside of the stator flanges, and the air was assumed to be shut off after approximately 2 minutes. This accomplished two objectives: the thermal response of the stator case was increased which provided improved build-up clearance, and the calculated clearance reduction, with fan impingement air, was sufficient to achieve the performance improvement. A transient and steady state analysis was conducted with these assumptions and compared to the two previous analyses. The results of these analyses on stage clearances are compared on Figure 13. Similar results were found on Stage 2 clearances.

Assumptions 1 and 2 above required that the grind shape for the ACC turbine be the same as the grind employed on the current design. The only difference was an increase in the grind average clearance.

3.3.2.3 Performance Estimates

The pretest performance stackups were completed using engine derivatives which accounted for the following:

1. The effects of Stage 1 and Stage 2 clearance changes
2. The cycle penalty inherent with using fan air
3. Fan air supply scoop losses and spent impingement air dump gains.

Figure 14 shows the effectiveness in reducing cruise SFC for a given level of external fan impingement air for the internally heated flanges and for the deletion of external flow.

3.3.3 Engine Testing

In order to demonstrate the performance of the High Pressure Turbine Active Clearance Control System a two-part engine test was required.

The first phase of the engine test gathered transient, steady state and High Energy X-Ray (HEX) data. The pretest analysis was then adjusted to match the test cell temperatures, and new clearance predictions were calculated. These

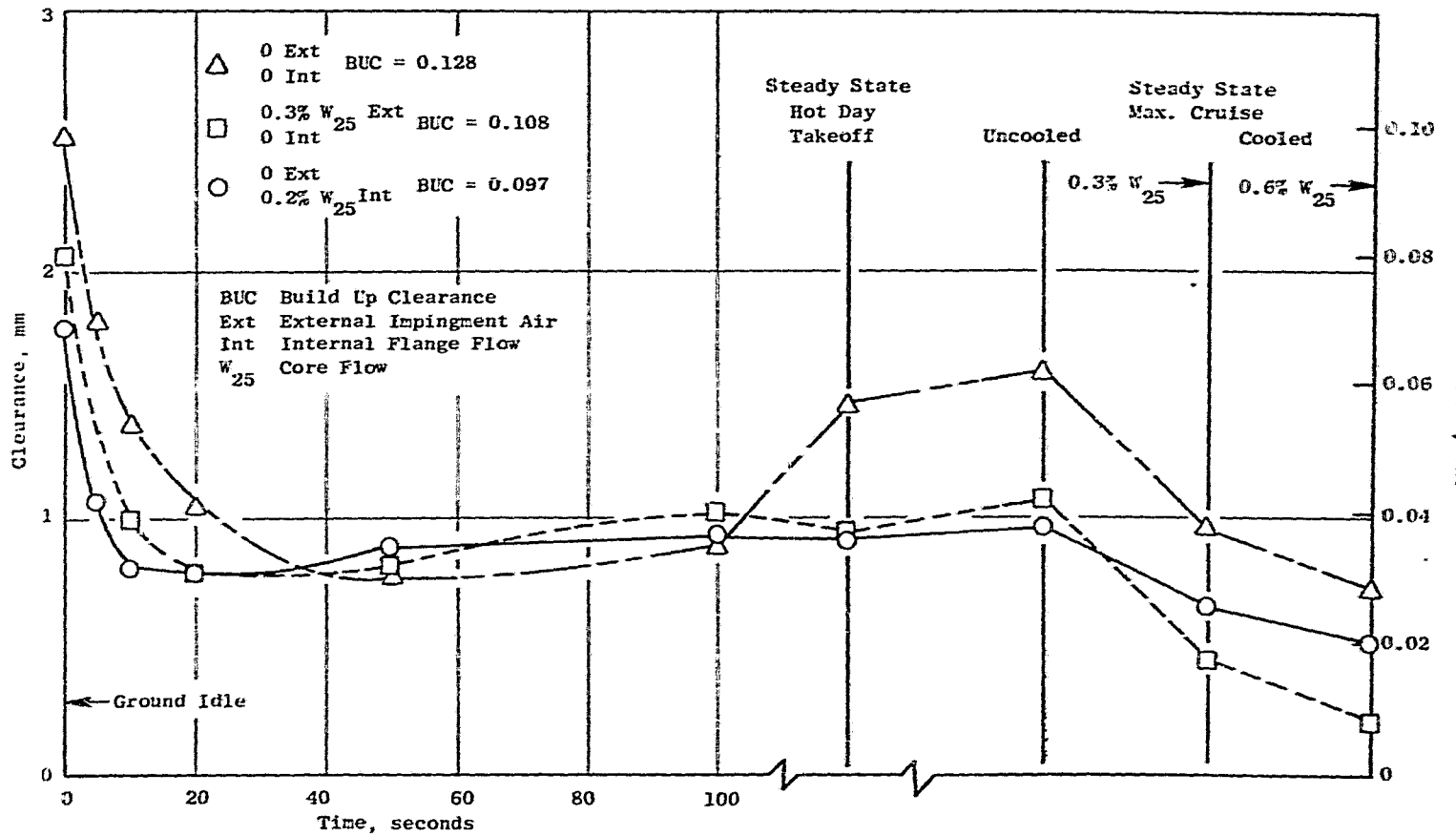

Figure 13. First Stage HPT Clearance Comparison.

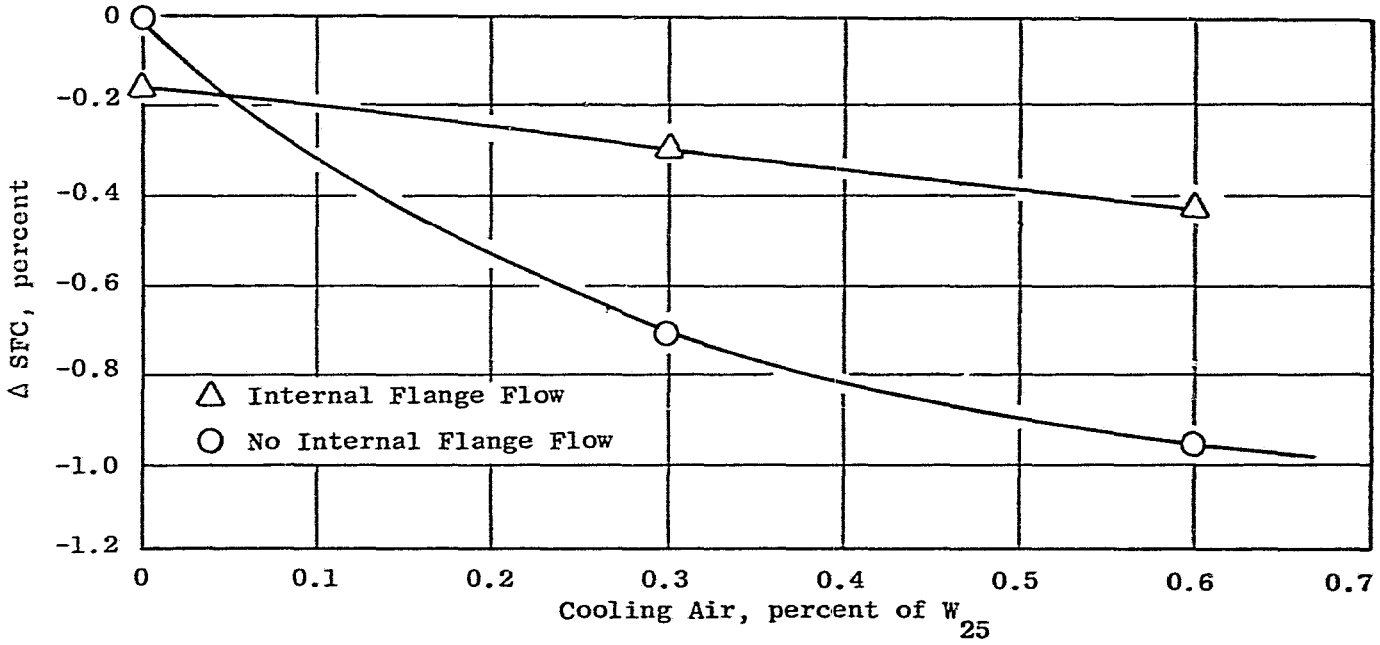

Figure 14. Performance Comparisons HPT ACC.

"test cell clearances" were then compared to the HEX radiographs. After an accurate match of temperature and clearance was completed new sea level performance improvement estimates were calculated.

After completion of the temperature survey, the engine was tested in a calibrated engine test cell and performance data were obtained. A comparison was then made between the measured performance improvement and the calculated performance improvement. Figure 15 illustrates the process used during the engine test to compare the measured engine performance to the calculated engine performance.

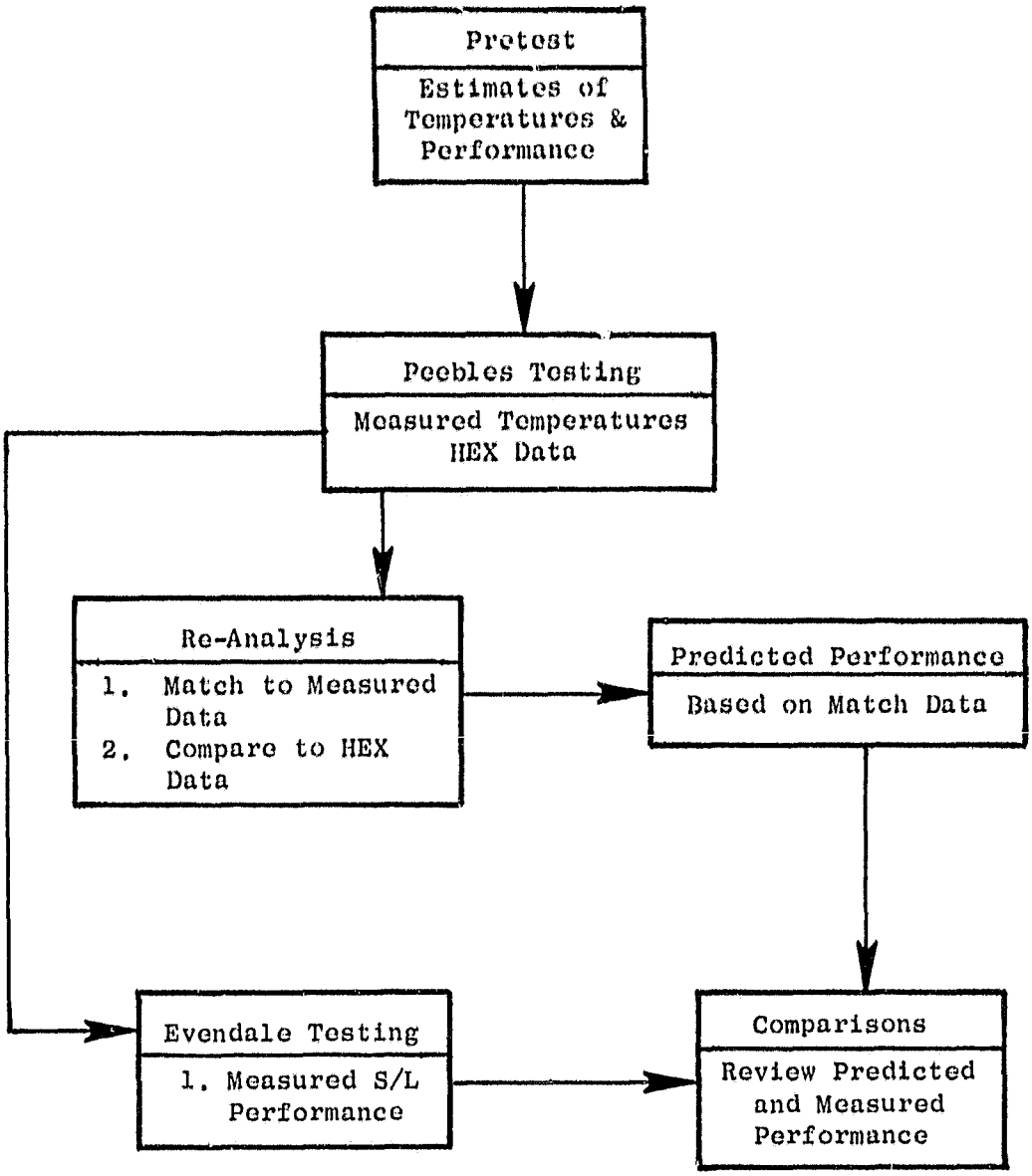

Figure 15. Engine Testing Procedure.

4.0 CONTROL COMPONENT AND SYSTEM BENCH TEST

Described herein are the high temperature air flow calibration tests performed for the motor-operated butterfly valve which was used during engine tests of the HPT cooling system.

4.1 TEST OBJECTIVES

The objectives of this test were to measure and record the flow characteristics of the HPT Active Clearance Control fan air supply valve.

4.2 INSTRUMENTATION AND TEST SETUP

The following test instrumentation was used to measure the flow parameters of the HPT variable area control valve.

Equipment	Parameter	Range	Minimum Accuracy
Single Phase, 400 Hz Power Supply	Voltage Source	0-150 VRMS	--
Frequency Meter	Frequency	400 ± 10 HZ	± 3%
AC Voltmeter	Voltage	0-150 VRMS	± 2%
Ammeter	Current	0-5 AMPS MAX	± 1%
Ohmmeter (2 Required)	Switch Continuity Pot. resistance	0-5K OHM MAX	± 1% F.S.
Degree Potentiometer	Temperature	0 to 150F	+ 1°F
Stop Watch	Time	0-30 Sec	+ .2 Sec
Hi Pot	Dielectric	0-2500 VAC	± 5%
Hi Pot	Leakage Current	0-5 MA	± 4%
Pressure Gage	Proof Pressure	0-500 psig	± 1% F.S.
Pressure Gage	Inlet Pressure Leakage and Manual Override	0-60	1% F.S.
Orifice or Flow Meter	Leakage	0-1 lb/min.	2%

Equipment	Parameter	Range	Minimum Accuracy
H_2O Manometer	ΔP across Orifice Meter	0-30 inches	+ 2% F.S.
Continuity Box (Optional)	Switch Continuity	Lamp Current 1 AMP MAX	N/A

The test set up is depicted on Figure 16.

4.2.1 Test Procedure

The valve was installed on a line with air at 180° F ± 10° F psig available for testing. The test valve was opened to the 10° open position by energizing pins "1" and "3" on the actuator with the 115 V.A.C. 400 Hz power supply until the correct fractional resistance was read from the ohmmeter. The fractional resistance for any required valve opening is given by:

$$r = \frac{R}{R_t} = \frac{R_1}{R_t} + \frac{R_2 - R_1}{R_t}\left(\frac{\theta}{90}\right) \qquad (1)$$

where R = resistance of potentiometer at desired vane opening

R_t = total potentiometer resistance (resistance between potentiometer pins 1 and 3)

R_1 = resistance at fully closed (resistance between potentiometer pins 2 and 3)

R_2 = resistance at fully open (vane opening = 90°) (pins 2 and 3)

θ^2 = desired vane opening, degrees

The flow control valve was slowly opened downstream of the test valve until a ΔP was read across the valve. Records of ΔP, P, P_1, T_1, R, R_t, and flow for this rate and for four higher flow rates through the valve were made. Additional data was recorded for the flow rate measurement, such as orifice inlet temperature, orifice ΔP and ambient pressure and temperature. After the data for the highest flow rate had been recorded, the valve was opened 10° more and the procedure, outlined above, was repeated, starting at the minimum flow which registered a readable ΔP across the valve. Data were obtained for every 10° of valve opening from 0 - 90°.

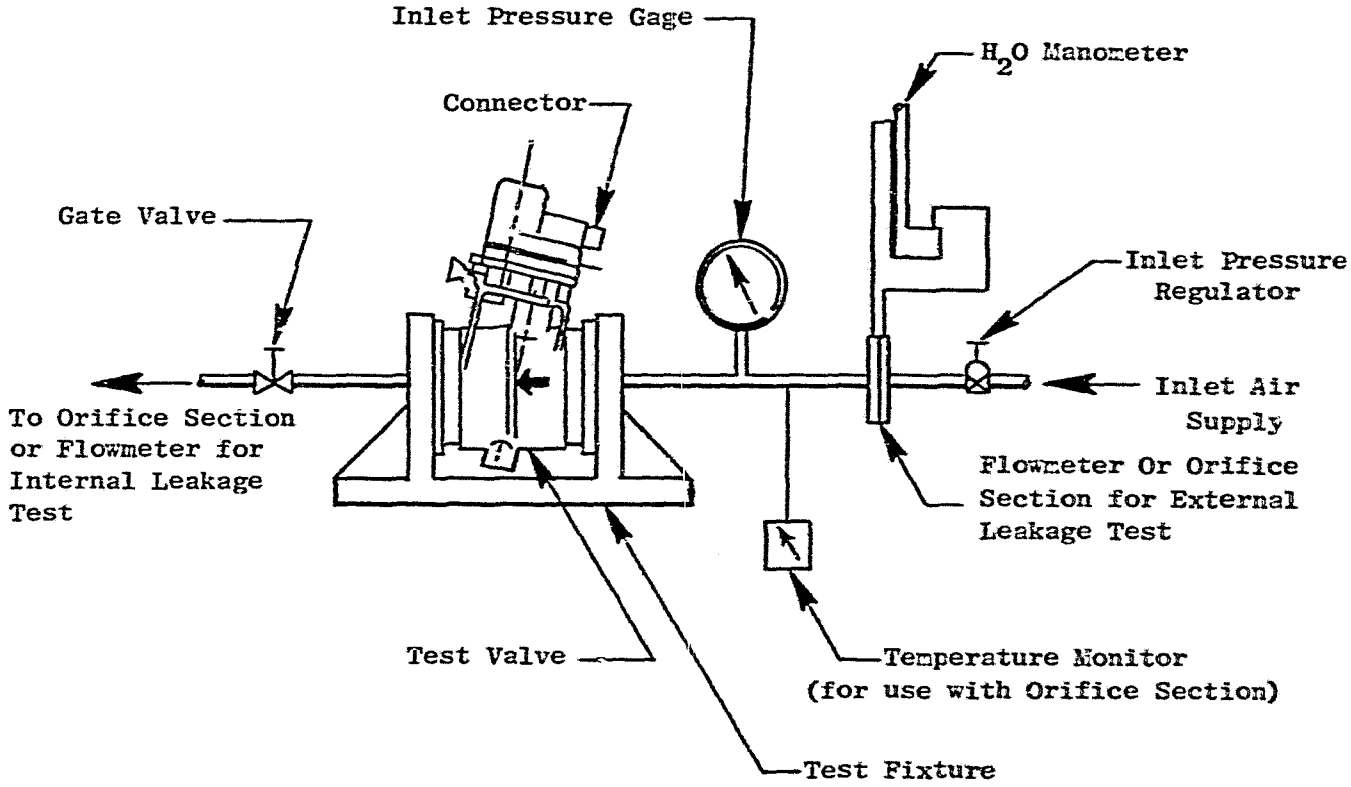

Figure 16. Room Temperature Test Setup.

From the data obtained, a family of curves, one curve for each fractional resistance R, was generated. Each curve showed:

$$\frac{\Delta P}{P_1} \text{ versus } \frac{W\sqrt{T}}{P_1} ,$$

where ΔP = pressure drop across valve,

P_1 = valve inlet pressure

W = flow rate

T = inlet temperature

4.2.2 Test Results

The measured test data were used to produce nondimensional air flow calibration curves for each valve, showing the valve flow function $\left(\frac{W\sqrt{T}}{P_1}\right)$ versus valve pressure ratio $\left(\frac{\Delta P}{P_1}\right)$. A separate curve was provided for every ten degrees of valve opening.

The final calibration curve is shown in Figure 17. This is the calibration curve for the valve that was installed in the test vehicle.

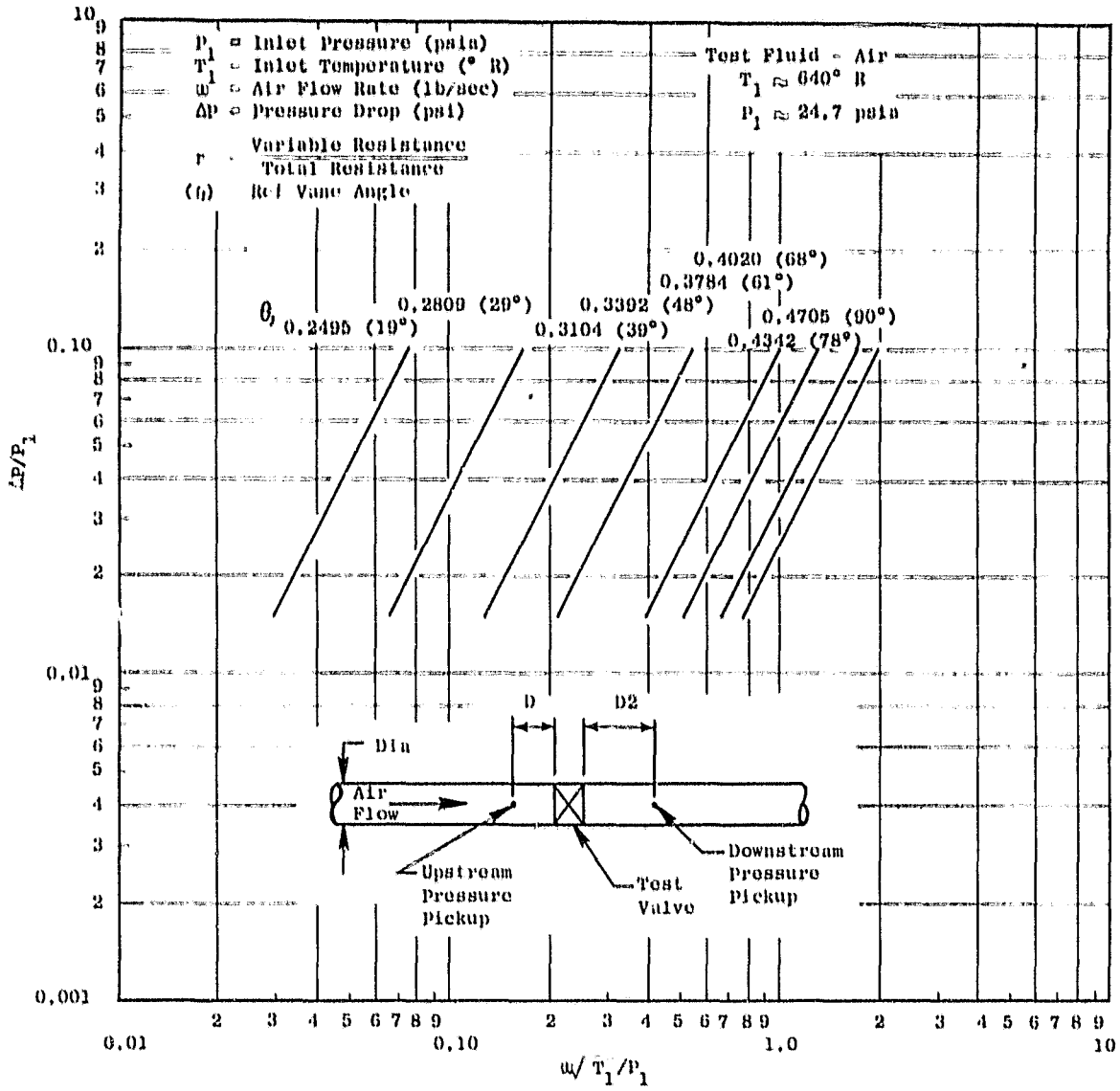

Figure 17. Valve Flow Versus Valve Pressure Ratio.

5.0 VIBRATION TESTING

This section of the report is concerned with the vibratory testing of the HPT ACC configuration piping and control components.

5.1 TEST OBJECTIVES

The objective of this test was to obtain the vibratory response of the active clearance control external configuration piping and control components. The data were analyzed to ensure that the vibratory frequencies were not in resonance with the engine operating range frequencies.

5.2 INSTRUMENTATION AND TEST PROCEDURE

The test data were obtained using a Fourier Analysis System and impulse test techniques. The test procedure involved epoxying a small, low mass (0.5 gram) accelerometer to the test part in the plane of excitation and then lightly tapping the part with a load cell attached to a small hammer.

This "pulse" imparts low level excitation to all frequencies in the analysis range and, therefore, will excite all system resonances. The accelerometer and load cell response signals are then filtered, sampled at a high speed, digitized, and stored in the analyzer, where these "time histories" are transformed into the frequency domain using a Fast Fourier Transform algorithm. The output response from the accelerometer is then divided by the input response from the load cell and displayed as an Inertance plot (i.e., Acceleration/Force vs. Frequency). This procedure is shown schematically in Figure 18.

Accelerometer locations and orientations are noted in Figures 19 and 20. All hammer "pulse" excitation was in the same direction as the accelerometer orientation.

The data as output by the Fast Fourier Transform algorithm consisted of the following:

1) Graphical representation of the inertance (acceleration/force) vs. response frequency
2) A graphical representation of the phase angle between input and output
3) A tabulation of frequency, inertance and phase angle arrangement in descending values of inertance.

A typical Fast Fourier Transform output is shown in Figure 21.

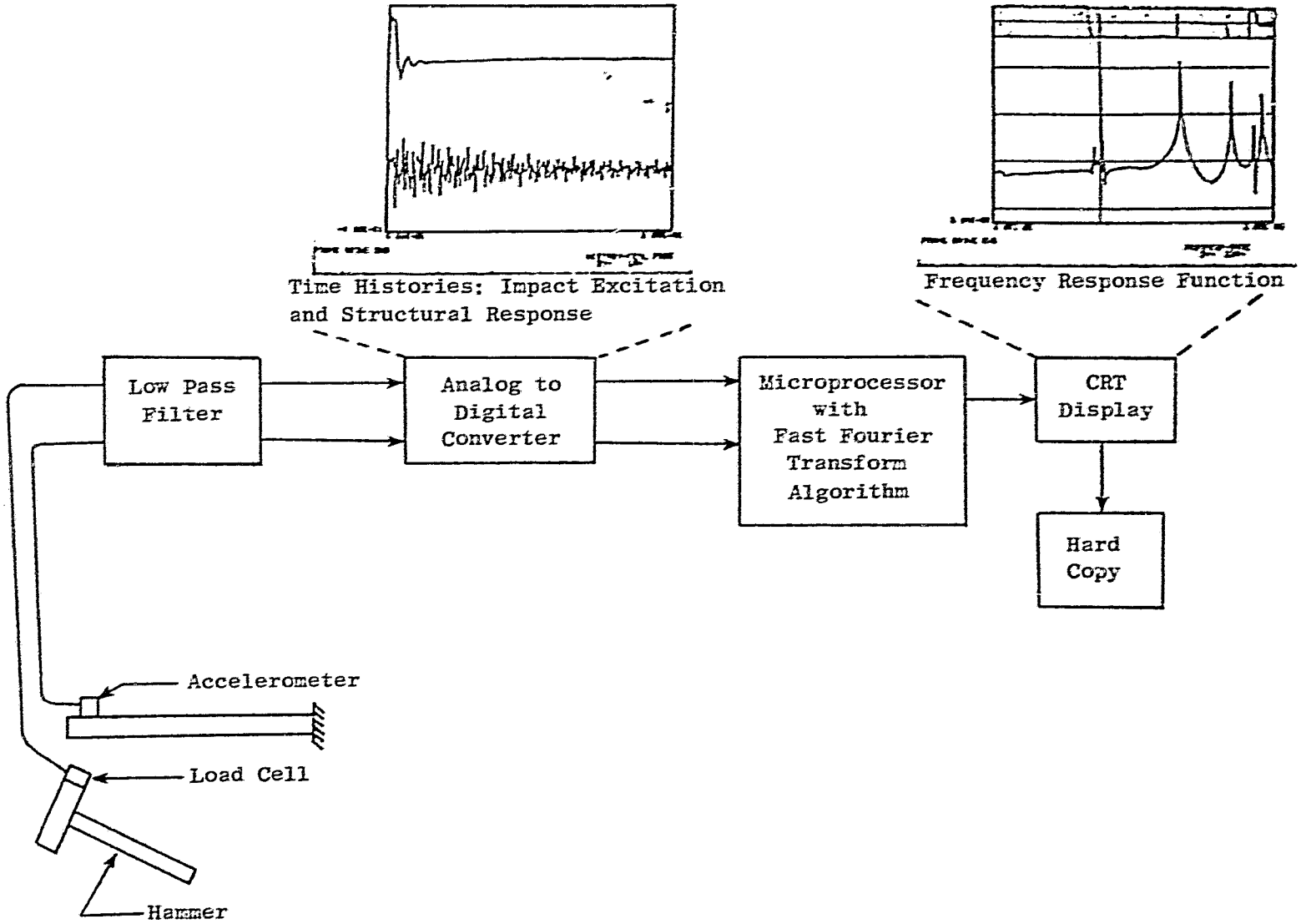

Figure 18. Fourier Analysis System.

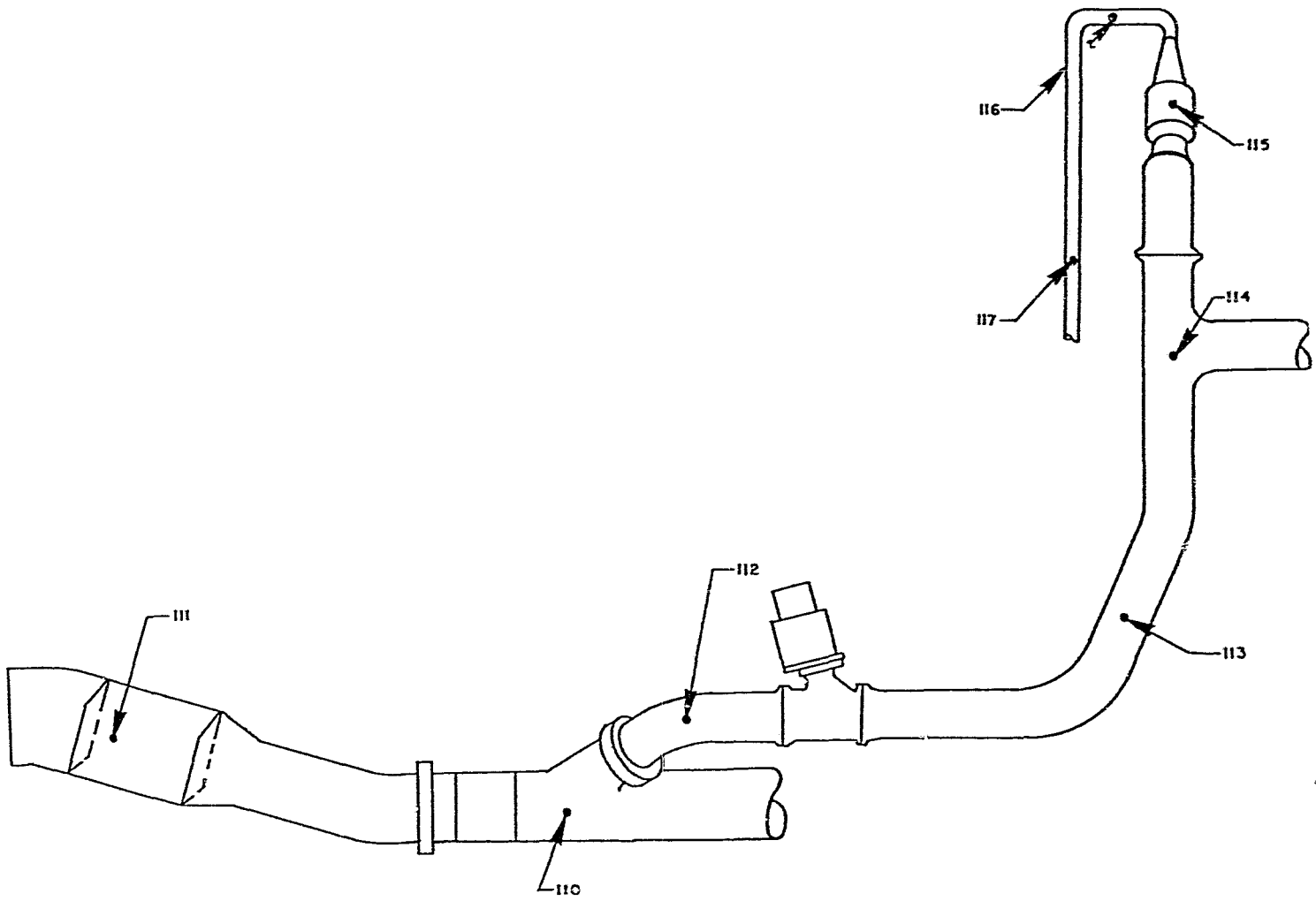

Figure 19. ACC Ducting Assembly - Accelerometer Location and Number.

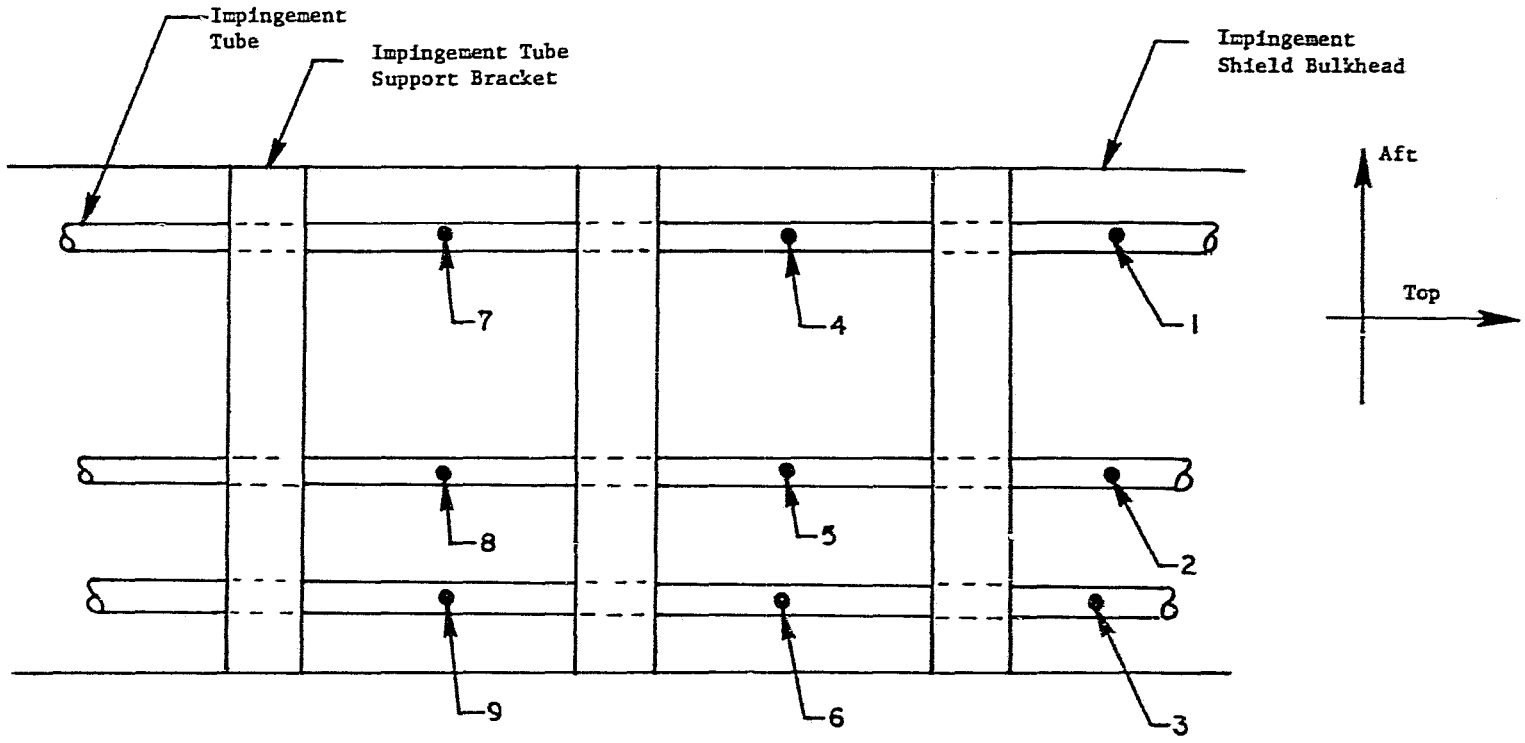

Figure 20. Impingement Assembly - Accelerometer Location and Number.

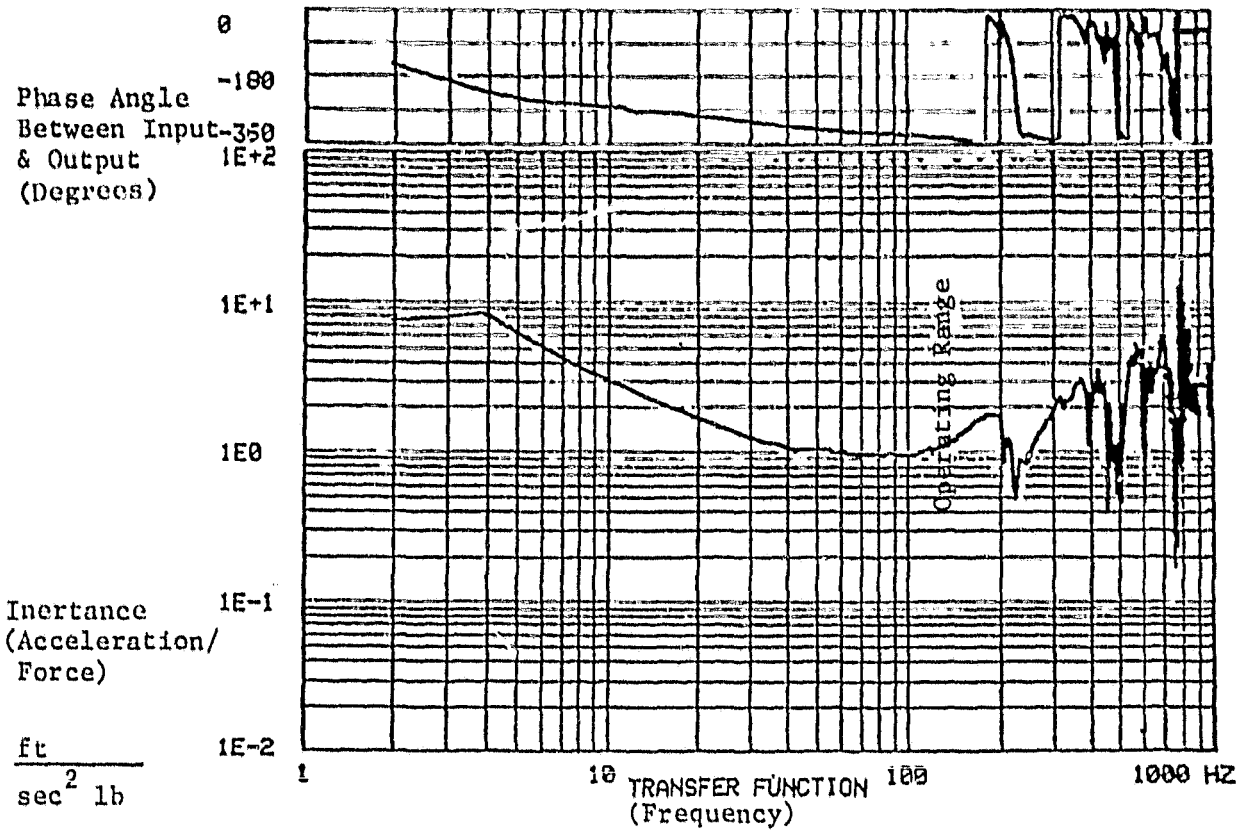

RANK	CHANNEL NO.	FREQUENCY	F1(N)	F2(N)
1	295	5.76 E+2	5.17 E+0	-6.84 E+1
2	299	5.83 E+2	5.10 E+0	-7.71 E+1
3	285	5.56 E+2	4.38 E+0	-3.33 E+1
4	220	4.29 E+2	3.59 E+0	-7.03 E+1
5	193	3.76 E+2	3.10 E+0	-4.93 E+1
6	228	4.45 E+2	3.06 E+0	-8.92 E+1
7	195	3.80 E+2	3.04 E+0	-5.59 E+1
8	163	3.18 E+2	2.29 E+0	-1.38 E+1
9	174	3.39 E+2	2.22 E+0	-1.97 E+1
10	240	4.66 E+2	2.10 E+0	-8.37 E+1
11	99	1.93 E+2	1.79 E+0	-3.26 E+1
12	93	1.81 E+2	1.78 E+0	-1.29 E+1
13	97	1.89 E+2	1.79 E+0	-2.57 E+1
14	107	2.08 E+2	1.23 E+0	-5.34 E+1
15	259	5.05 E+2	1.21 E+0	-1.40 E+1
16	67	1.30 E+2	1.11 E+0	-3.43 E+2

Figure 21. Typical Fast Fourier Transform Output.

5.3 TEST FACILITY AND TEST SETUP

The vibratory survey was conducted in two parts. The first part was completed at Evendale and included a vibration survey of the impingement tubes and the impingement tube support brackets. The second part was completed in the engine preparation building at Peebles test facility and included a complete vibratory survey of all installed piping, valves, brackets and fittings. The two-part test was deemed necessary because with the installation of engine instrumentation, impingement shield covers and other external configuration hardware, the impingement tubes and support brackets are inaccessible.

The vibratory scan of the impingement tubes was conducted with the forward and aft impingement shield bulkheads, impingement tubes, support brackets and the air impingement manifold installed and secured to the engine HPT case. See Figure 22 for details. The interconnection between the air impingement manifold and the HPT air supply system was not completed, and the impingement shield covers were removed. However, for this portion of the test, the main interest was the vibratory response of the impingement tubes between the support brackets and not the response of the entire piping system. The elimination of the interconnection and the impingement shield covers would not alter that particular response.

The second part of the vibration survey was completed at Peebles and consisted of a vibratory scan of the entire piping system with all hardware installed on the engine.

5.4 TEST RESULTS

Prior to discussing the results of the vibration survey, it is pertinent to define the temperature correction factor which takes into account that the vibratory frequencies are a function of the operating temperature of the part. It can be shown for a linear elastic system that the temperature correction factor is as follows:

$$\left(\frac{E_H}{E_c}\right)^{1/2} = \frac{f_H}{f_c}$$

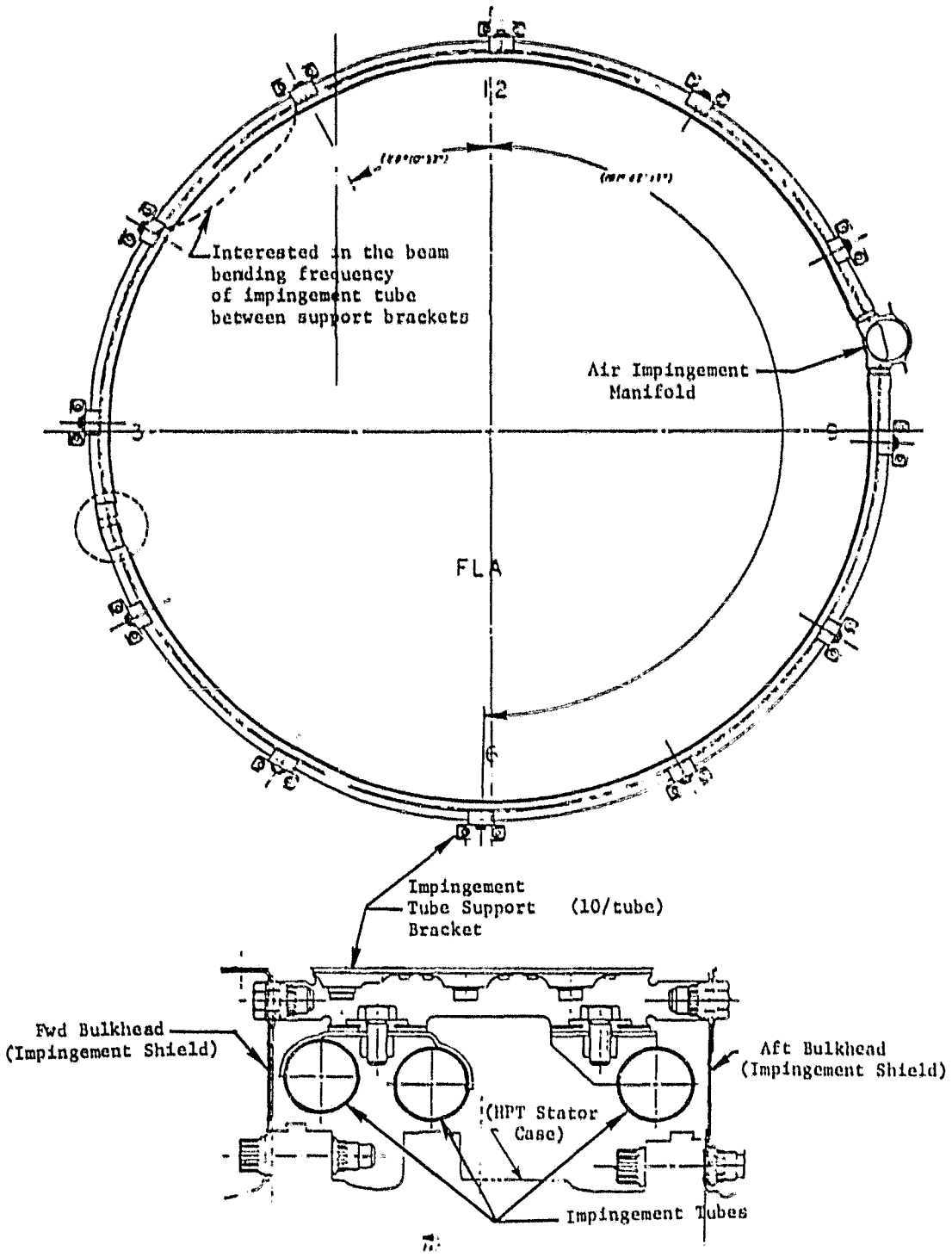

Figure 22. Impingement Tube Vibratory Scan.

where:

f_H = vibratory frequency at operating temperature

f_c = vibratory frequency at test temperature

E_H = Modulus of elasticity at operating temperature

E_c = Modulus of elasticity at test temperature

$(E_H/E_c)^{1/2}$ = temperature correction factor

The effects of pressurization on the vibratory frequencies were neglected.

5.4.1 Vibratory Frequencies

The results of the vibratory survey show that accelerometers 111 and 116 (see Figure 19) show a significant resonance. The remaining responses appear highly dampened or occur well above engine operating speed frequencies.

5.4.1.1 Frequency Response of Accelerometer #116

The frequency response of accelerometer #116 (Figure 23) shows a very strong undampened response at 187 Hertz. This accelerometer is located on the CDP tube whose purpose is to supply CDP air to the impingement system during a takeoff burst.

The CDP tube is subjected to an operating temperature of the compressor discharge air (T_3). In addition, the tube is anchored to the compressor case, and would respond to core operating frequencies.

Analysis indicated the following:

T_3 (max) = 540°C (1005°F)

XN25 (max) = 9767 rpm (core speed)

E_c = 28.41×10^{-6}, 21°C (70°F) [AISI 321 Stainless Steel]

E_H = 21.865×10^{-6}, 540°C (1005°F)

$$\left(\frac{E_H}{E_c}\right)^{1/2} = .8773$$

$f_{H\ tube}$ = 187 (.8773) = 164. (Hz)

core operating frequency = $\frac{9767}{60}$ = 163 (Hz)

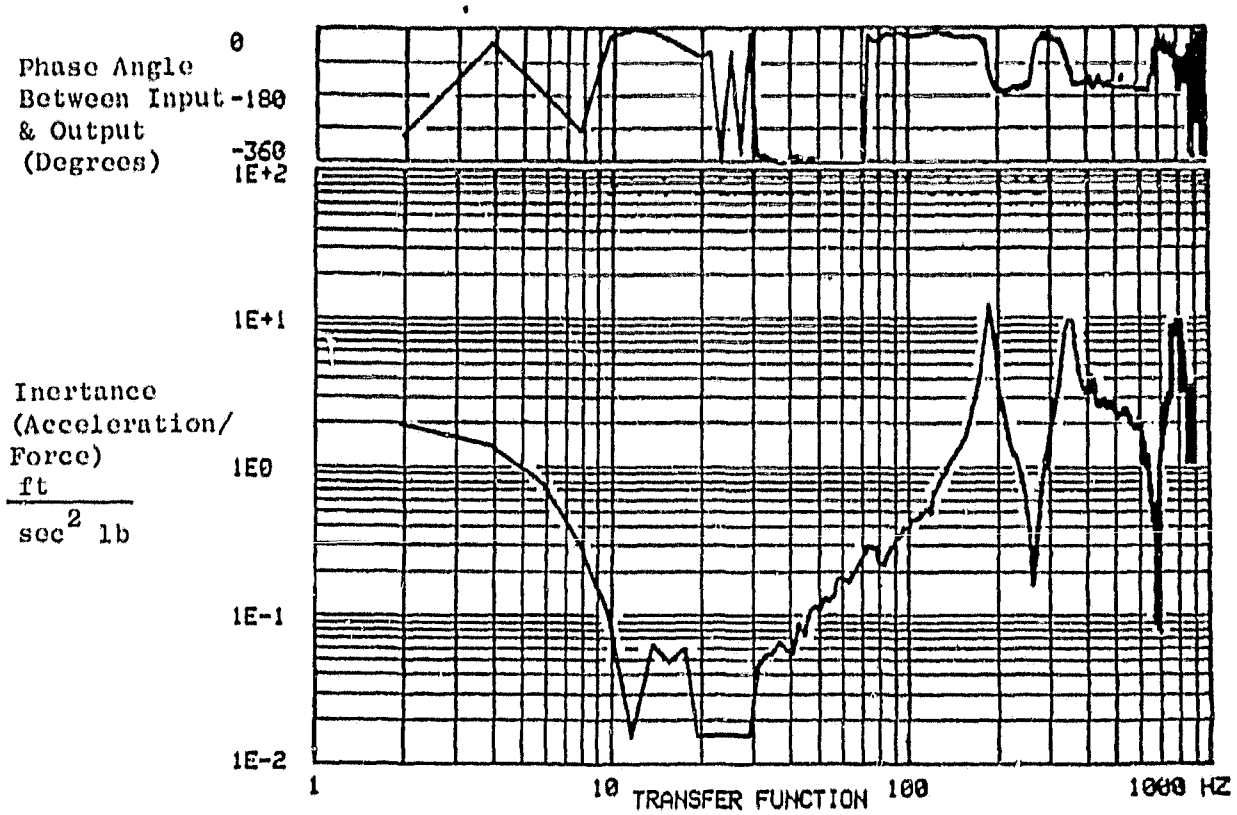

RANK	CHANNEL NO.	FREQUENCY	F1(N)	F2(N)
1	96	1.87 E+2	1.21 E+1	-9.17 E+1
2	178	3.47 E+2	9.75 E+0	-8.90 E+1
3	181	3.53 E+2	9.76 E+0	-1 05 E+2
4	202	3 94 E+2	3.42 E+0	-1.45 E+2
5	118	2.30 E+2	1.20 E+0	-1.56 E+2
6	124	2.42 E+2	9.02 E-1	-1.55 E+2
7	60	1.17 E+2	5.20 E-1	-1.34 E+1

Figure 23. Accelerometer No. 116 Direction Radial.

Because the engine would be maintaining this operating condition for an extended period of time, it was judged that not enough safety margin existed in this section of tube. A review of the test plan showed that the instrumented engine tests would be run during June-July (with higher ambient temperatures) and both core speed and T_3 would be lower than pre-test limits, which assumed a cold day operation. Based on revised estimates:

T_3 (max test) = 510°C (950°F)

XN25 (max test) = 9500 rpm (core speed)

E_c = 28.41×10^6, 21°C (70°F)

E_H = 22.25×10^6, 510°C (950°F)

$\left(\frac{E_H}{E_c}\right)^{1/2}$ = .885

f_H tube = 187 (.885) = 166 (Hz)

core operating frequency = $\frac{9500}{60}$ = 158 (Hz)

At this operating condition, a 5 percent margin of safety exists between the maximum engine operating rpm frequency and the resonance tube frequency. Although this is not adequate for a production design, it was deemed adequate for a development piece of hardware. During the engine test, T_3 and core speed were held to the limits specified above.

5.4.1.2 Frequency Response of Accelerometer #111

The frequency response of accelerometer 111 shows a somewhat dampened response at 140 (Hz) as can be seen in Figure 24. This accelerometer was located on the forward section of the air supply scoop, and was subjected to T_{13} (fan discharge temperature). The air supply scoop was anchored to the engine front frame, and was directly subjected to core operating frequencies. However, the air scoop was checked against both core and fan operating speed frequencies.

T_{13} (max) = 69°C (156°F)

fan speed XN112 (max) = 3600 rpm

core speed XN125 = 6146 (ground idle)
8750 (min. cruise)
9000 (avg. cruise)
9200 (max. cruise)
9500 (take-off)

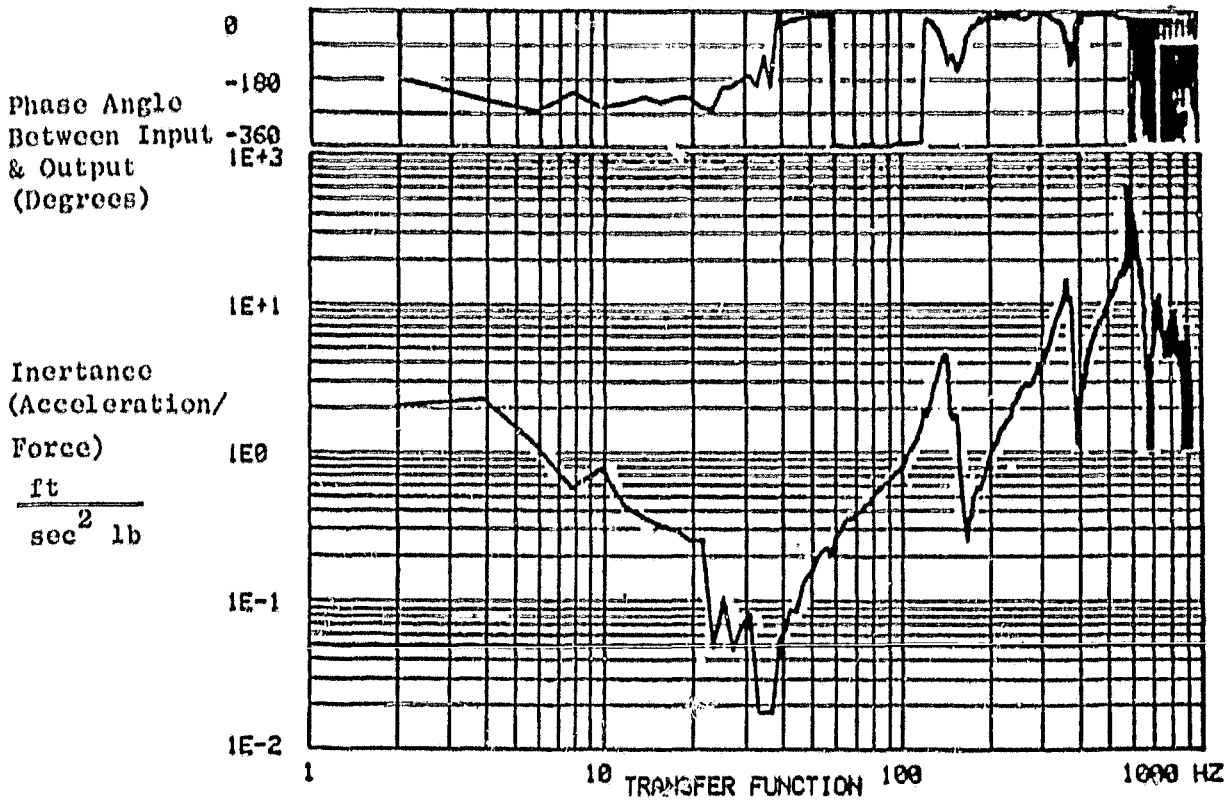

RANK	CHANNEL NO.	FREQUENCY	F1(N)	F2(N)
1	186	3.63 E+2	1.45 E+1	-6.48 E+1
2	193	3.76 E+2	1.11 E+1	-9.91 E+1
3	72	1.40 E+2	4.61 E+0	-8.63 E+1
4	138	2.69 E+2	2.93 E+0	-1.60 E+1
5	141	2.75 E+2	2.92 E+0	-1.43 E+1
6	134	2.61 E+2	2.80 E+0	-1.38 E+1
7	123	2.40 E+2	2.13 E+0	-4.47 E+0
8	61	1.19 E+2	1.99 E+0	-1.16 E+1
9	78	1.52 E+2	1.81 E+0	-1.20 E+2
10	121	2.36 E+2	1.78 E+0	-1.02 E+1
11	94	1.83 E+2	5.95 E-1	-3.81 E+1

Figure 24. Accelerometer No. 111 Direction Radial.

E_c = 28.41×10^6, 21°C (70°F)

E_H = 27.9×10^6, 69°C (156°F)

$\left(\frac{E_H}{E_c}\right)^{1/2}$ = .991

$f_{H\ scoop}$ = 140 (.991) = 138.7 (Hz)

fan operating frequency = $\frac{3600}{60}$ = 60 (Hz)

core operating frequency = 102.4 (Hz) at ground idle
145.8 (Hz) at min. cruise
150.0 (Hz) at avg. cruise
153.0 (Hz) at max. cruise
158.0 (Hz) at take-off

The air scoop vibratory frequency was well above max. fan speed, and falls between the ground idle and minimum cruise steady state points. The engine would reach the 138.7 (Hz) transiently, and the air scoop would not be in resonance with the engine.

5.5 DISCUSSION

The results of the vibratory survey show that, except for the CDP supply pipe, the resonant frequencies of the HP turbine active clearance control piping were well above the engine operating speed frequencies.

The CDP pipe showed a resonant frequency which is 5 percent above maximum engine operating speed. Although this may not be adequate for a production design, it is adequate for development hardware. For production, additional margin could be obtained by rearranging the bracket supports.

One additional frequency existed on the HPT/LPT air supply scoop which fell between two steady state engine operating conditions. No engine operating problems were expected since this response is somewhat dampened and would only see transient excitation.

In conclusion, it can be stated that there were no vibratory resonances in the HPT ACC piping system which were judged to impair safe engine operation.

6.0 HIGH ENERGY X-RAY TRANSIENT/ENDURANCE TESTING

This section of the report is centered on the engine testing completed at the General Electric Peebles Test Operation, Peebles, Ohio. This section of the report describes the test objective, test facility, instrumentation, piping, flow calibration, temperature survey, high energy x-ray (HEX) testing, high energy x-ray (HEX) data and matched analytical data comparisons.

Results of both transient and steady state temperature surveys are presented and compared to the matched analytical data. The HEX data for both transients and steady state operating conditions are presented and the HEX clearance measurements are compared to the clearance measurements based on matched temperature data.

6.1 TEST OBJECTIVES

The test objectives of the instrumented engine at the Peebles Test Operation (PTO) were as follows:

1. Obtain transient and steady state temperature data during various engine throttle burst, throttle chops and throttle reburst cycles.
2. Concurrent with 1 above, obtain high energy x-ray (HEX) radiographs to be used to measure the HP turbine tip clearance.
3. Demonstrate the capability of the active clearance control hardware to withstand cyclic endurance testing.

In addition to the above, a complete flow calibration of the HPT active clearance control piping system was completed.

6.2 TEST FACILITY

The testing was completed at the Peebles Outdoor Test Facility, Site III-A, where HEX measurements were taken and transient and cyclic endurance testing were conducted.

The digital system at Peebles Site III-A is directly linked with the Data Management System (DMS) at Site IV. A quick look format can be generated and selected engine data printed out at the Site III-A control room.

The following data channels are available at Site III-A:

1) 88 pressure channels (steady state only)
2) 192 temperature channels plus 8 reference channels
3) 10 frequency channels

Transient temperature data is recorded on "floppy disk" at a maximum rate of 300 channels per second. Up to 15 temperature channels can be simultaneously monitored on Sanborn charts and recorded on the "floppy disk" system.

In addition to the transient and steady state systems already described the site has the following capacity:

1) Engine parameter monitoring
2) HEX/fluoroscopy
3) Voice recorders
4) Vibration readout

6.3 INSTRUMENTATION

6.3.1 Active Clearance Control Instrumentation

The instrumentation used to measure and record the temperatures and pressures in the ACC piping system and hot structure remained unchanged during the course of the Peebles testing, and consisted of a total of 121 thermocouples and 49 pressure taps. The instrumentation is broken down into various categories. A brief description follows.

Cooling Supply Instrumentation

Cooling supply instrumentation consisted of two static pressure and 1 total temperature/total pressure probe in each of the LPT, HPT and CDP air supply systems. See Figure 25 for additional detail.

Impingement System Instrumentation

The impingement system instrumentation consisted of 10 static pressure probes and 5 temperature probes. Six of the pressure probes and 3 of the temperature probes were located at the stagnation points of the air impingement tubes and served as total pressure/temperature probes which were utilized to verify individual impingement tube air flow. See Figure 26 for additional details.

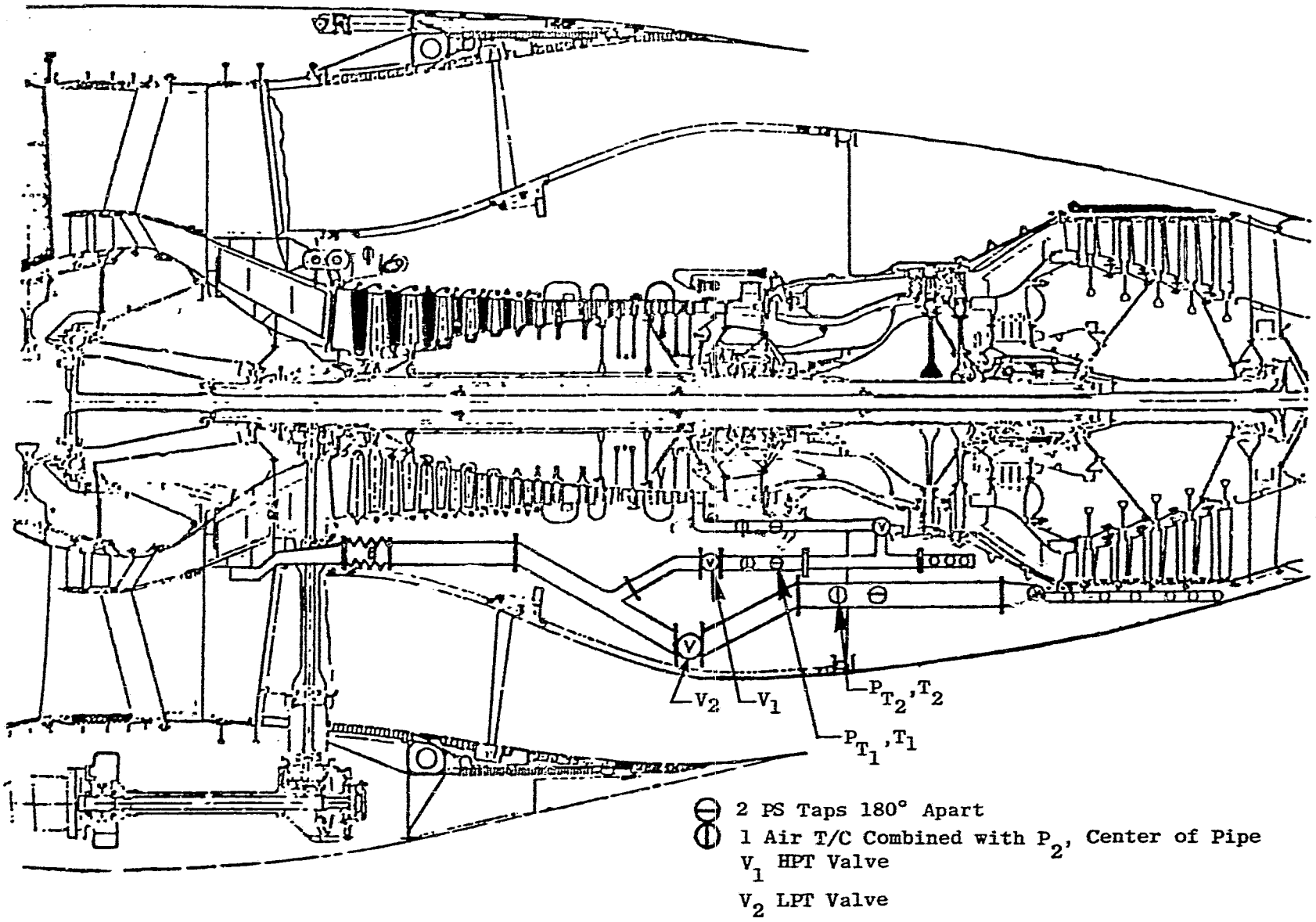

Figure 25. Cooling Supply Instrumentation.

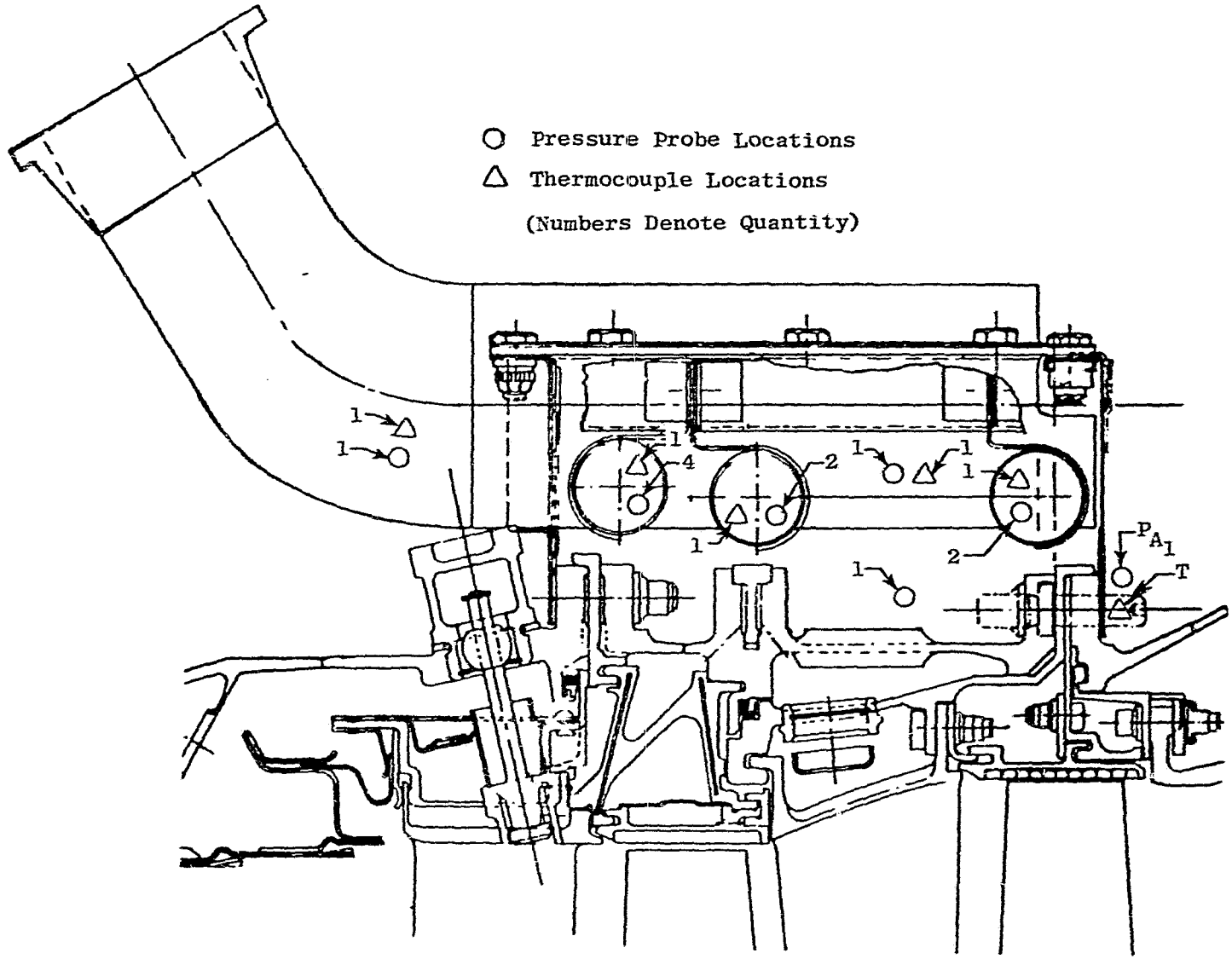

Figure 26. Impingement System Instrumentation.

HPT Case and Internal Structure Instrumentation

These components contained the bulk of the active clearance control instrumentation, which was comprised of 27 pressure probes, 35 surface thermocouples, 40 imbedded flange thermocouples, and 21 air thermocouples. Figure 27 depicts the axial location of the various pressure probes and thermocouples. The instrumentation was oriented in several different circumferential locations, and the imbedded flange thermocouples were located in such a manner that both circumferential and radial temperature gradients could be determined. The remaining active clearance control instrumentation was located on the impingement bulkheads, inside the impingement shield and several surface thermocouples located on the control valves. In addition to the above was the standard engine instrumentation required to monitor engine operating condition.

6.3.2 Engine Instrumentation

Engine station designations used for the testing were in accordance with ARP755A. These designations as related to the CF6-6 included:

- 0 Ambient
- 11 Fan Inlet
- 13 Fan Discharge
- 18 Fan Nozzle Throat
- 25 Core Inlet
- 30 Compressor Discharge
- 40 HP Turbine Inlet
- 49 LP Turbine Inlet
- 50 LP Turbine Exit
- 80 Core Nozzle Throat

Figure 28 illustrates these plane locations on a CF6-6 engine cross section and identifies the engine instrumentation.

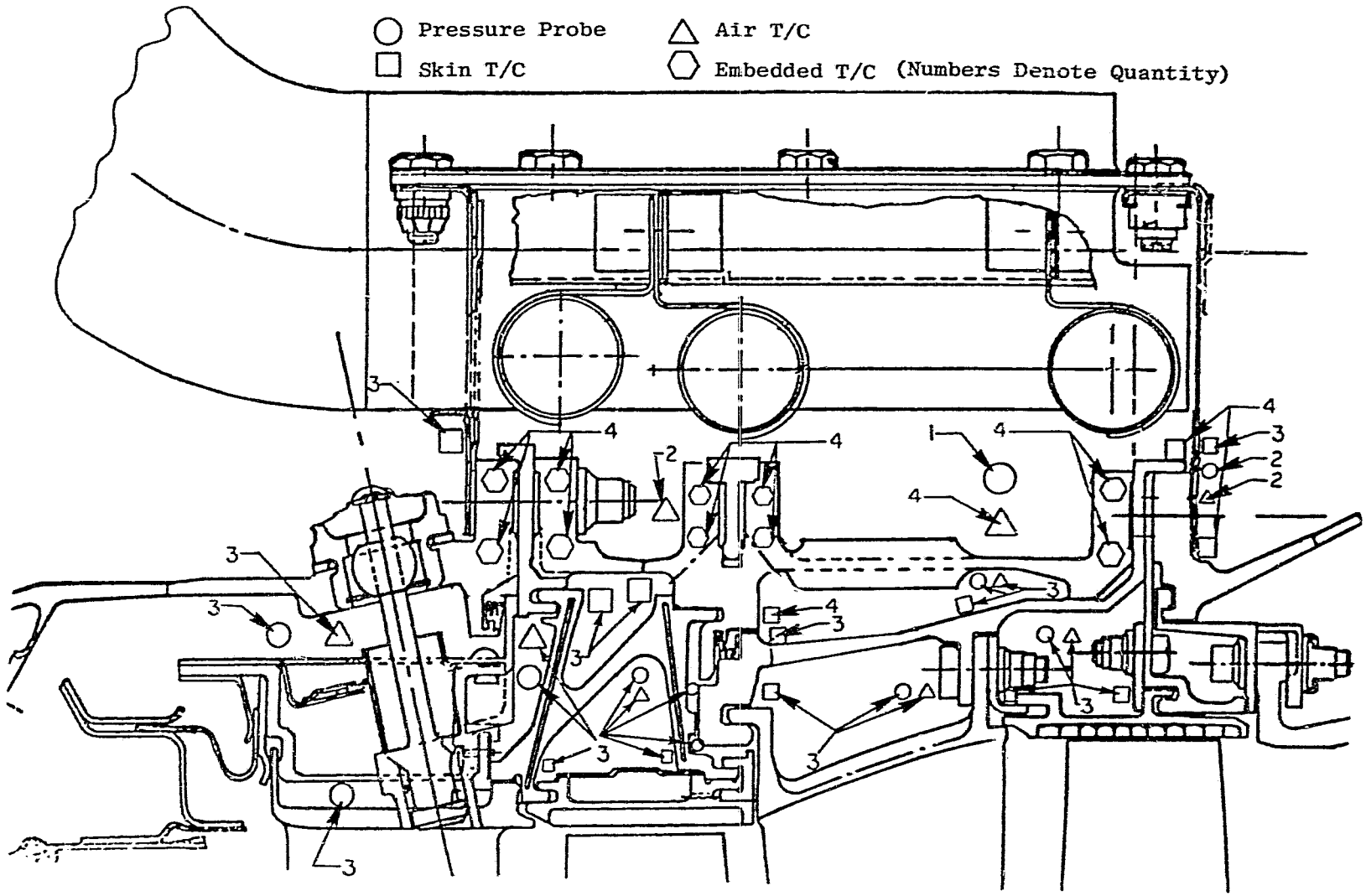

Figure 27. HPT Case and Internal Structure Instrumentation.

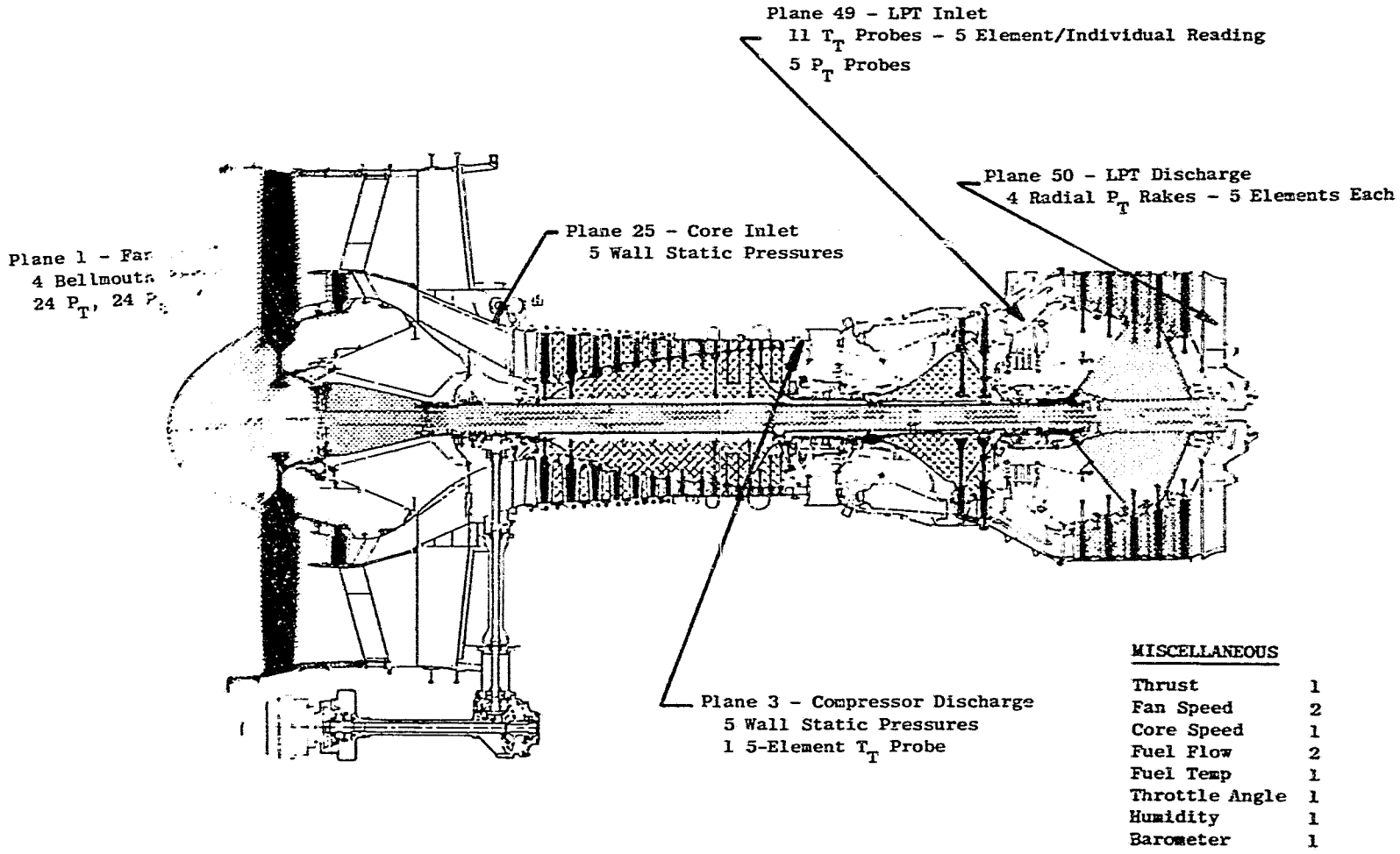

Figure 28. Engine Instrumentation.

The following test instrumentation was used to measure engine performance and to monitor engine operation. The instrumentation is broken down into two categories: general instrumentation, aerodynamic instrumentation.

General

- Barometric Pressure - The local barometric pressure measured using a recording Microbarograph.
- Humidity - The absolute humidity measured in grains of moisture per pound of dry air using a humidity indicator.
- Cell Static Pressure (P_0) - Test cell static pressure measured at four locations in the cell.
- Fan Speed (XNL) - Low pressure rotor speed measured using two fan-case-mounted, fan-speed sensors.
- Core Speed (XNH) - High pressure rotor speed measured using engine core-speed sensor driven off the end of the lube and scavenge pump.
- Main Fuel Flow (WFM) - volumetric flowmeter, facility mounted.
- Verification Fuel Flow (WFV) - Second fuel flowmeter mounted in series with WFM.
- Fuel Temperature - Temperature of fuel measured at the facility flowmeters using a single chromel/alumel probe in the fuel line.
- Fuel Sample Specific Gravity (SCSAMP) - Specific gravity of the fuel sample measured using a hydrometer.
- Fuel Sample Temperature (TSAMP) - Fuel sample temperature measured during the specific gravity measurement.
- Fuel Lower Heating Value (LHV) - Lower heating value of the fuel sample as determined by a bomb colorimeter.
- Thrust (FG) - Thrust-frame, axial force measuring using three strain-gage-type load cells for redundant measurement.

- Variable Stator Vane Position (VSV) - Readout of the Linear Variable Displacement Transducer (LVDT) attached to the high pressure compressor variable stator pump handle.

Aerodynamic Pressure and Temperatures

The following rakes, probes, and static pressure taps were installed to measure airflow temperature and pressure as required to define component performance. (See Figure 28.)

- Fan Inlet (Plane 1)
  Bellmouth rakes were installed to measure static pressure, total pressure, and total temperature at the fan inlet. Four rakes, each having six total pressure probes, six static pressure probes, and two total temperature probes.

- Compressor Inlet (Plane 25)
  Five flow-path-wall static pressure taps.

- Compressor Discharge (Plane 3)

  Five of the borescope port plugs in the compressor rear frame were modified to permit compressor discharge static pressure measurement. A single 5-element thermocouple probe was used to measure compressor discharge temperature.

- Low Pressure Turbine Inlet (Plane 49)

  Temperature in this plane was measured by eleven 5-element rakes with individual probe readout to permit monitoring of temperature profiles. Pressure was measured using five probes each having five elements all feeding a single fitting.

- Low Pressure Turbine Discharge (Plane 50)

  Low pressure turbine discharge pressure was measured using four rakes having five elements each.

6.4 ACTIVE CLEARANCE CONTROL PIPING FLOW CALIBRATION

6.4.1 Test Objectives

The objective of this test was to obtain data which define the airflow characteristics of the active clearance control High Pressure Turbine cooling system and associated tubing. Specifically the objective was to define the flow function versus pressure ratio for the entire HPT active clearance control system downstream of the HPT control valve.

6.4.2 Test Hardware

The test hardware included the complete HPT active clearance control configuration piping as follows: HPT/LPT fan air supply system; HPT, LPT, CDP air control valves, HPT air impingement tubes and manifold; and HPT air impingement shield. HPT active clearance control hardware is illustrated in Figure 29.

6.4.3 Instrumentation

The impingement system instrumentation, as described in Section 6.3.1, was utilized to record the necessary temperature and pressures used to calculate the ACC piping flow function. (See Figures 28 and 29 for additional details of the instrumentation utilized for the flow calibration).

6.4.4 Test Procedure

The test setup is shown in Figure 30 and consisted of a metering section installed upstream of the HPT control valve. The metering section supply tubing was plumbed to the facility air line.

The test procedure consisted of pressurizing the upstream section of the control valve with shop air and then opening the valve until the desired pressure was read at P_{T1}, (Figure 30). The flow through the metering section was calculated and all pressures and temperatures down stream of the HPT control valve were recorded. With these data the flow function could then be calculated. Throughout this testing, the LPT control valve remained closed.

6.4.5 Test Results

The results of the flow calibration are presented in terms of flow function vs. pressure ratio. These are defined as:

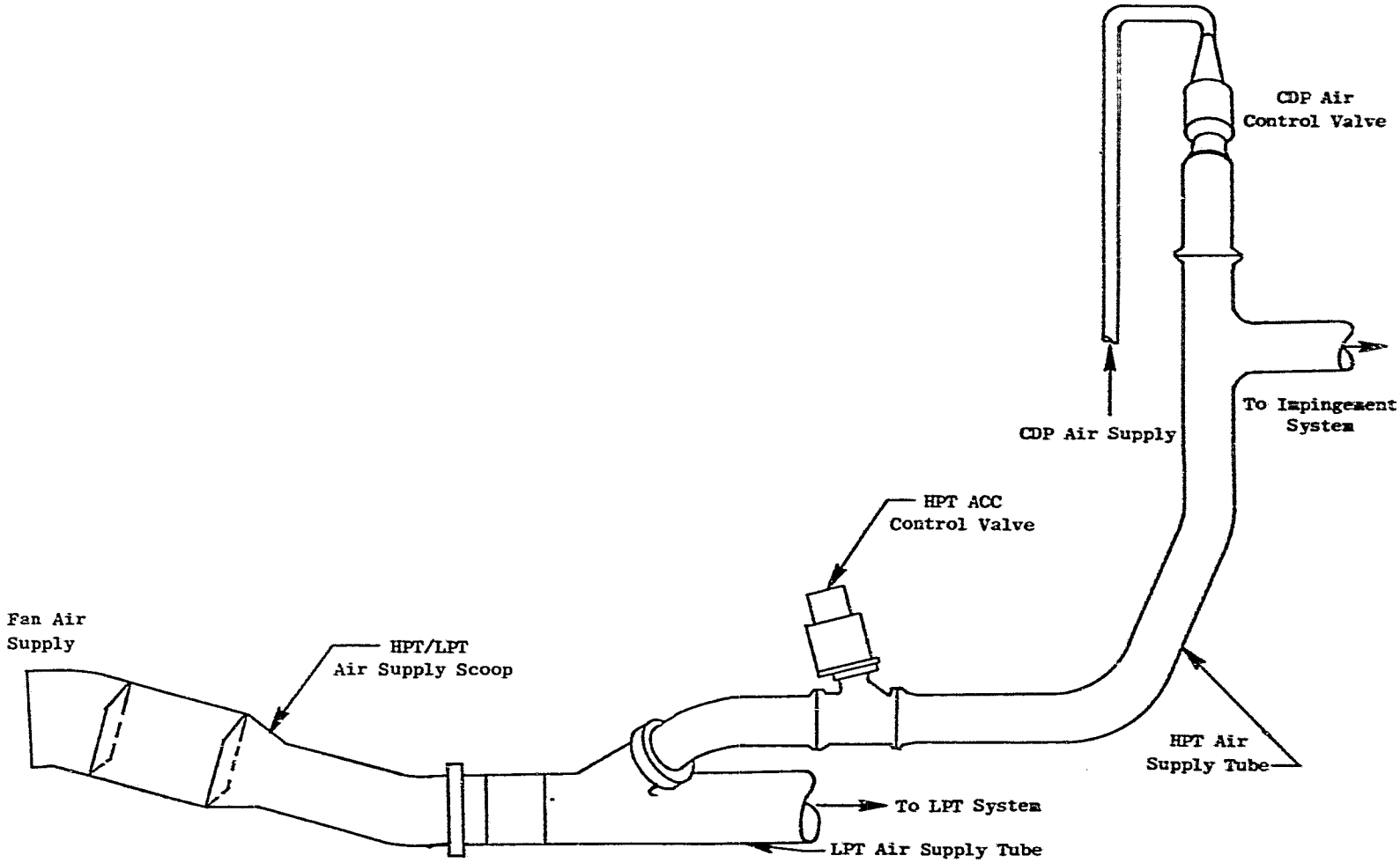

Figure 29. HPT Active Clearance Control Hardware.

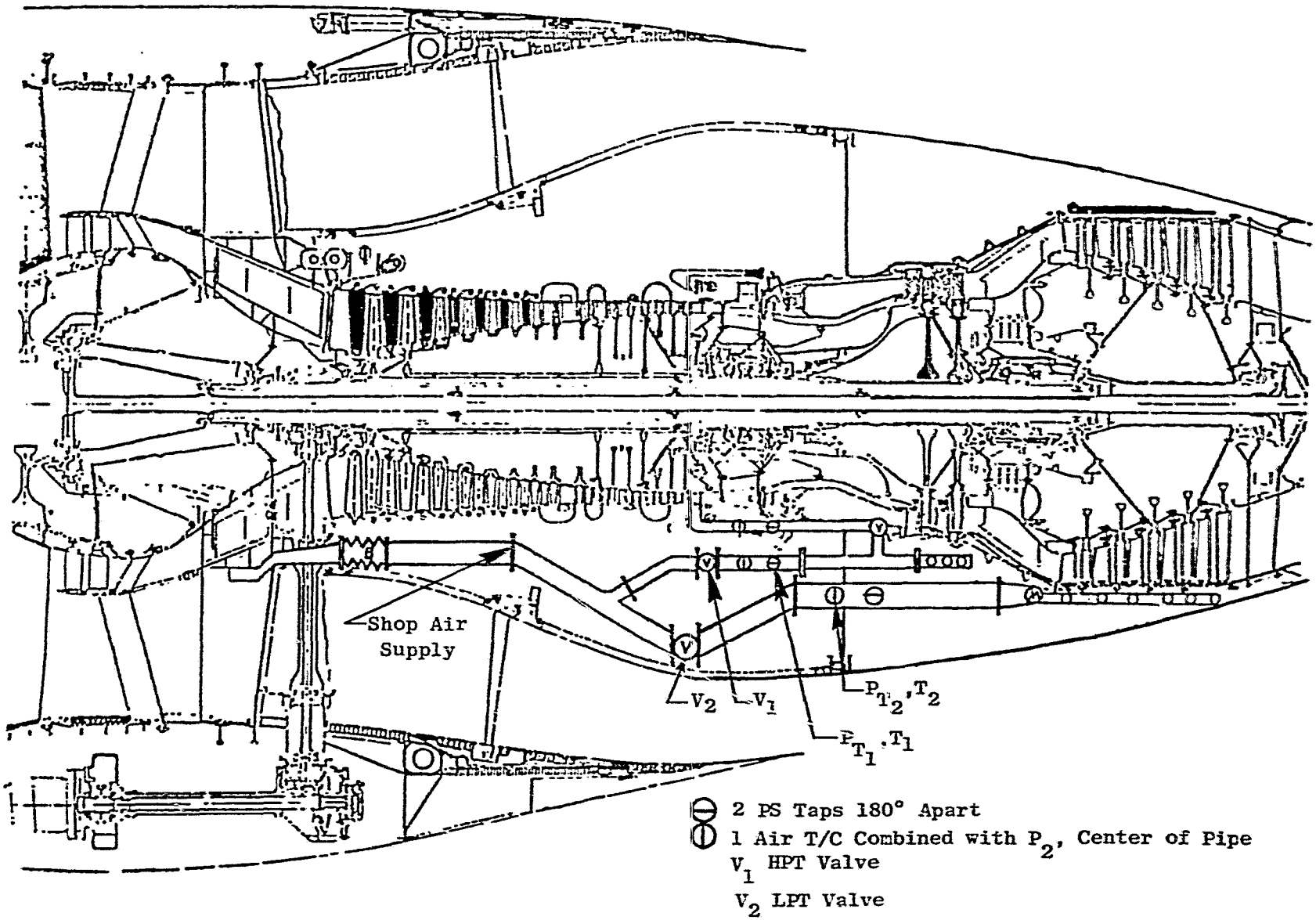

Figure 30. Flow Calibration Instrumentation - Cooling Supply.

Flow Function - $(W\sqrt{T_T})/P_T$

where, W = airflow to manifold, kg/sec (lb/sec)

T_T = total temperature, ^{o} K (^{o} R) in the manifold supply pipe

P_T = total pressure, N/cm^2 (psia) in the manifold supply pipe

Pressure Ratio - P_T/P_S

where, P_T = total pressure, N/cm^2 (psia)

P_S = static (barometric) pressure, N/cm^2 (psia)

The flow function vs. pressure ratio curve for the HPT Active Clearance Control Piping System is presented in Figure 31.

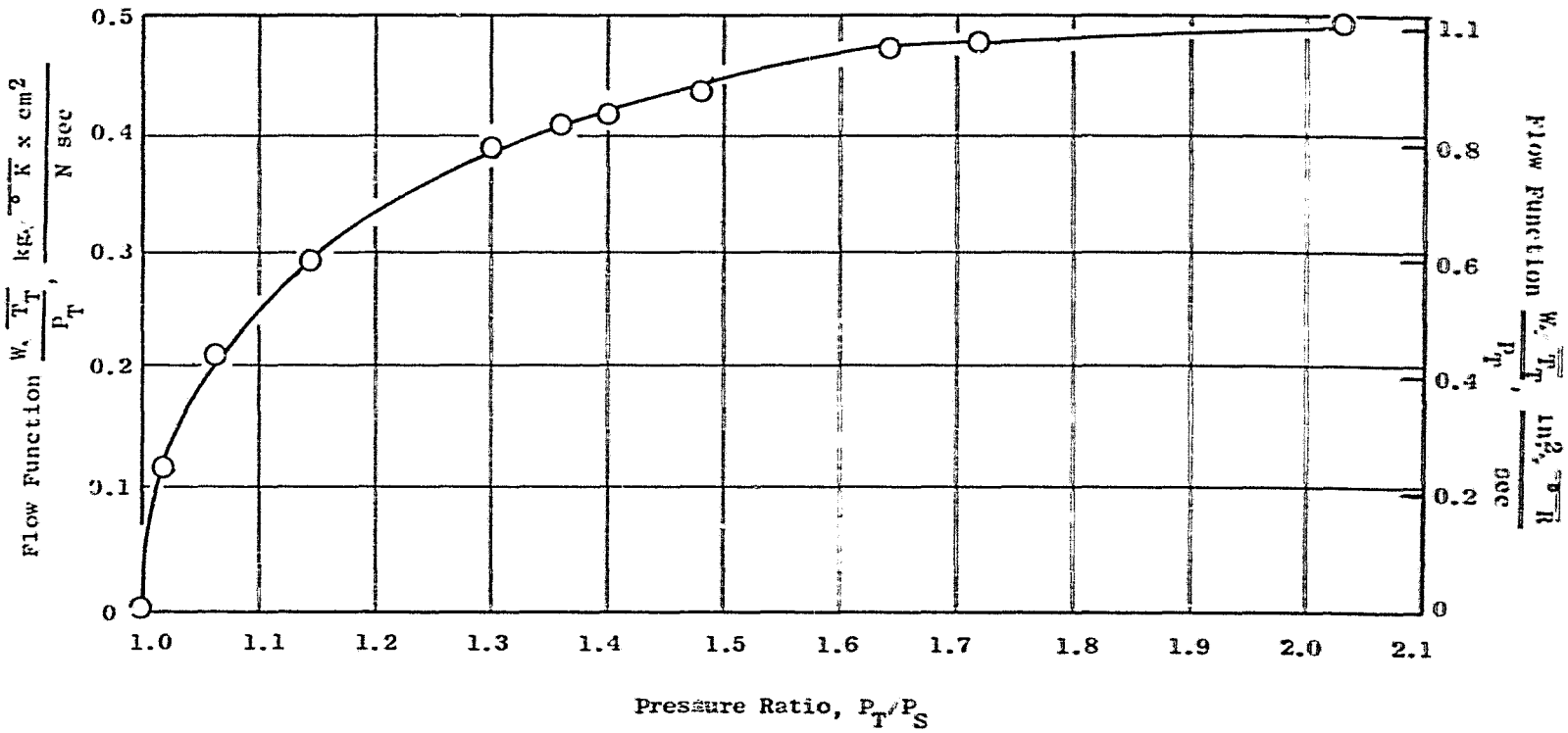

Figure 31. Flow Function Versus Pressure Ratio for the HPT Active Clearance Control Piping System.

6.5 TEMPERATURE DATA

6.5.1 Introduction

Steady state and transient temperature data were obtained by operating the engine through a series of transient and steady state cycles. During this phase, structural temperatures and high energy x-ray (HEX) radiographs were recorded. The temperature data were then used to adjust the analytical models used to predict clearances, and the HEX data were then compared to the clearance predictions based on matched temperature data. This section of the report is devoted to a discussion of the measured and matched temperatures. Section 6.6 discusses the High Energy X-Ray portion of the test, and Section 6.7 elaborates on the comparison between the HEX data and the matched analytical data.

6.5.2 Test Objectives

The objective of this testing was to obtain detailed temperature response data of the HPT ACC stator structure. These data were then compared to the pretest estimates, adjustments made to the analytical model and new clearance predictions completed based on the matched temperature data.

6.5.3 Transient Temperature Data

Transient and steady state temperature and HEX data were recorded for the following:

1. Engine throttle burst and chops from ground idle (G/I) to takeoff (T/O), and steady state
2. 10 typical engine revenue service cycles ("C" cycles)
3. A series of hot rotor throttle rebursts with the following dwell times: 60, 240, 180 and 130 seconds.
4. Steady state cruise temperatures.

Figures 32 through 37 illustrate the various engine cycles run. Included on these figures are the prescribed time intervals for taking HEX data.

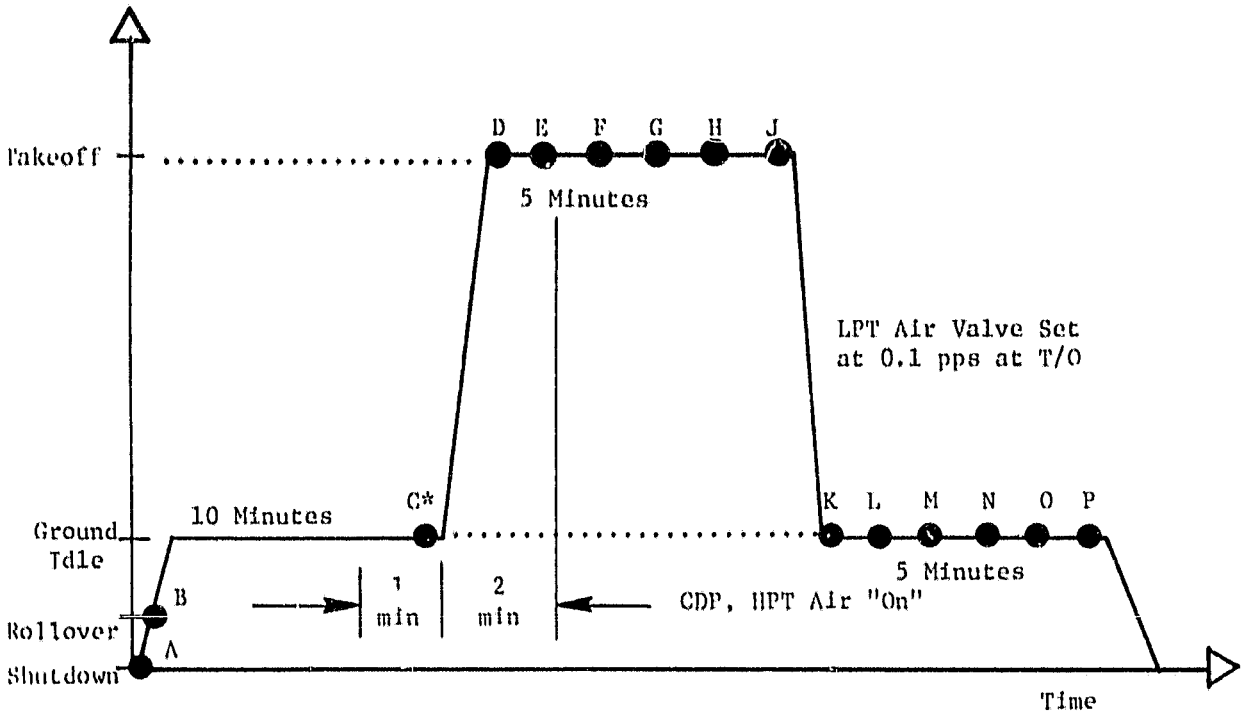

Cycle Point		Engine Time/Condition
A	-	Engine Shutdown
B	-	Engine Starting Rollover
C	-	Steady-State Ground Idle for 10 Minutes
D	-	Throttle Burst to Takeoff + 10 Seconds
E	-	Throttle Burst to Takeoff + 25 Seconds
F	-	Throttle Burst to Takeoff + 50 Seconds
G	-	Throttle Burst to Takeoff + 100 Seconds
H	-	Throttle Burst to Takeoff + 180 Seconds
J	-	Throttle Burst to Takeoff + 300 Seconds
K	-	Throttle Chop to Ground Idle + 10 Seconds
L	-	Throttle Chop to Ground Idle + 25 Seconds
M	-	Throttle Chop to Ground Idle + 50 Seconds
N	-	Throttle Chop to Ground Idle + 100 Seconds
O	-	Throttle Chop to Ground Idle + 180 Seconds
P	-	Throttle Chop to Ground Idle + 300 Seconds

*After Film "C" has Been Exposed, Change Out 3 Cassettes Prior to Burst to T/O

Figure 32. Throttle Burst and Chop Test Cycle.

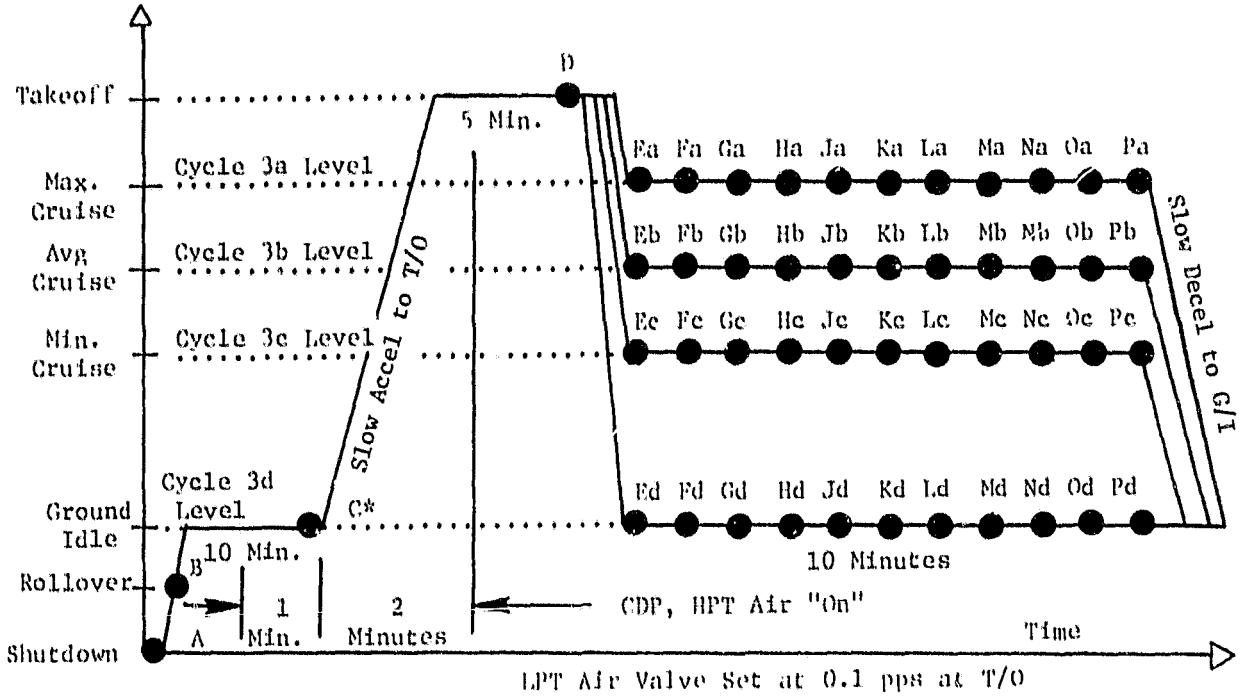

Cycle Point		Engine Time/Condition
A	-	Engine Shutdown
B	-	Engine Starting Rollover
C	-	Steady-State Ground Idle for 10 Minutes
D	-	Steady-State Takeoff Power for 5 Minutes
Ex	-	Throttle Chop, Takeoff to 3x Power Level + 5 Seconds
Fx	-	Throttle Chop, Takeoff to 3x Power Level + 20 Seconds
Gx	-	Throttle Chop, Takeoff to 3x Power Level + 40 Seconds
Hx	-	Throttle Chop, Takeoff to 3x Power Level + 60 Seconds
Jx	-	Throttle Chop, Takeoff to 3x Power Level + 90 Seconds
Kx	-	Throttle Chop, Takeoff to 3x Power Level + 130 Seconds
Lx	-	Throttle Chop, Takeoff to 3x Power Level + 180 Seconds
Mx	-	Throttle Chop, Takeoff to 3x Power Level + 240 Seconds
Nx	-	Throttle Chop, Takeoff to 3x Power Level + 300 Seconds
Ox	-	Throttle Chop, Takeoff to 3x Power Level + 450 Seconds
Px	-	Throttle Chop, Takeoff to 3x Power Level + 600 Seconds

*After Film "C" has Been Exposed, Change Out 3 Cassettes Prior to Acceleration to T/O.

Figure 33. Takeoff to Intermediate Power Level Test Cycle.

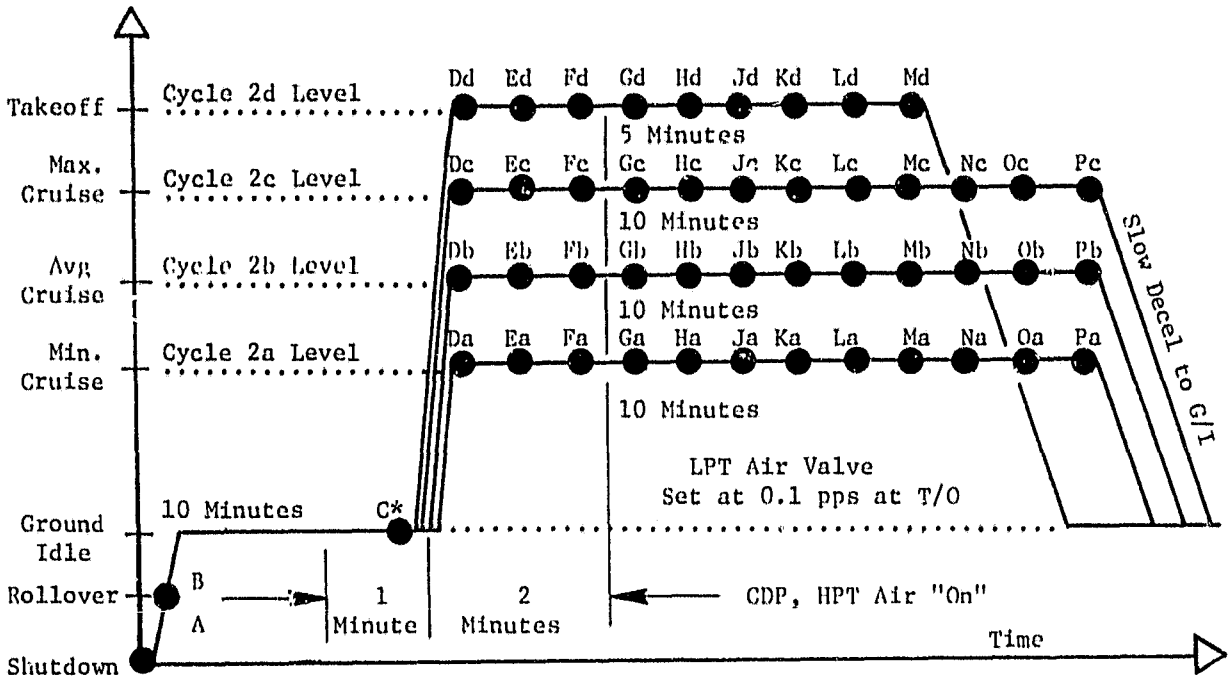

Cycle Point		Engine Time/Condition
A	-	Engine Shutdown
B	-	Engine Starting Rollover
C	-	Steady-State Ground Idle for 10 Minutes
Dx	-	Throttle Burst to 2x Power Level + 10 Seconds
Ex	-	Throttle Burst to 2x Power Level + 25 Seconds
Fx	-	Throttle Burst to 2x Power Level + 40 Seconds
Gx	-	Throttle Burst to 2x Power Level + 60 Seconds
Hx	-	Throttle Burst to 2x Power Level + 90 Seconds
Jx	-	Throttle Burst to 2x Power Level + 130 Seconds
Kx	-	Throttle Burst to 2x Power Level + 180 Seconds
Lx	-	Throttle Burst to 2x Power Level + 240 Seconds
Mx	-	Throttle Burst to 2x Power Level + 300 Seconds
Nx	-	Throttle Burst to 2x Power Level + 400 Seconds
Ox	-	Throttle Burst to 2x Power Level + 500 Seconds
Px	-	Throttle Burst to 2x Power Level + 600 Seconds

*After Film "C" has Been Exposed, Change Out 3 Cassettes Prior to Acceleration to T/O.

Figure 34. Ground Idle to Intermediate Power Thermal Test Cycle.

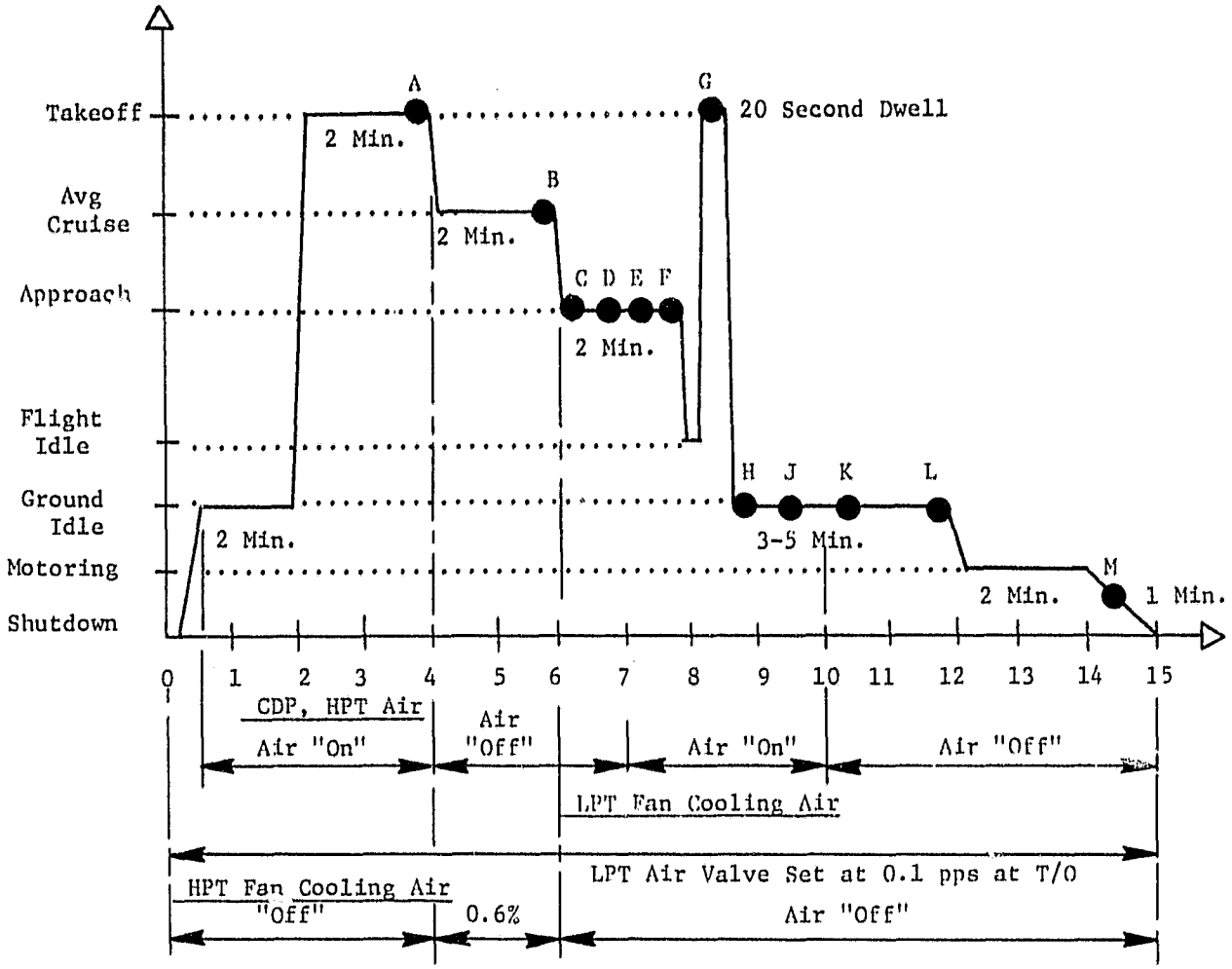

Cycle Point		Engine Time/Condition
A	-	Engine Two Minutes at Takeoff Power
B	-	Engine Two Minutes at Average Cruise Power
C	-	Throttle Chop, Avg Cruise to Approach + 5 Seconds
D	-	Throttle Chop, Avg Cruise to Approach + 25 Seconds
E	-	Throttle Chop, Avg Cruise to Approach + 60 Seconds
F	-	Throttle Chop, Avg Cruise to Approach + 120 Seconds
G	-	On Point at Takeoff During "Bodie" Burst
H	-	Return to Ground Idle from "Bodie" Burst + 5 Seconds
J	-	Return to Ground Idle from "Bodie" Burst + 25 Seconds
K	-	Return to Ground Idle from "Bodie" Burst + 60 Seconds
L	-	Return to Ground Idle from "Bodie" Burst + 210 Seconds
M	-	Engine at Warm Rollover

Figure 35. CF6-6 Simulated Service "C" Cycle.

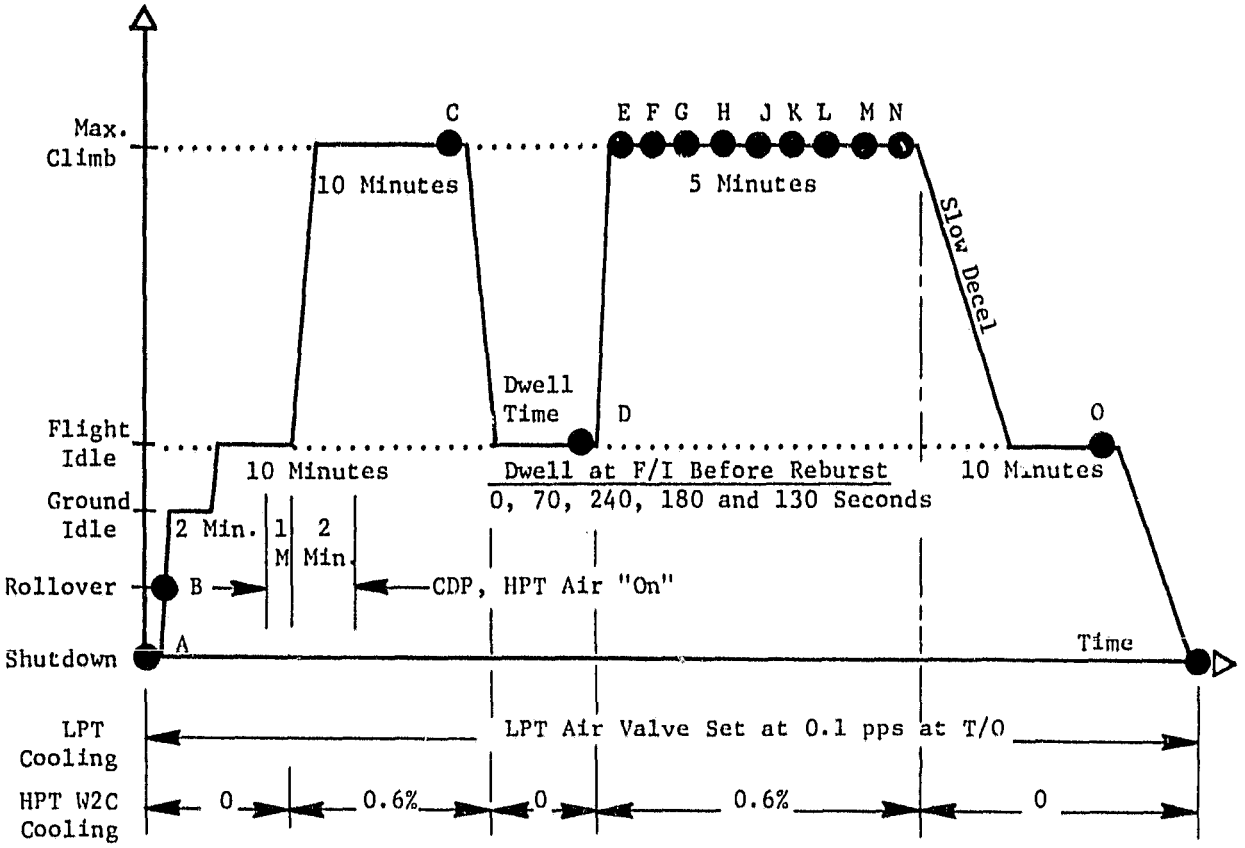

Cycle Point		Engine State/Condition
A	-	Engine Shutdown
B	-	Engine Starting Rollover
C	-	Steady-State Maximum Climb for 10 Minutes
D*	-	Flight Idle at End of Dwell Time
E	-	Hot Rotor Reburst to Maximum Climb + 10 Seconds
F	-	Hot Rotor Reburst to Maximum Climb + 25 Seconds
G	-	Hot Rotor Reburst to Maximum Climb + 40 Seconds
H	-	Hot Rotor Reburst to Maximum Climb + 60 Seconds
J	-	Hot Rotor Reburst to Maximum Climb + 90 Seconds
K	-	Hot Rotor Reburst to Maximum Climb + 135 Seconds
L	-	Hot Rotor Reburst to Maximum Climb + 180 Seconds
M	-	Hot Rotor Reburst to Maximum Climb + 240 Seconds
N	-	Hot Rotor Reburst to Maximum Climb + 300 Seconds
O	-	Steady-State Flight Idle for 10 Minutes
P	-	Engine Shutdown

*No Cycle Point "D" During Zero Dwell Time Cycle

Figure 36. Hot Rotor Reburst Test Cycle.

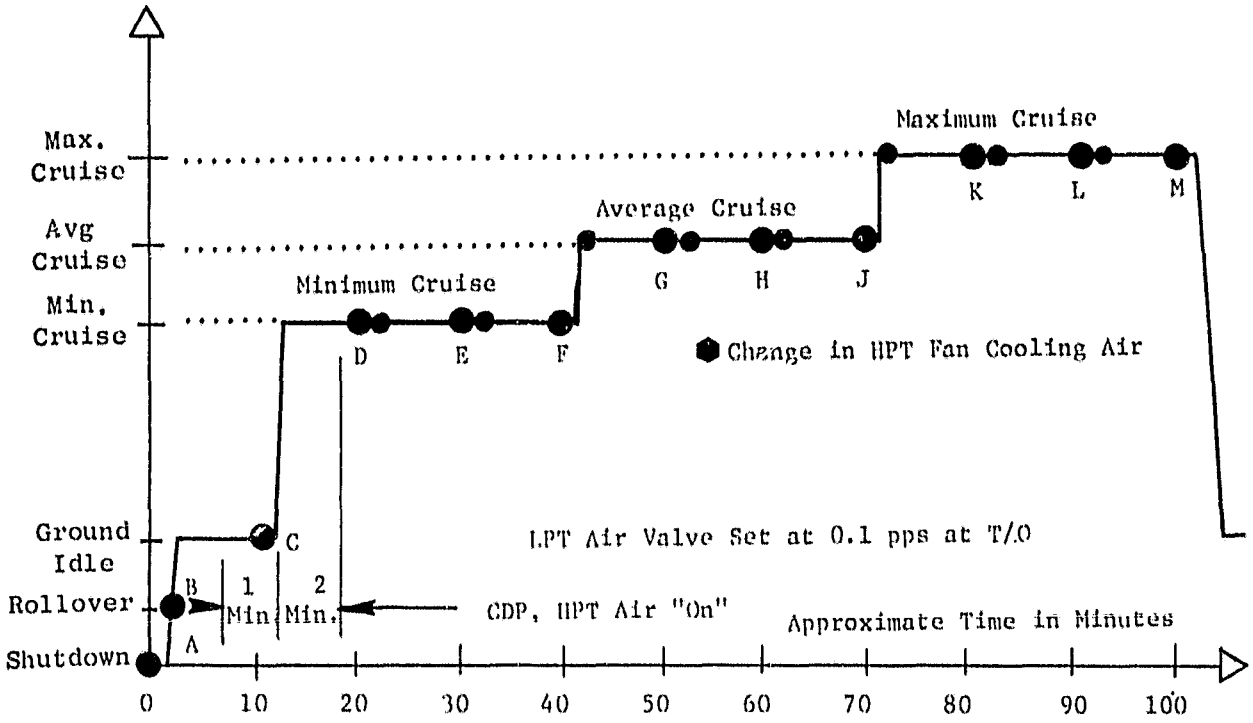

Cycle Point		Engine Time/Condition	HPT Acc Fan Air	TPS Item
A	-	Cold Engine Shutdown	------	22
B	-	Engine Rollover at Start	------	22
C	-	Steady-State Ground Idle	------	22
D	-	Steady-State Minimum Cruise	0.0% W2C	23
E	-	Steady-State Minimum Cruise	0.3% W2C	24
F	-	Steady-State Minimum Cruise	0.6% W2C	25
G	-	Steady-State Average Cruise	0.0% W2C	26
H	-	Steady-State Average Cruise	0.3% W2C	27
J	-	Steady-State Average Cruise	0.6% W2C	28
K	-	Steady-State Maximum Cruise	0.0% W2C	29
L	-	Steady-State Maximum Cruise	0.3% W2C	30
M	-	Steady-State Maximum Cruise	0.6% W2C	31

Figure 37. Steady-State HPT Active Clearance Control Cruise Test Cycle.

6.5.3.1 Engine Throttle Bursts and Chop Temperature Data

Figures 38 through 47 illustrate the comparison between the recorded temperature and predicted temperature data. The "comparisons" shown on the figures are for a typical accel to takeoff power. The temperature match shows reasonable agreement with measured temperatures in all flanges except for two local areas. Figures 38 through 47 illustrate the temperature match obtained.

6.5.3.2 Cyclic Endurance Testing

The purpose of this test was to demonstrate the capability of the ACC hardware to sustain a series of engine simulated revenue service cycles, and to demonstrate operation of the HPT CDP and LPT air control valves which were actuated by an automatic vlave controller developed as part of the program. Ten "C" cycles were completed, during which both HEX and temperatures were recorded. After completion of the testing, the HPT ACC hardware was inspected and was found to be in excellent condition.

6.5.3.3 HPT Rotor Throttle Reburst Testing

This portion of the testing demonstrated the capability of the HPT ACC stator hardware to undergo a series of hot rotor throttle rebursts without experiencing excessive deterioration. The engine cycle is illustrated in Figure 36. Five different throttle rebursts were completed each with a different dwell time. Tip notch photos were taken prior to and after the completion of the reburst testing sequence. Tip notch photos were not taken between each reburst because by this point in the testing program enough operating experience was gained to know that excessive deterioration would not occur. The HPT showed no evidence of experiencing a reburst rub during the course of this testing.

6.5.3.4 Steady State Cruise Testing

This phase of the testing exercised the HPT ACC system through a series of cooled and uncooled cruise cycles (Figure 37). This testing was not intended to gain performance estimates, but rather to gather steady state temperatures and HEX data to confirm the analytical estimates of clearance change during the cooling cycles. Figures 48 through 57 illustrate the matched temperature data for cooled and uncooled maximum cruise engine operating conditions.

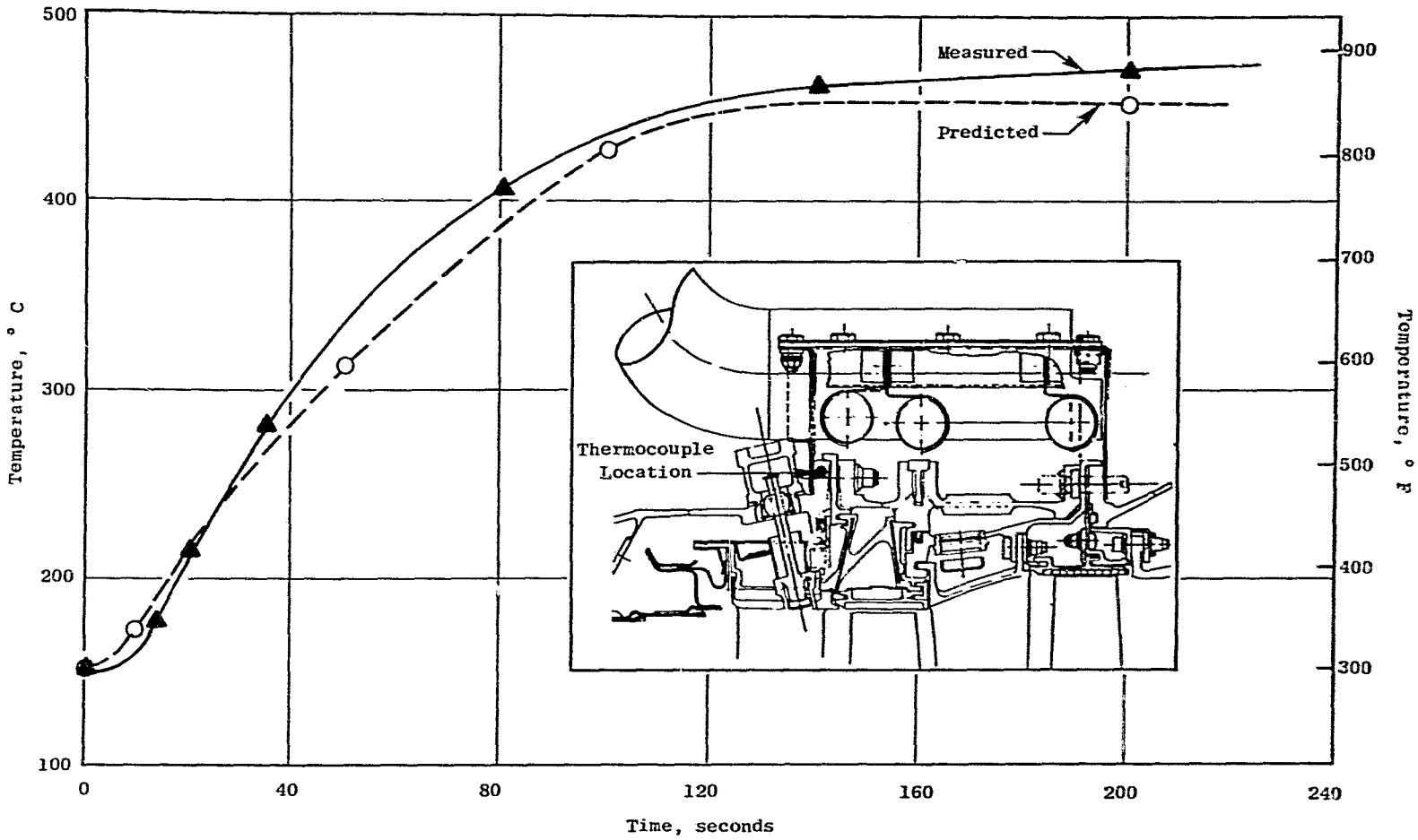

Figure 38. Temperature Match - Compressor Rear Frame Shallow Thermocouple.

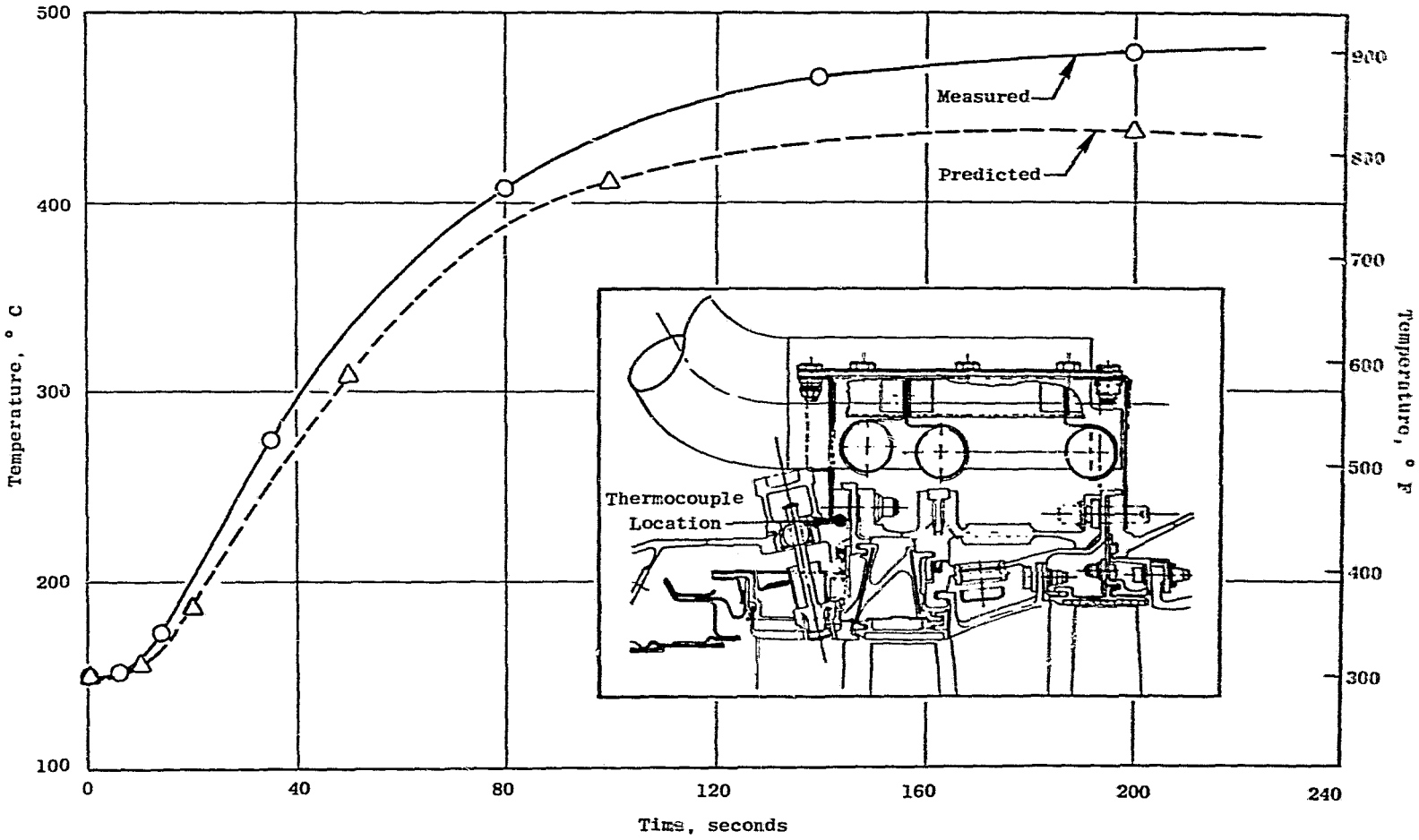

Figure 39. Temperature Match - Compressor Rear Frame Deep Thermocouple.

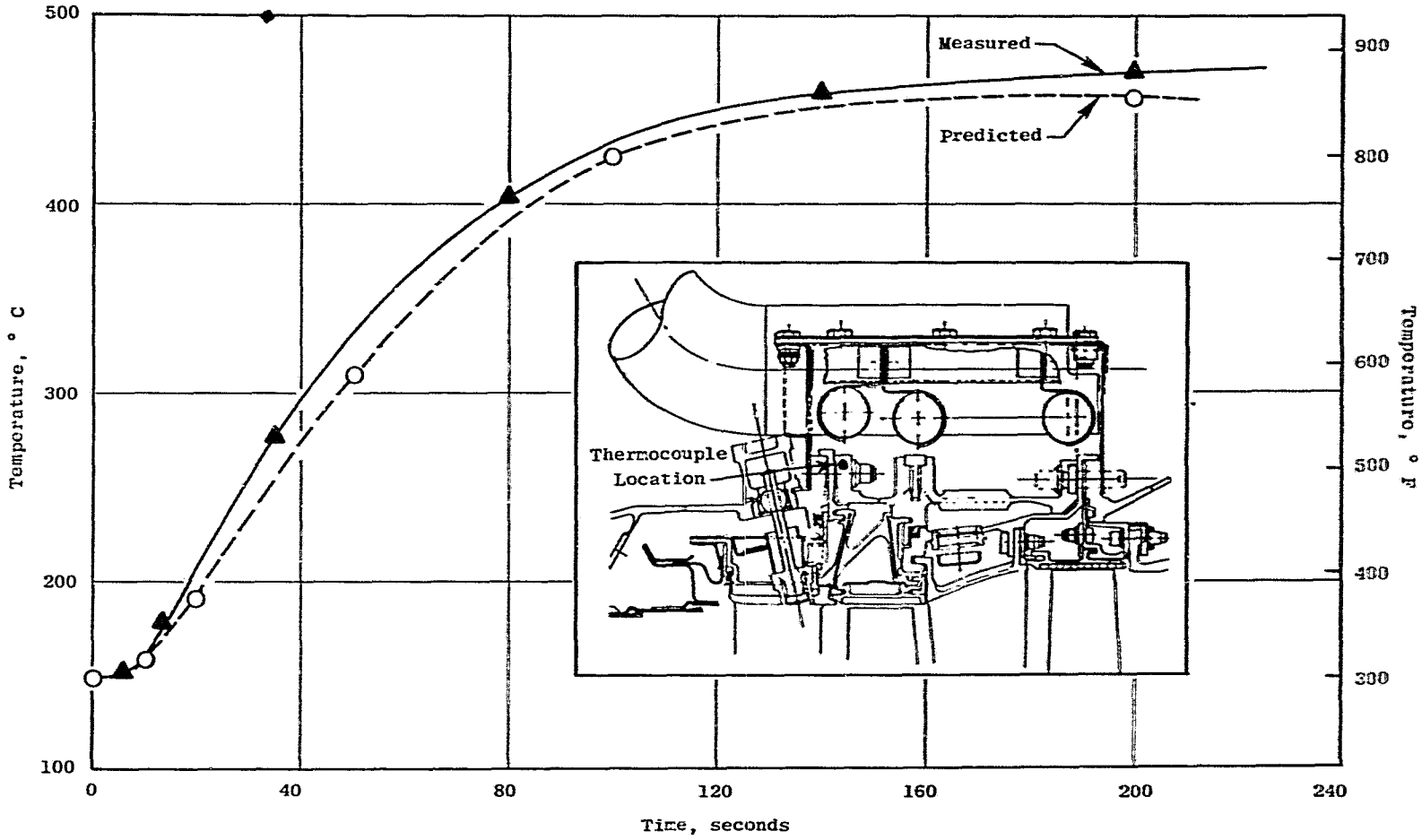

Figure 40. Temperature Match - HPT Forward Flange Shallow Thermocouple.

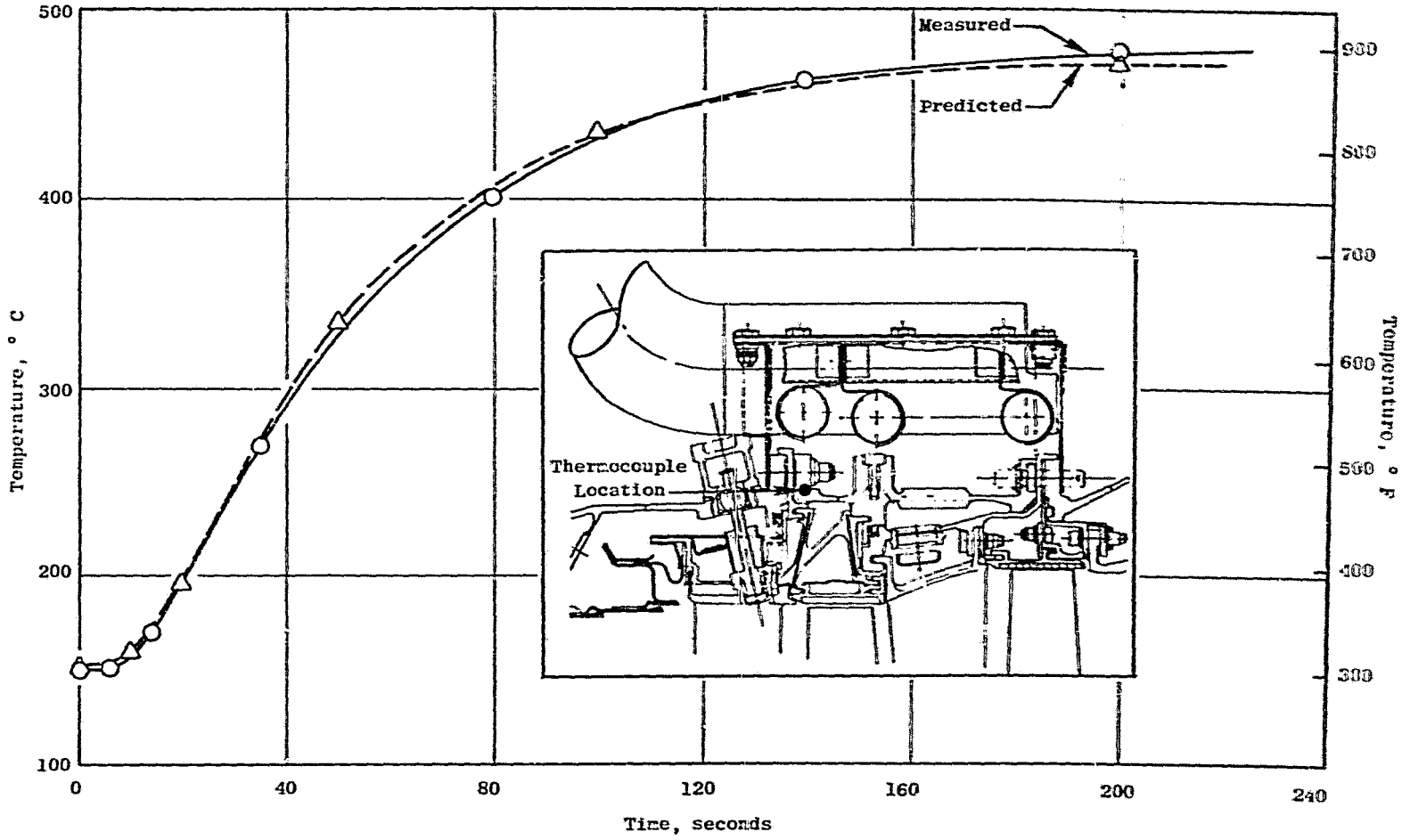

Figure 41. Temperature Match - HPT Forward Flange Deep Thermocouple.

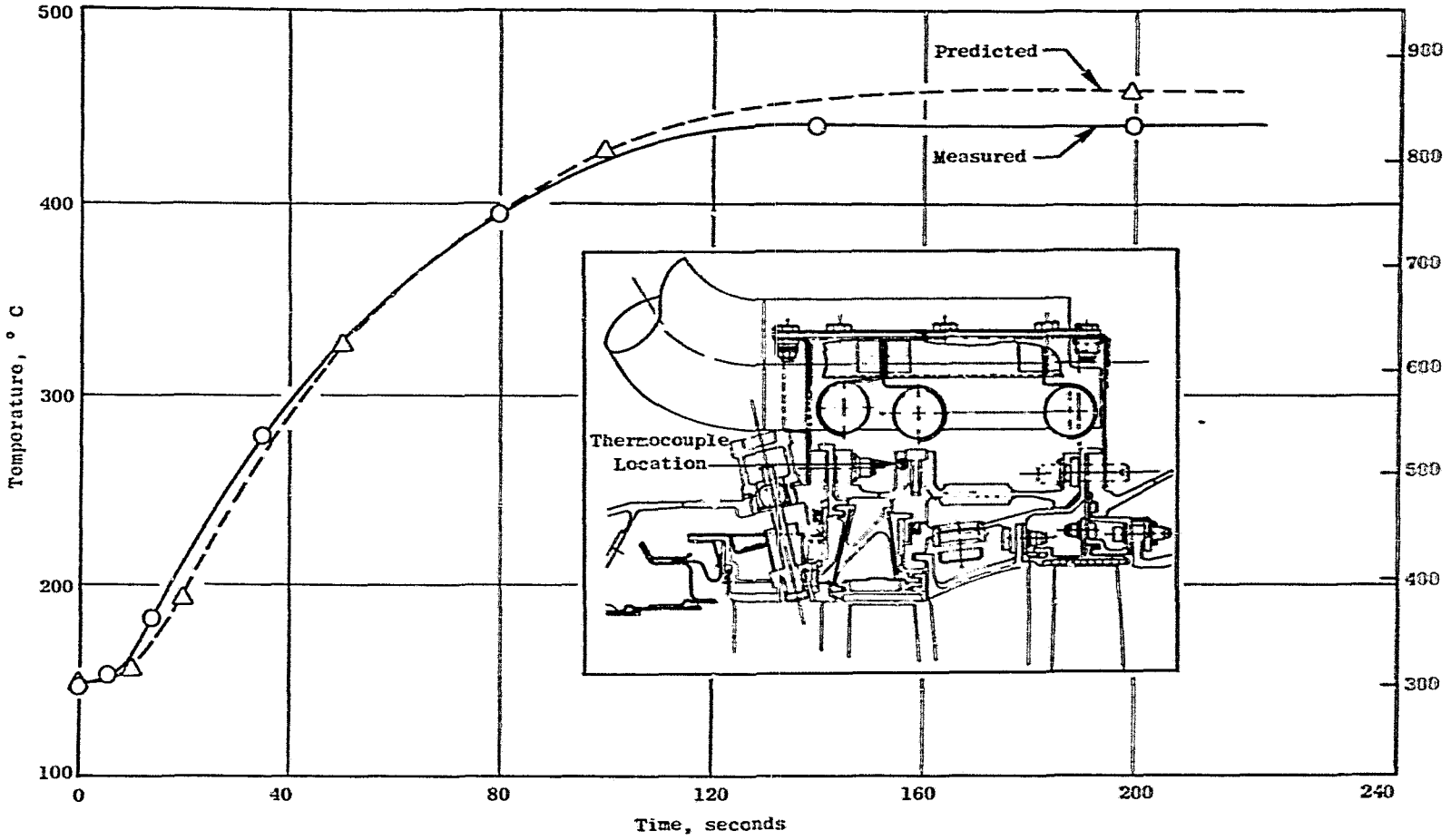

Figure 42. Temperature Match - HPT Mid Flange Shallow Thermocouple.

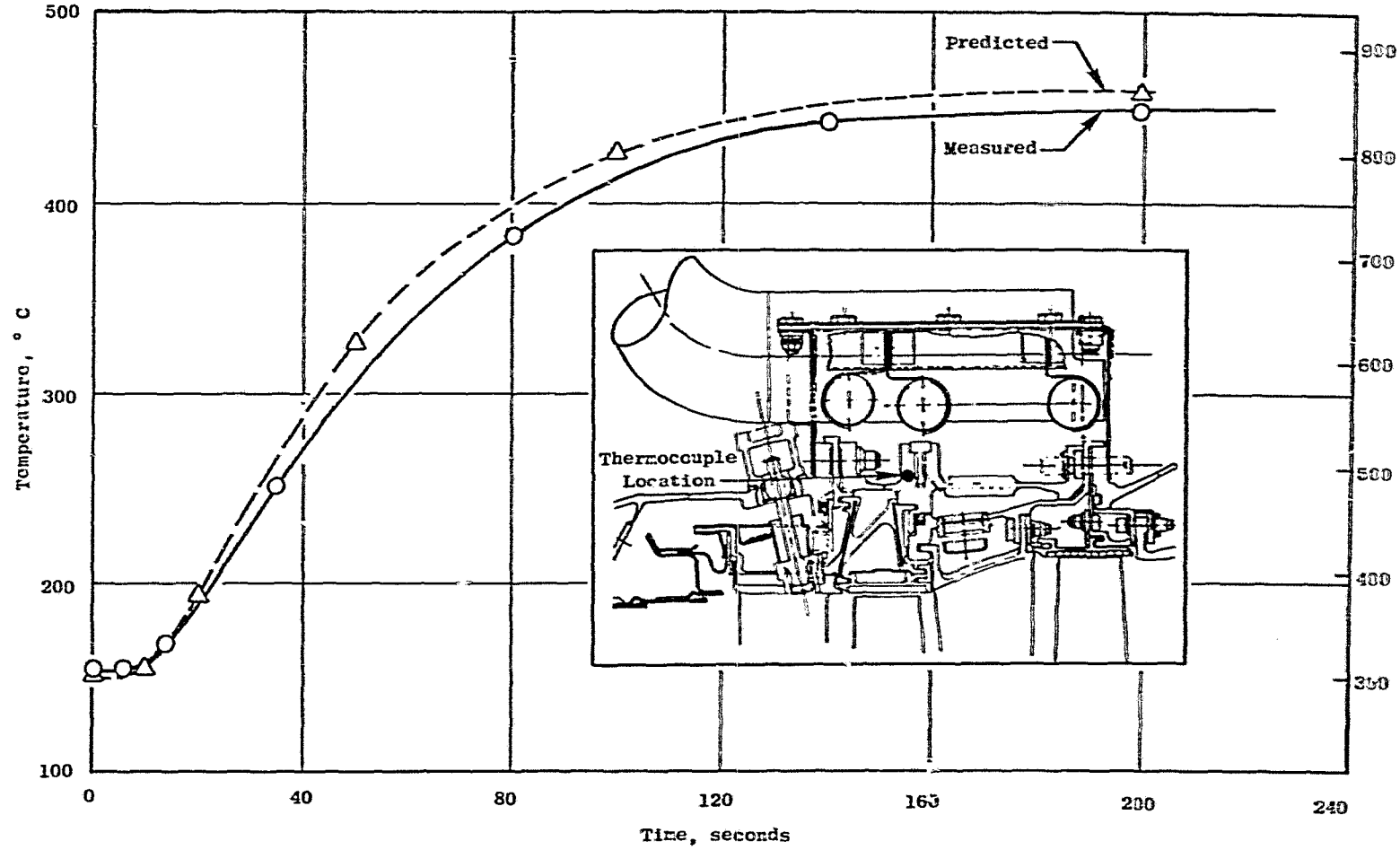

Figure 43. Temperature Match - HPT Mid Flange Deep Thermocouple.

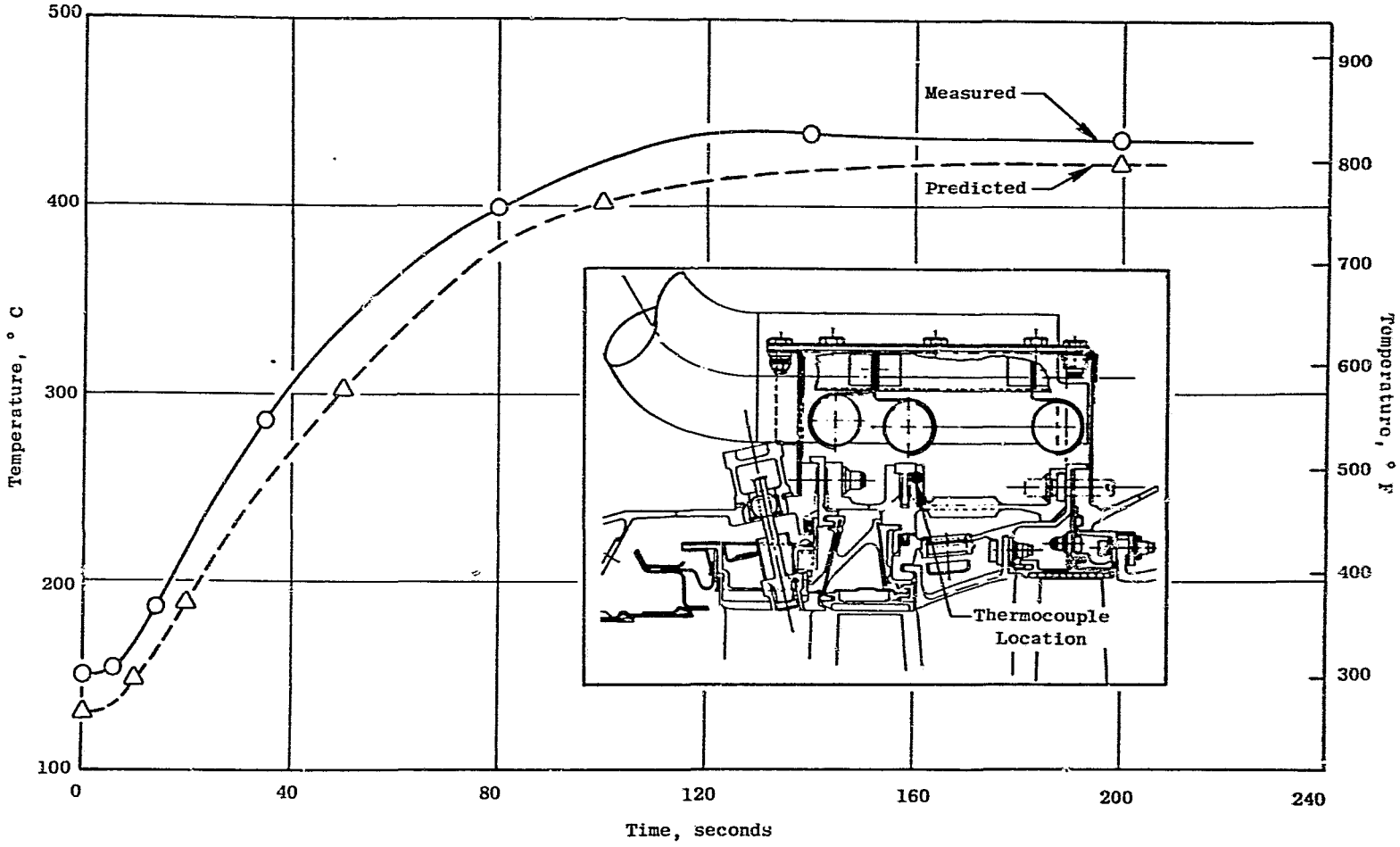

Figure 44. Temperature Match - HPT Mid Flange Shallow Thermocouple.

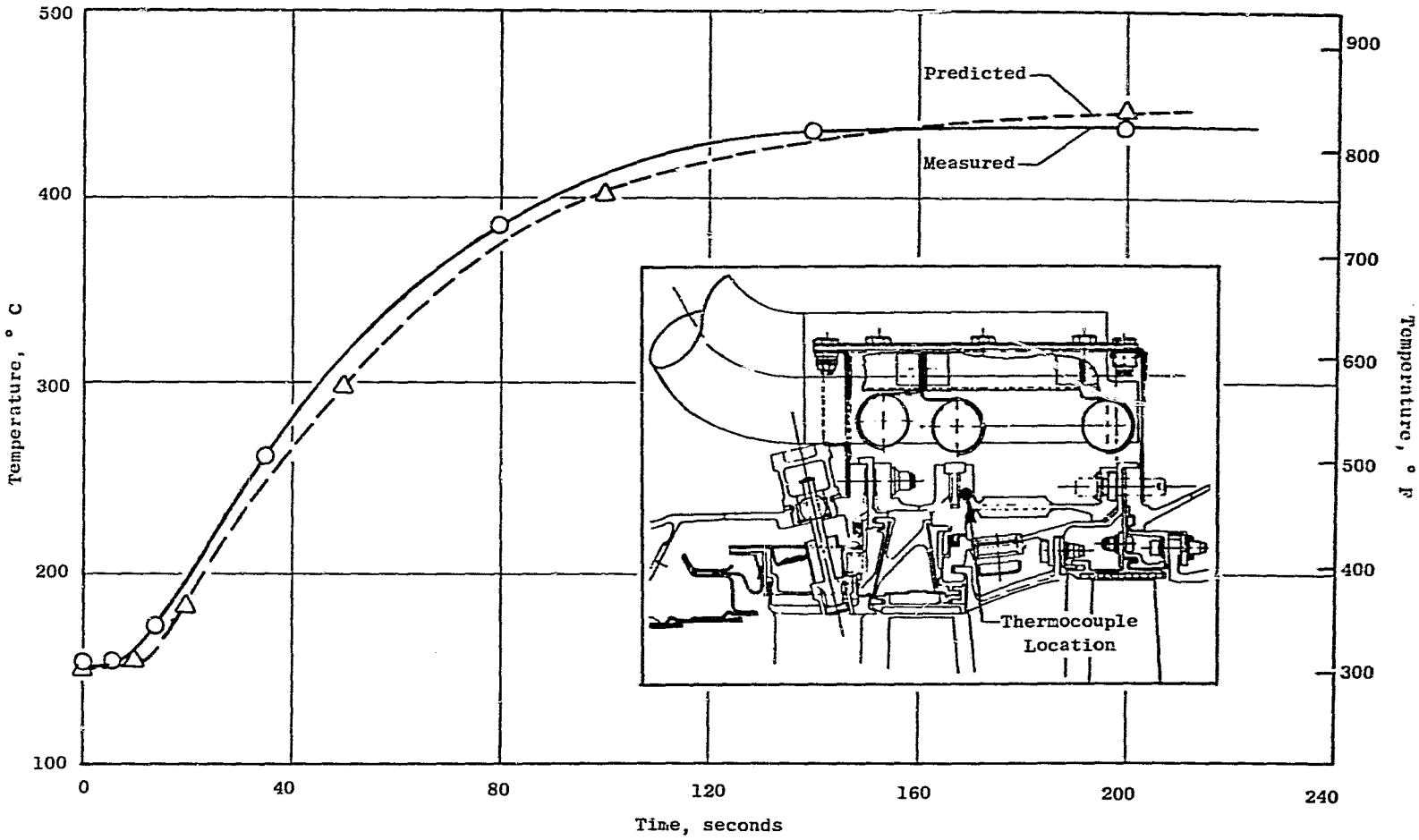

Figure 45. Temperature Match - HPT Mid Flange Deep Thermocouple.

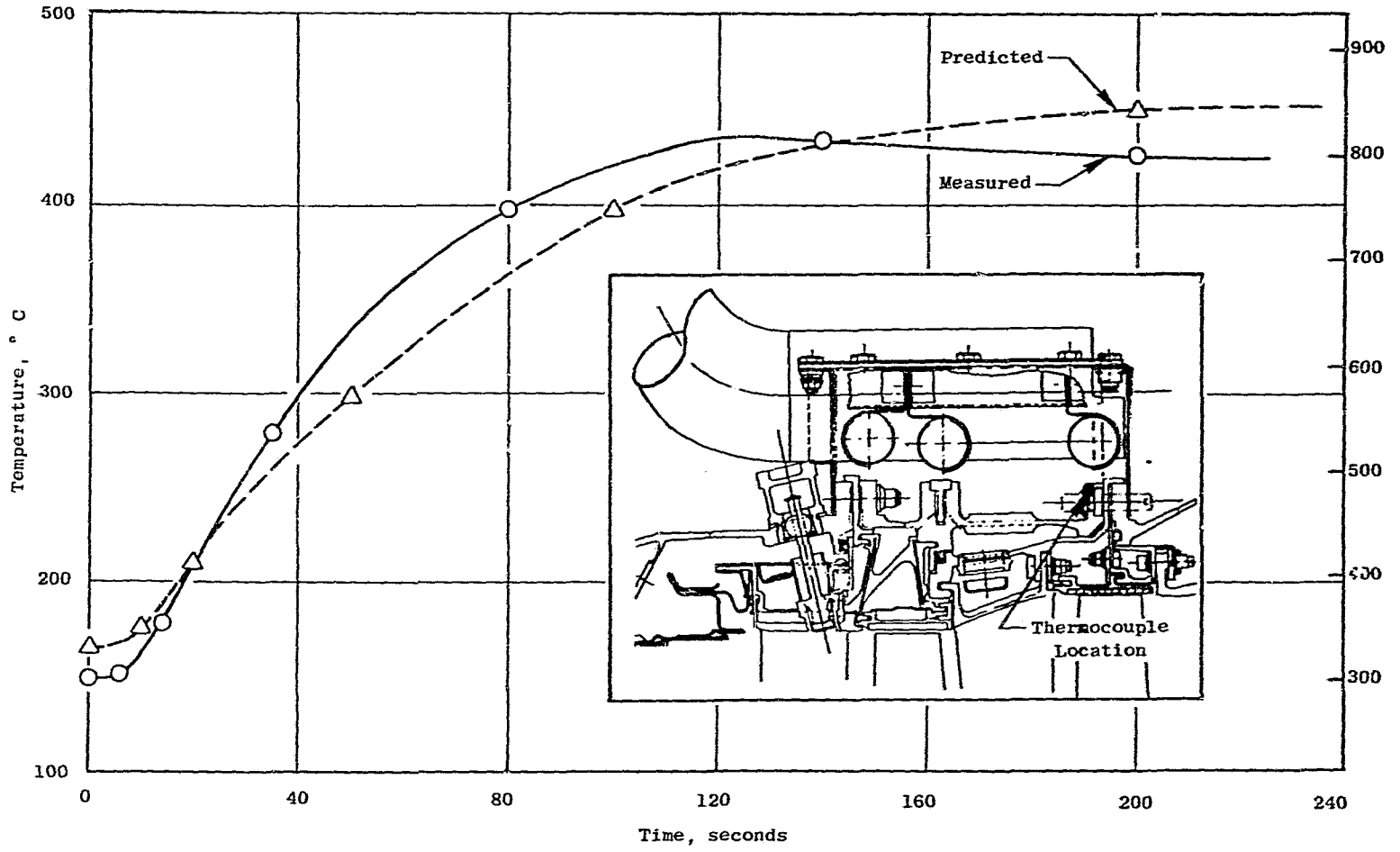

Figure 46. Temperature Match - HPT Rear Flange Shallow Thermocouple.

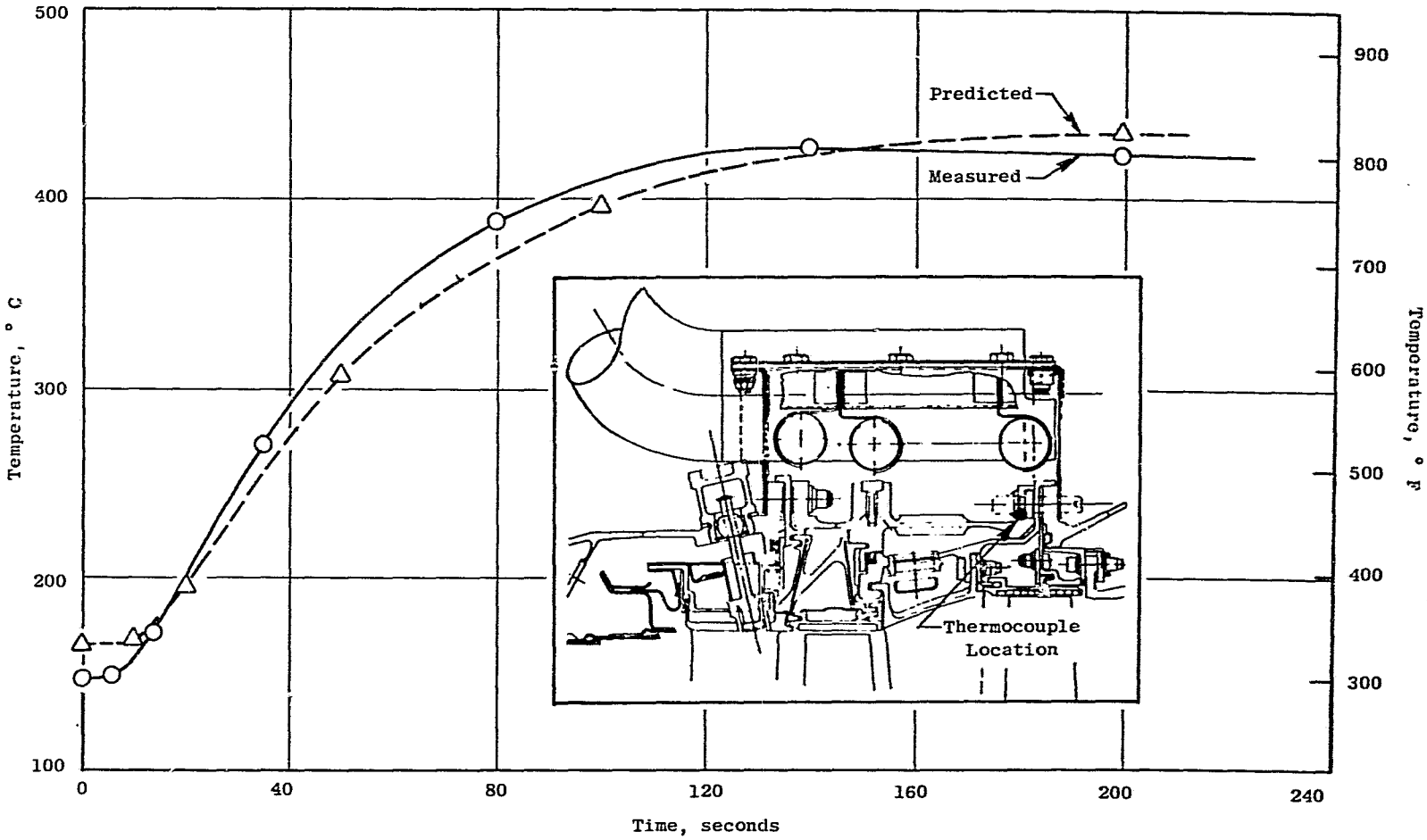

Figure 47. Temperature Match - HPT Rear Flange Deep Thermocouple.

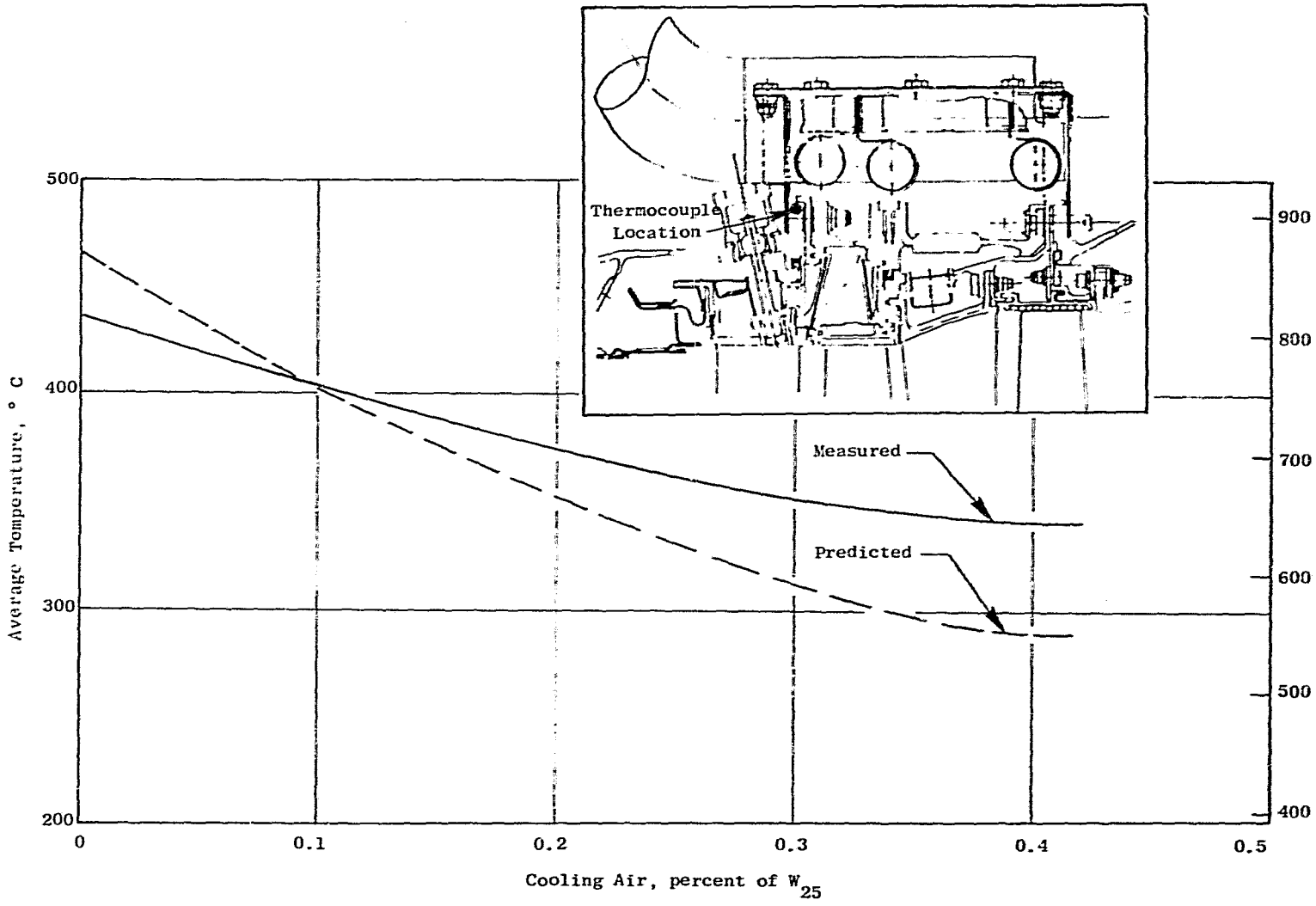

Figure 48. Temperature Match - Compressor Rear Frame Shallow Thermocouple.

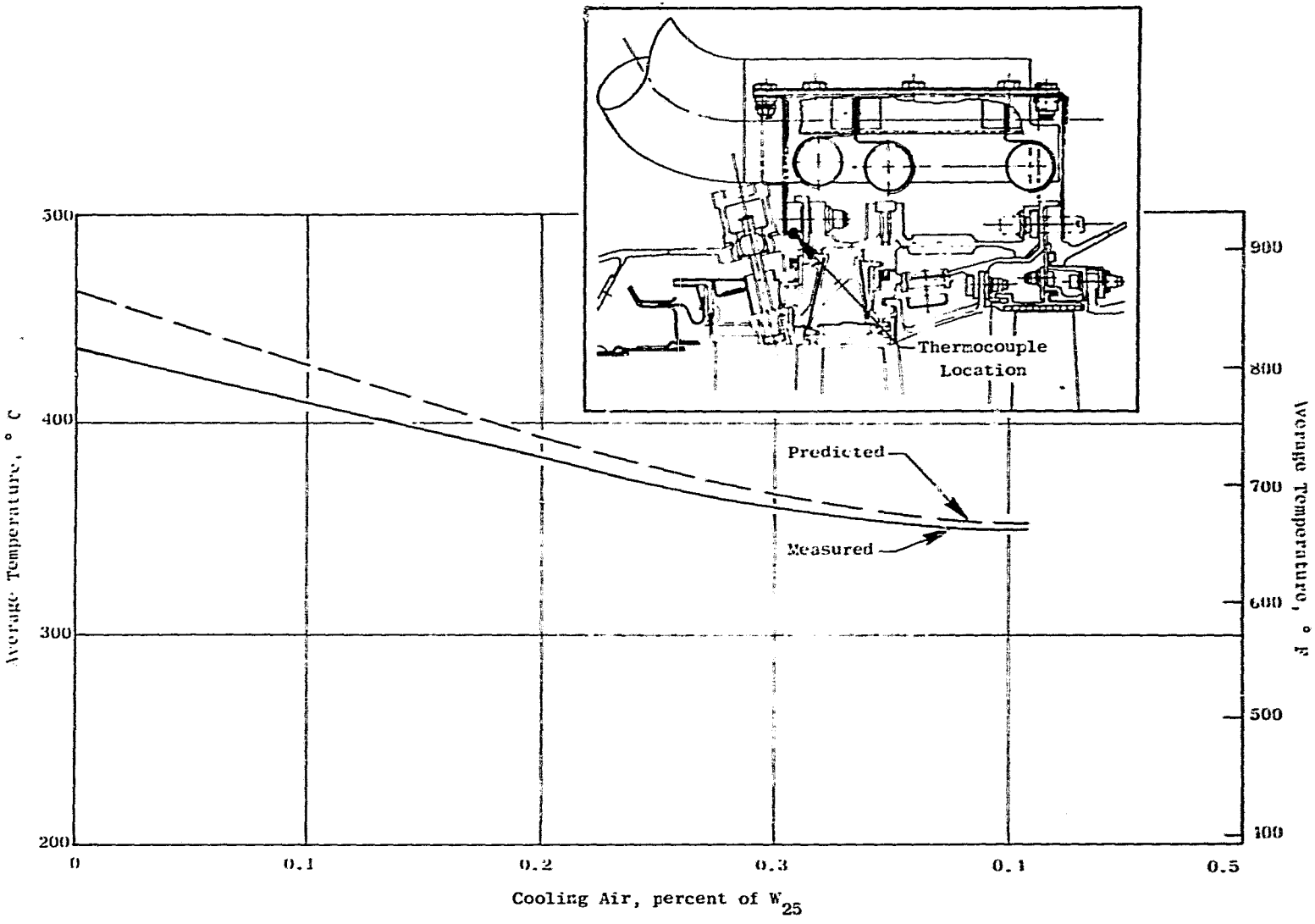

Figure 49. Temperature Match - Compressor Rear Frame Deep Thermocouple.

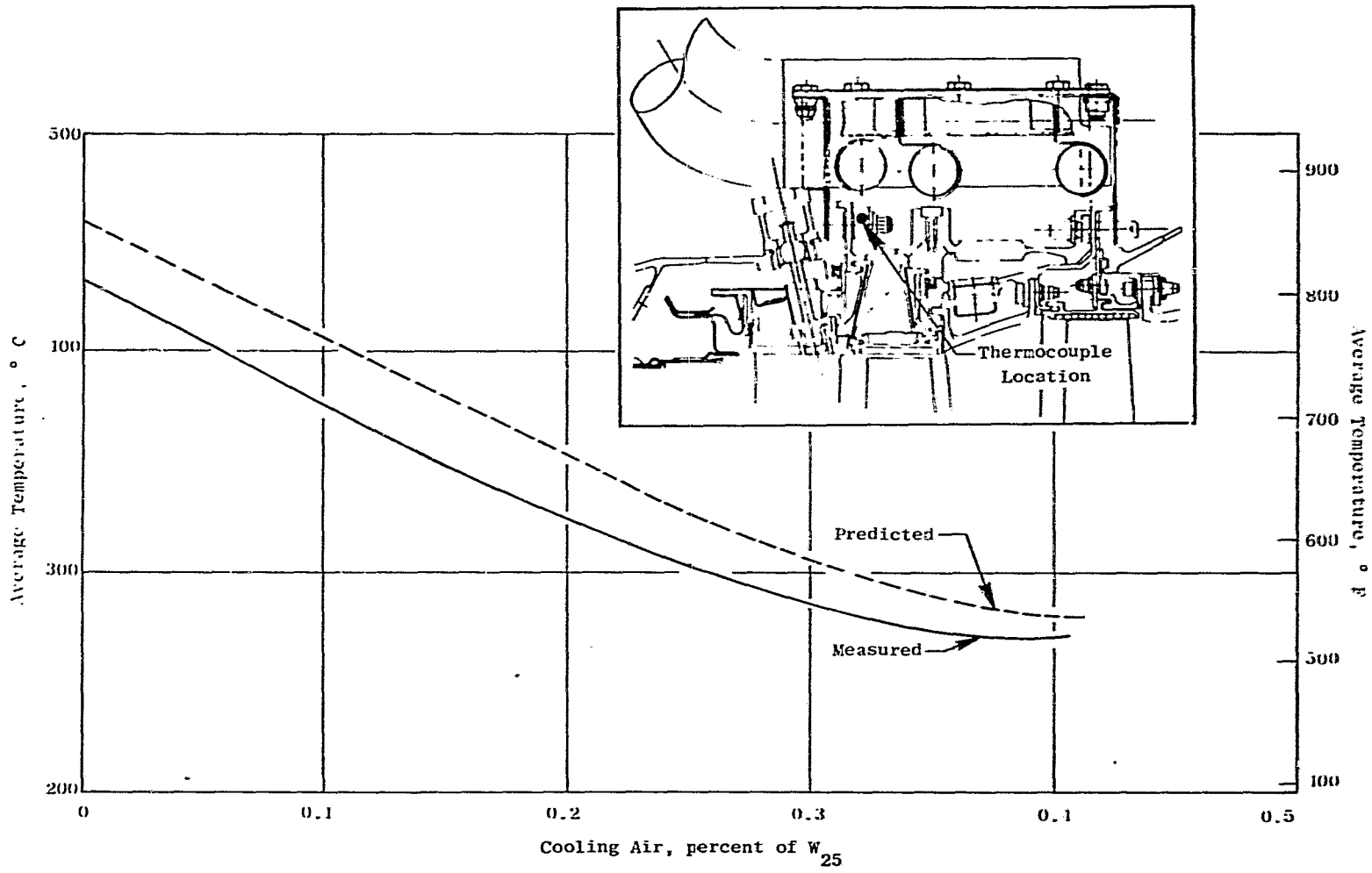

Figure 50. Temperature Match - HPT Forward Flange Shallow Thermocouple.

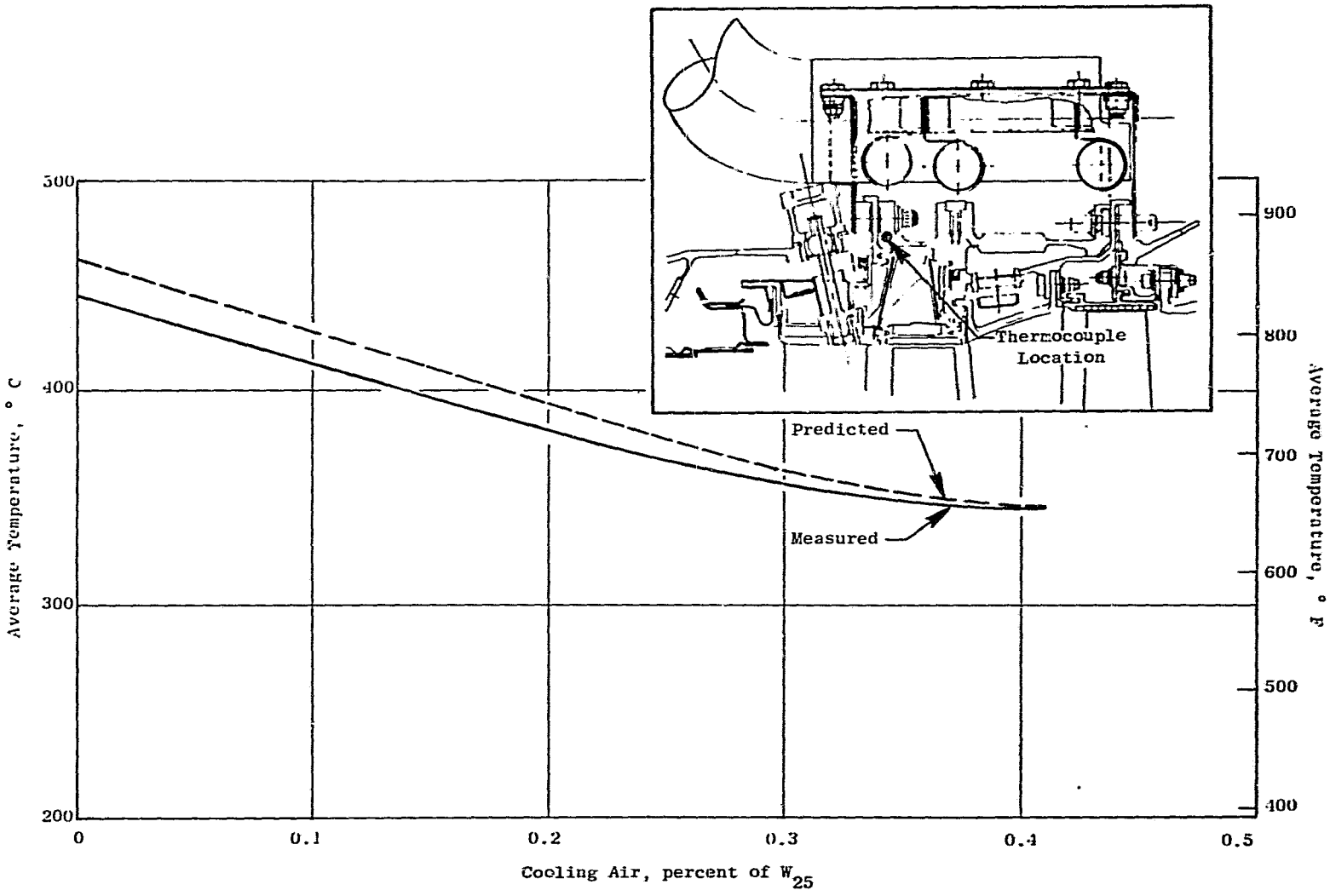

Figure 51. Temperature Match - HPT Forward Flange Deep Thermocouple.

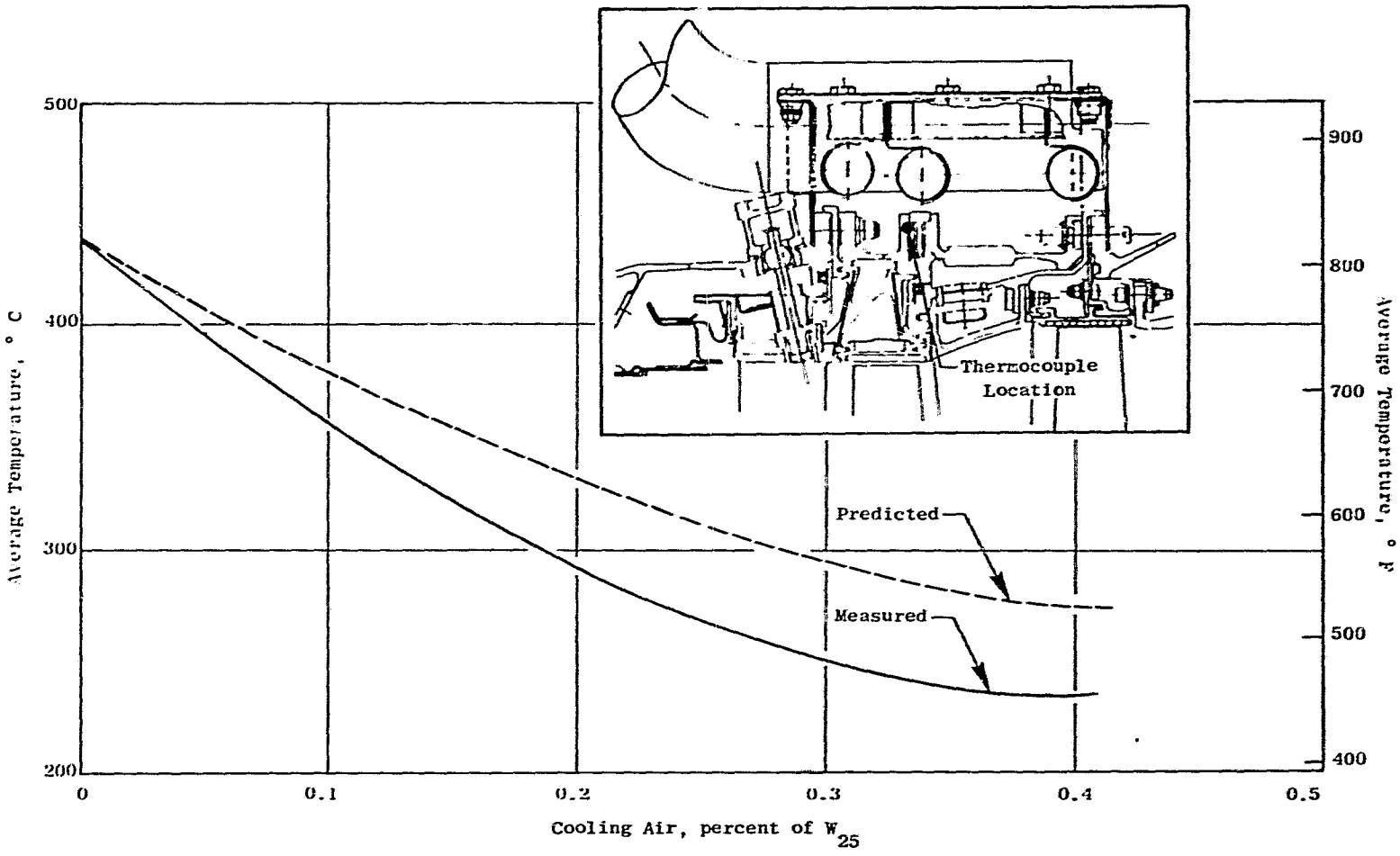

Figure 52. Temperature Match - HPT Mid Flange Shallow Thermocouple.

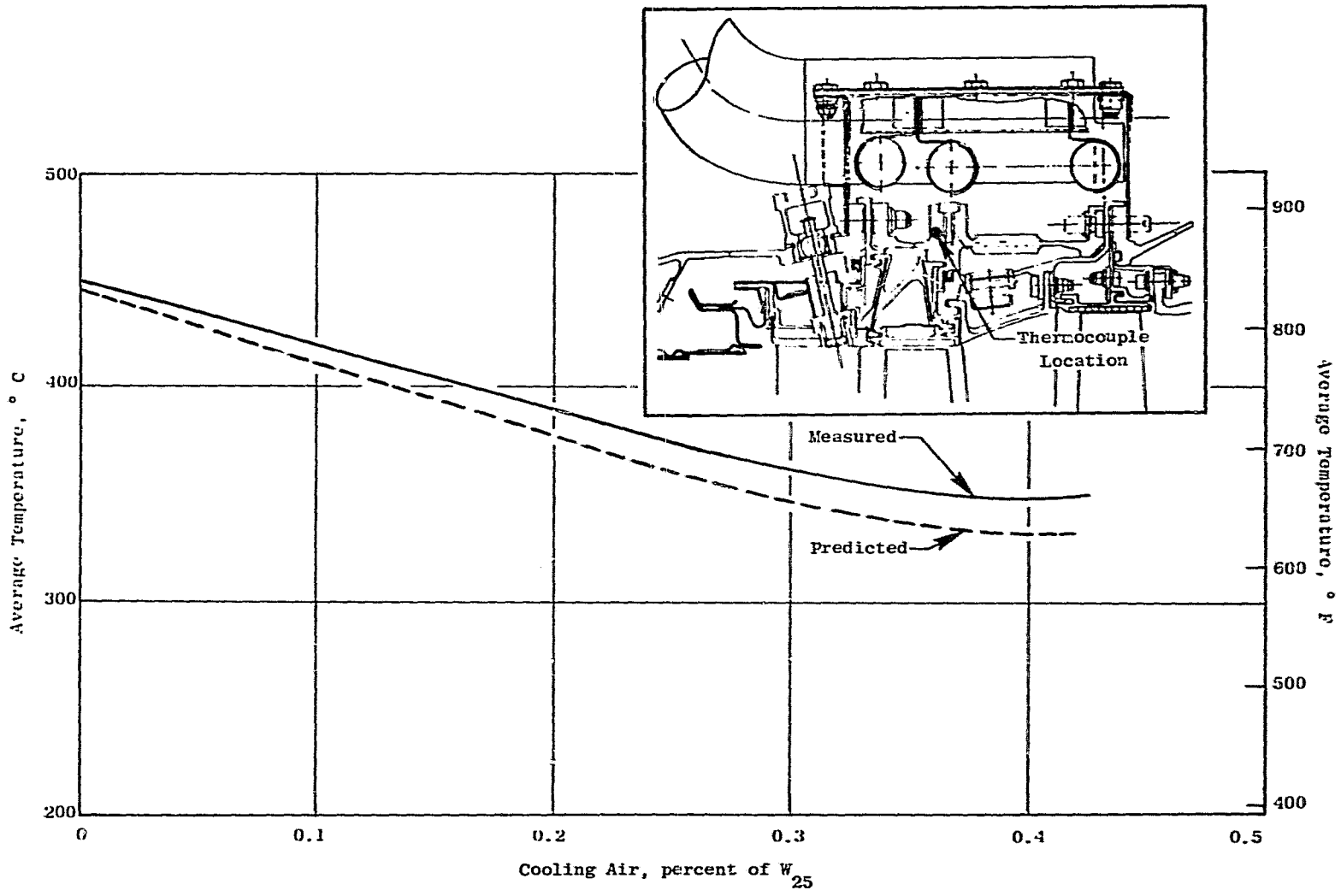

Figure 53. Temperature Match - HPT Mid Flange Deep Thermocouple.

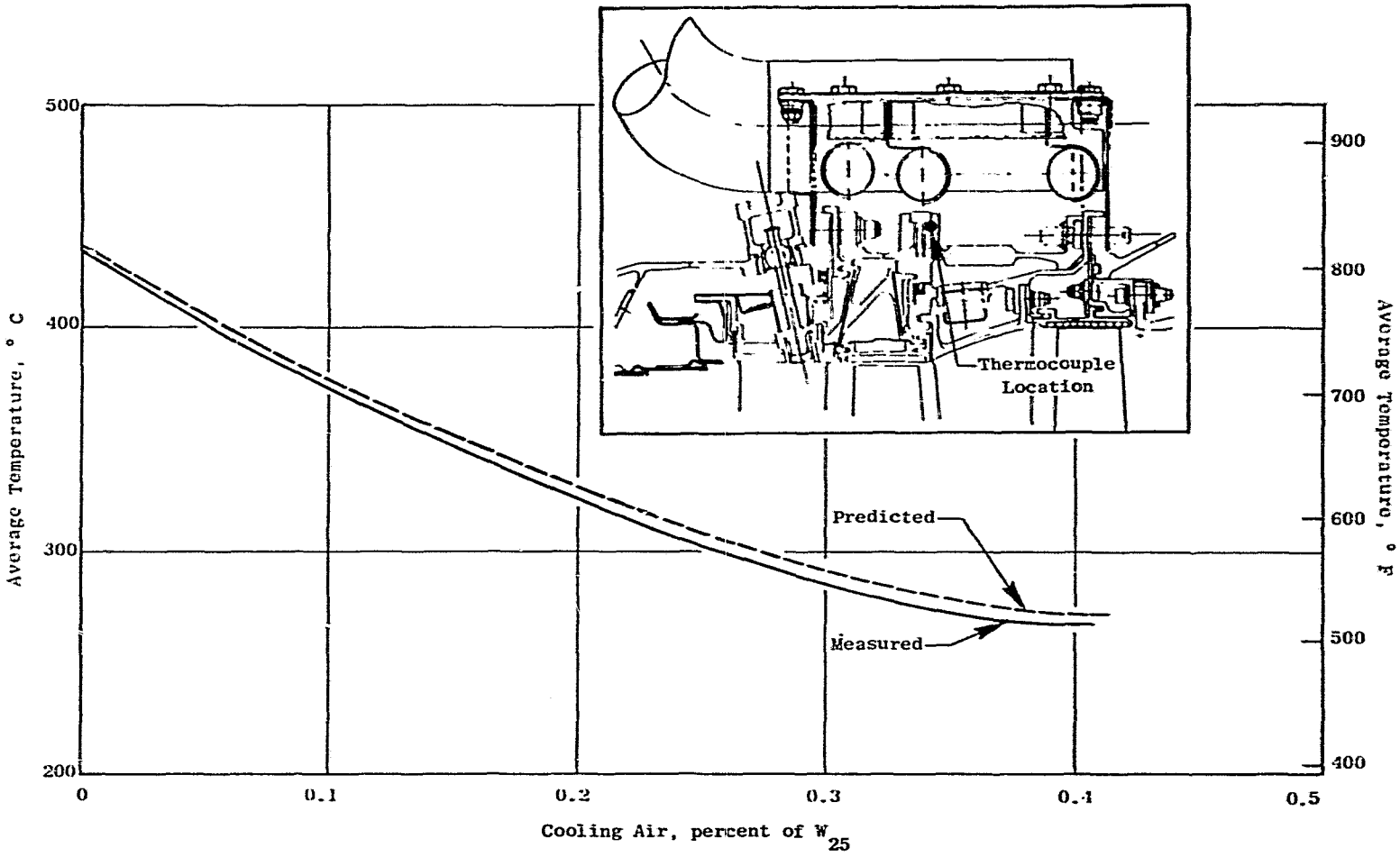

Figure 54. Temperature Match - HPT Mid Flange Shallow Thermocouple.

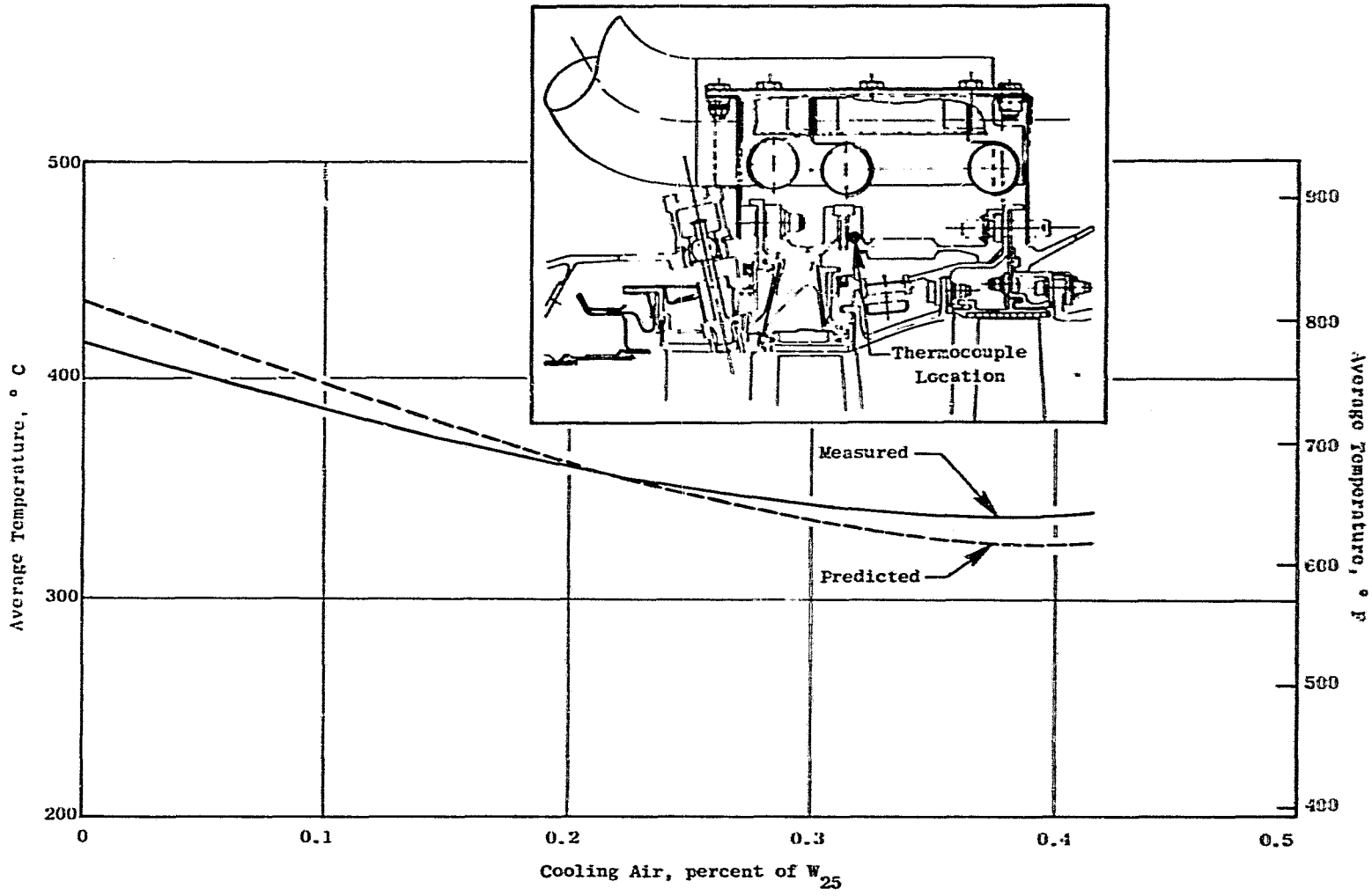

Figure 55. Temperature Match - HPT Mid Flange Deep Thermocouple.

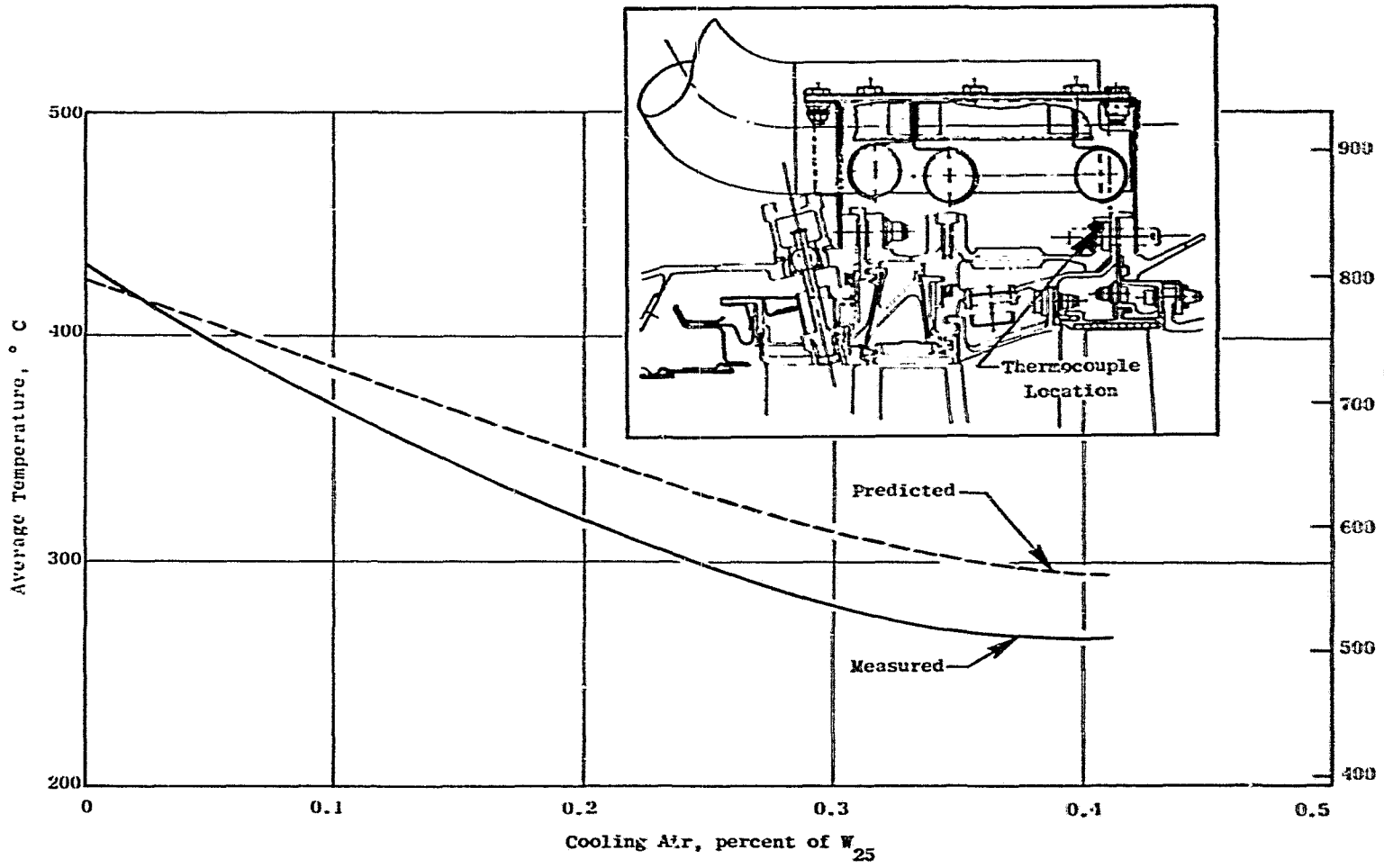

Figure 56. Temperature Match - HPT Rear Flange Shallow Thermocouple.

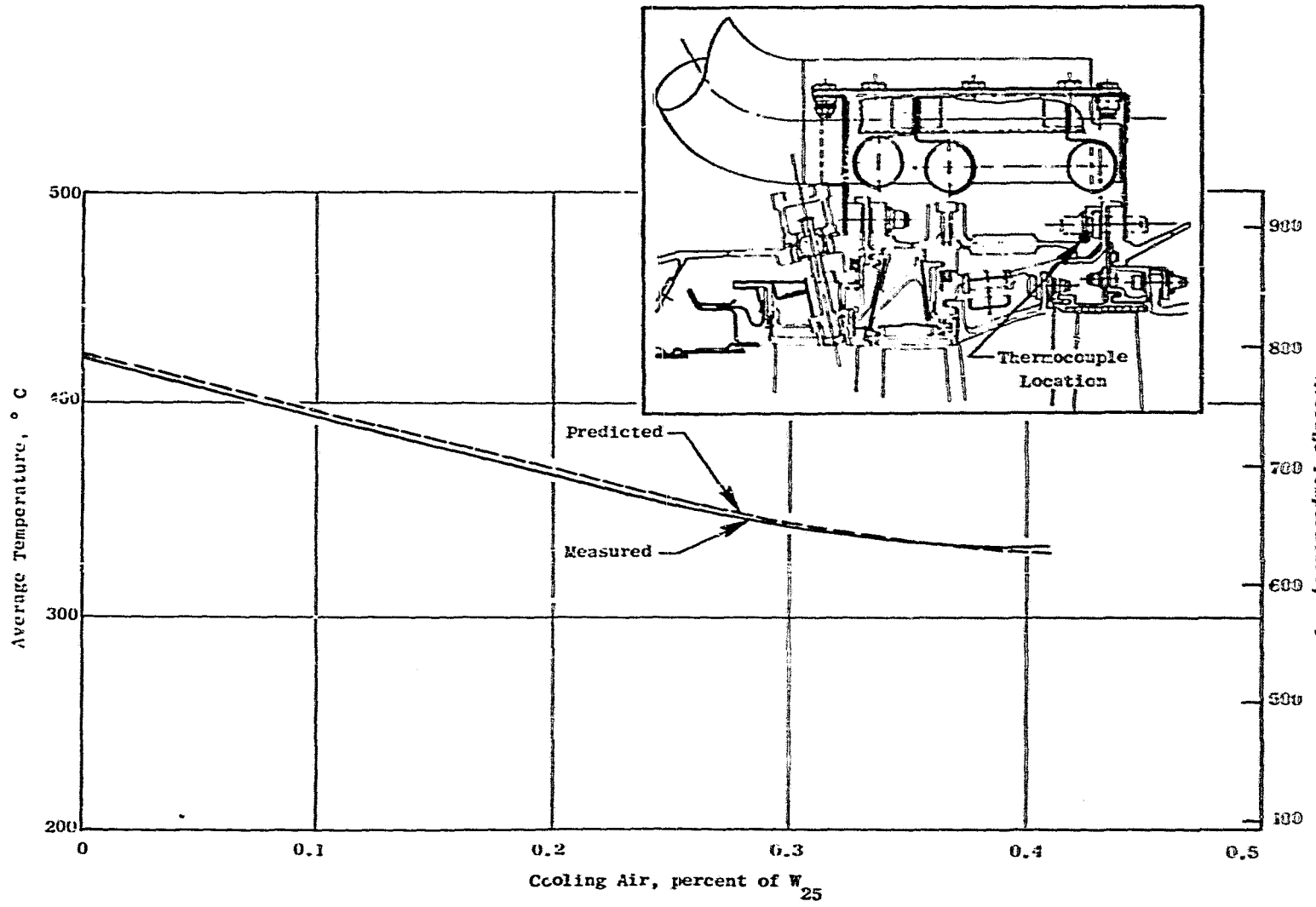

Figure 57. Temperature Match - HPT Rear Flange Deep Thermocouple.

Structurally the HPT casing flanges determine the stator radial position so that temperature matching in this area needs to be as accurate as possible. After adjusting for cycle conditions, the heat transfer coefficients were modified in order to obtain a match with the thermocouple data. A reasonable match was obtained for those thermocouple locations which experience has shown to govern the radial position of the shroud surface.

C-2

6.6 HEX DATA

This section of the report deals with High Energy X-Ray (HEX) portion of the engine test. Figures 58 and 59 show the engine installed at the HEX Test Site, and identify the major components of the HEX test facility.

6.6.1 Test Procedure

The radiographs were taken at the 6 o'clock position of the engine since this allowed the closest positioning of the film plane to the engine. Figures 60 and 61 show typical radiographs at the Stage 1 and Stage 2 HPT areas respectively. HEX radiographs were taken at steady state and during transient cycles. The fast film changer allowed 12 separate radiographs to be taken during the transients. The radiographs were processed and labeled at Peebles. The data reduction was completed at Evendale.

6.6.2 Analysis Procedure

To accurately measure an individual x-ray requires the use of an elaborate system composed of any X-Y positioning table, closed circuit television camera, and a television monitor. The monitor employs a "density profiler" facility which is used to make the actual measurements. The method of measuring is probably best explained using a simplified example.

Suppose that it is desired to measure the radial distance between a rotor seal tooth and its stator. Figure 61 shows what the x-ray image might look like on the television monitor. The x-rays are typically 4/3 actual size. The x-ray image will not appear with the edges well defined, but rather there will be a transition zone between light and dark. If the density or "brightness" is plotted along line "A" (Figure 62a) it will appear as shown at the right portion of the figure. To measure the x-ray image requires that this curve of density is bounded by the minimum and maximum brightness lines "B" and "C" which are set by the operator.

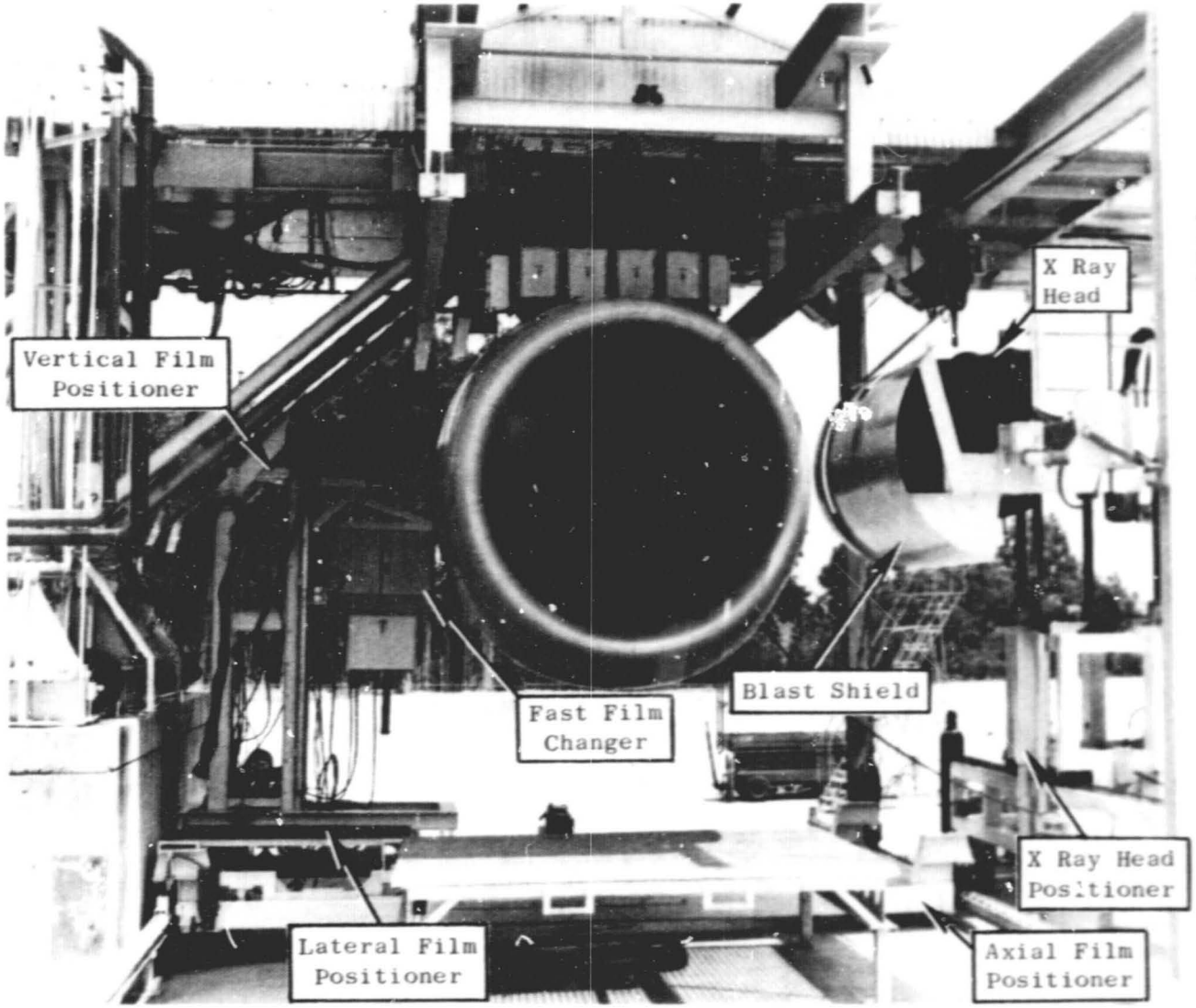

Figure 58. HEX Facility - Front View.

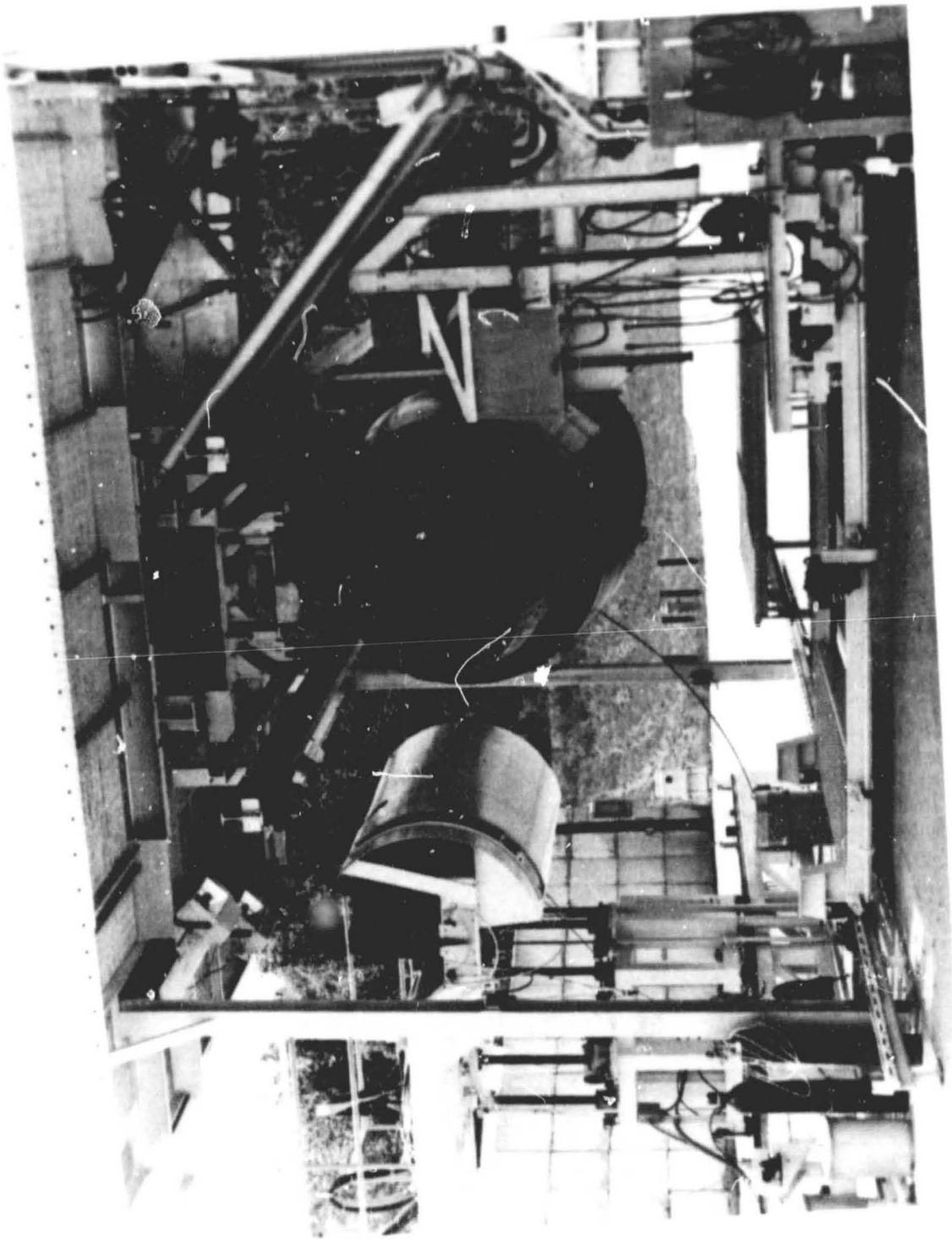

Figure 59. HEX Facility - Rear View.

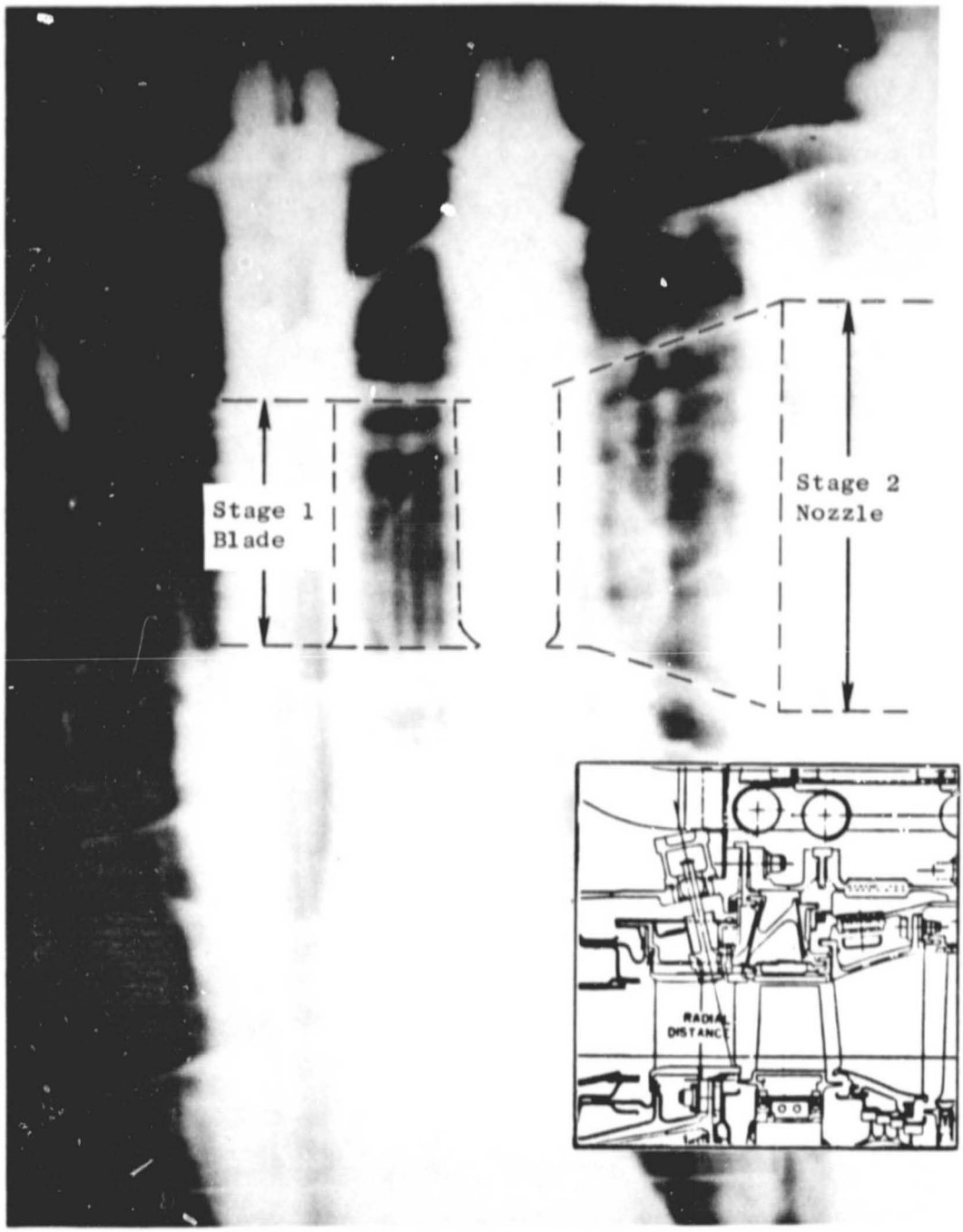

Figure 60. Stage 1 HEX Radiographs.

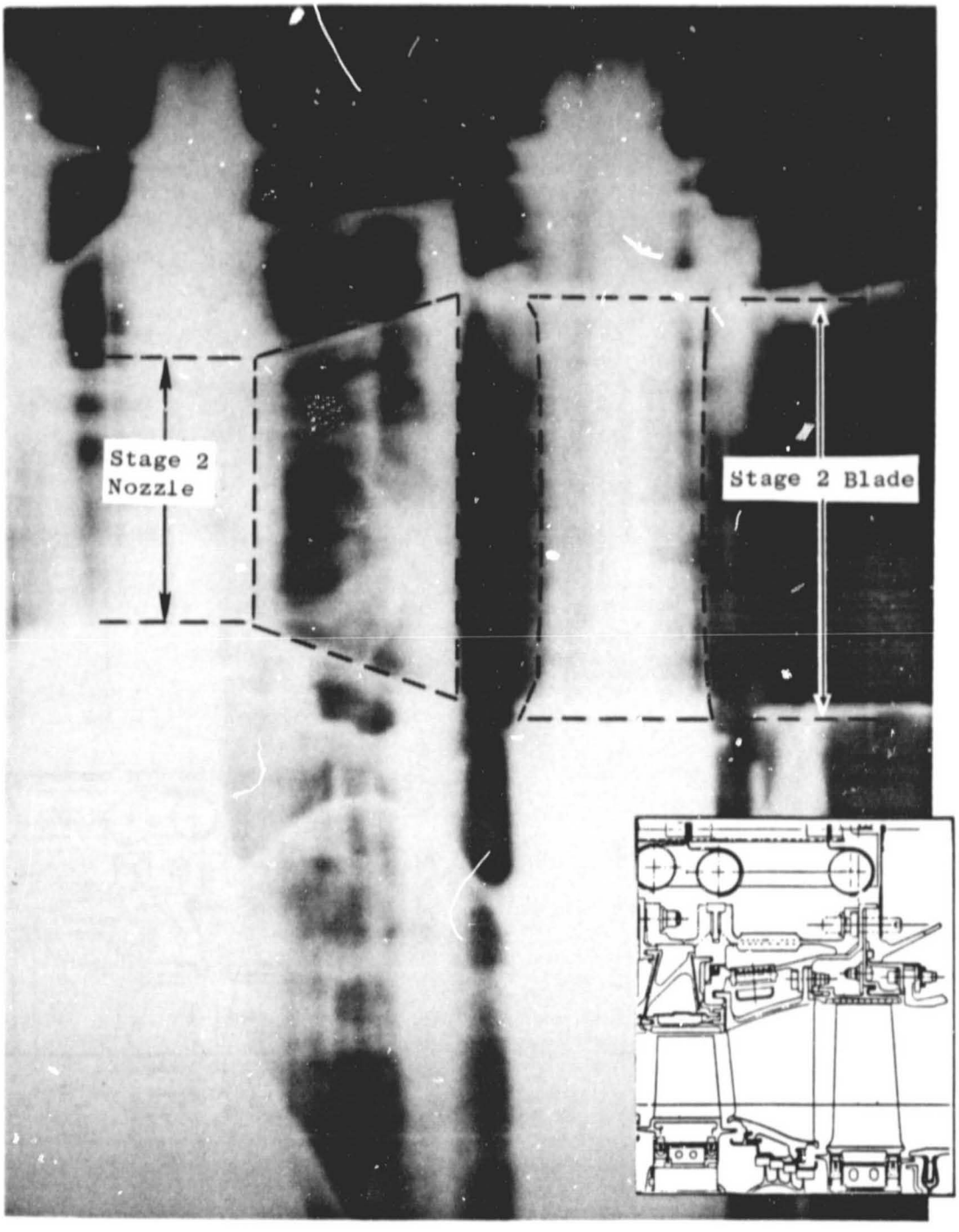

Figure 61. Stage 2 HEX Radiographs.

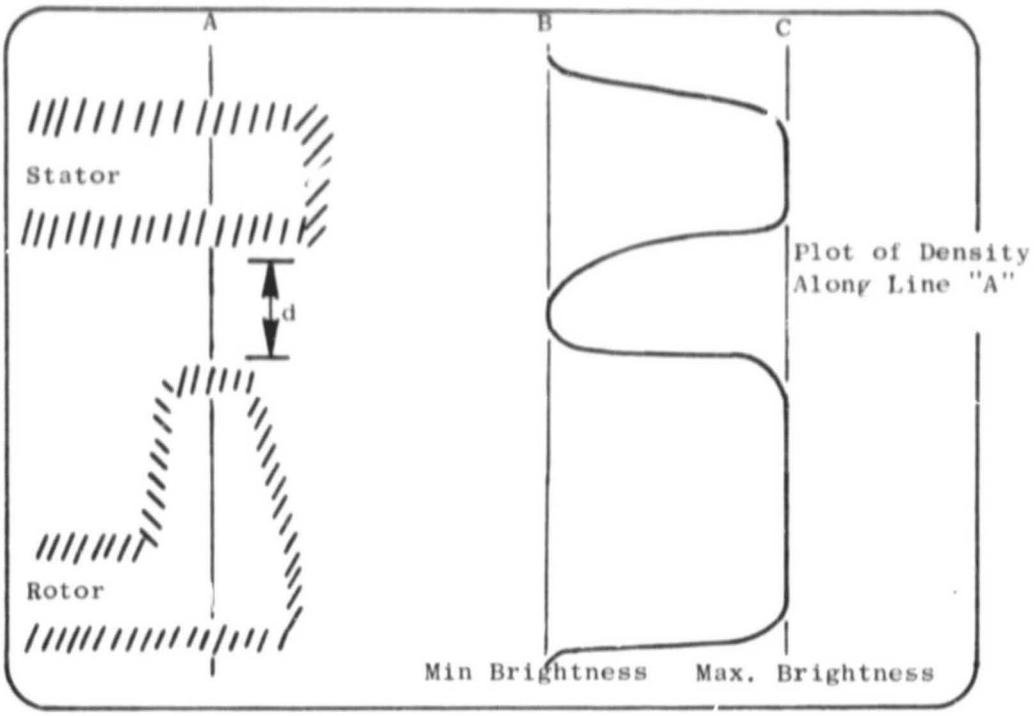

(a) X-ray Image on Television Monitor

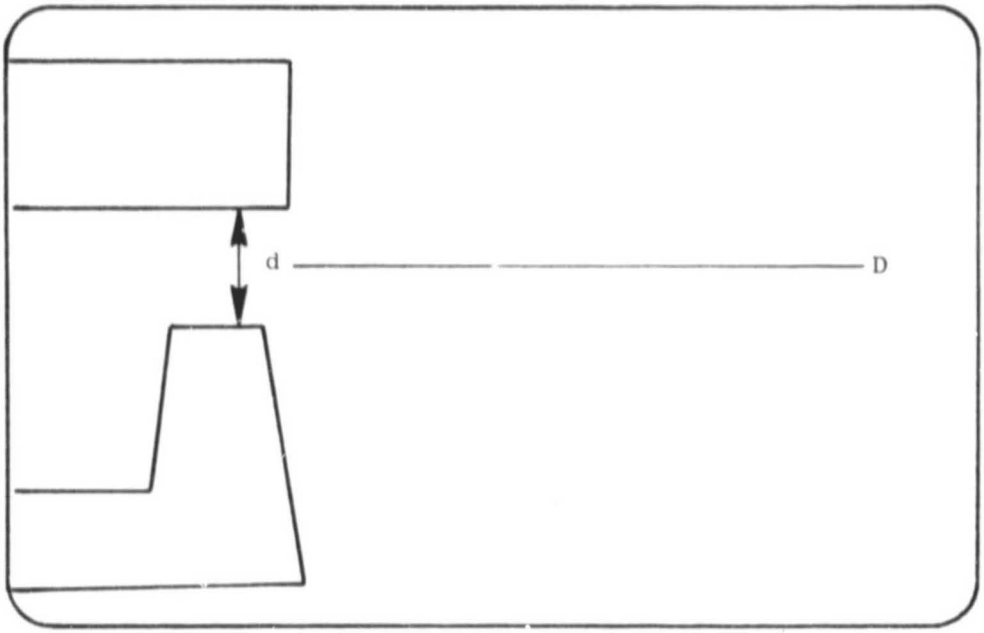

(b) Density Contour Obtained from Density Profiler.

Figure 62. X-Ray Image and Density Contour.

The density profiler then breaks up all light on the x-ray image between brightness levels B and C into 12 color contours displayed on a color television monitor. If the 12 contours are selectively turned off such that only the middle contour remains, the image on the screen will appear as in Figure 62b. The previously undefined edges of the rotor and stator are now replaced with a density contour line which is well defined. Note that the contour line does not necessarily lie on the edge of a part but between the min and max brightness levels.

Using the X-Y table and the horizontal reference line "D", the distance "d" can be accurately measured. The distance "d" is not usually 4/3 of the actual distance between rotor and stator but a smaller distance since, as mentioned previously, the contour line does not necessarily lie on the edge of a part. This points out an important limitation on the HEX system, i.e., absolute clearance cannot usually be measured, but consistent operator techniques will result in measuring accurate changes in clearance. To determine the seal rotor/stator clearance in Figure 62 would require that "d" be measured from a "cold" or non-running X-ray and compared with the value "d" measured in Figure 62. This gives the change in clearance and, assuming that the build-up clearance is known, the absolute clearance.

When measuring HP blade tip clearance, it is necessary to measure from the shroud to the blade platform because the airfoil is not dense enough to show on the x-rays. The airfoil thermal and mechanical growths are then calculated based on T4B and core speed. The airfoil calculated growths are then combined with HEX results and the resulting tip clearance is obtained.

Good measurement repeatability was obtained between the blade angle wing and shroud backing strip on Stage 1, and the blade angle wing and the forward shroud hook on Stage 2. Figures 63 and 64 illustrate the locations of the Stage 1 and Stage 2 measurements.

6.6.3 Test Results

Figures 65 through 69 illustrate the results of the HEX testing. These figures represent the change in the distance between the measurement points relative to a cold rollover point. To obtain actual rotor/stator clearance requires that the blade growth be factored into the measured data.

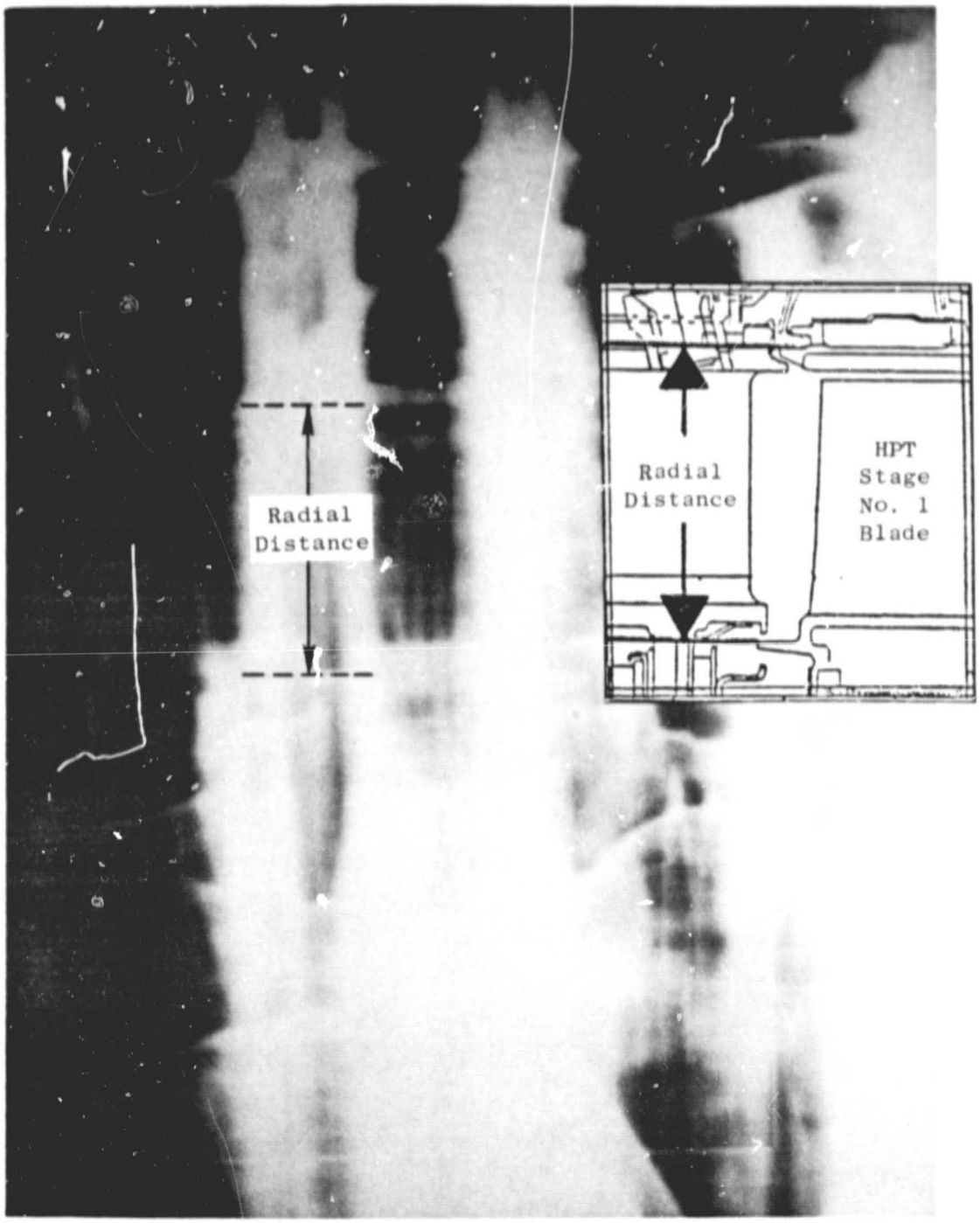

Figure 63. HEX Radiograph Stage 1 - Measurement.

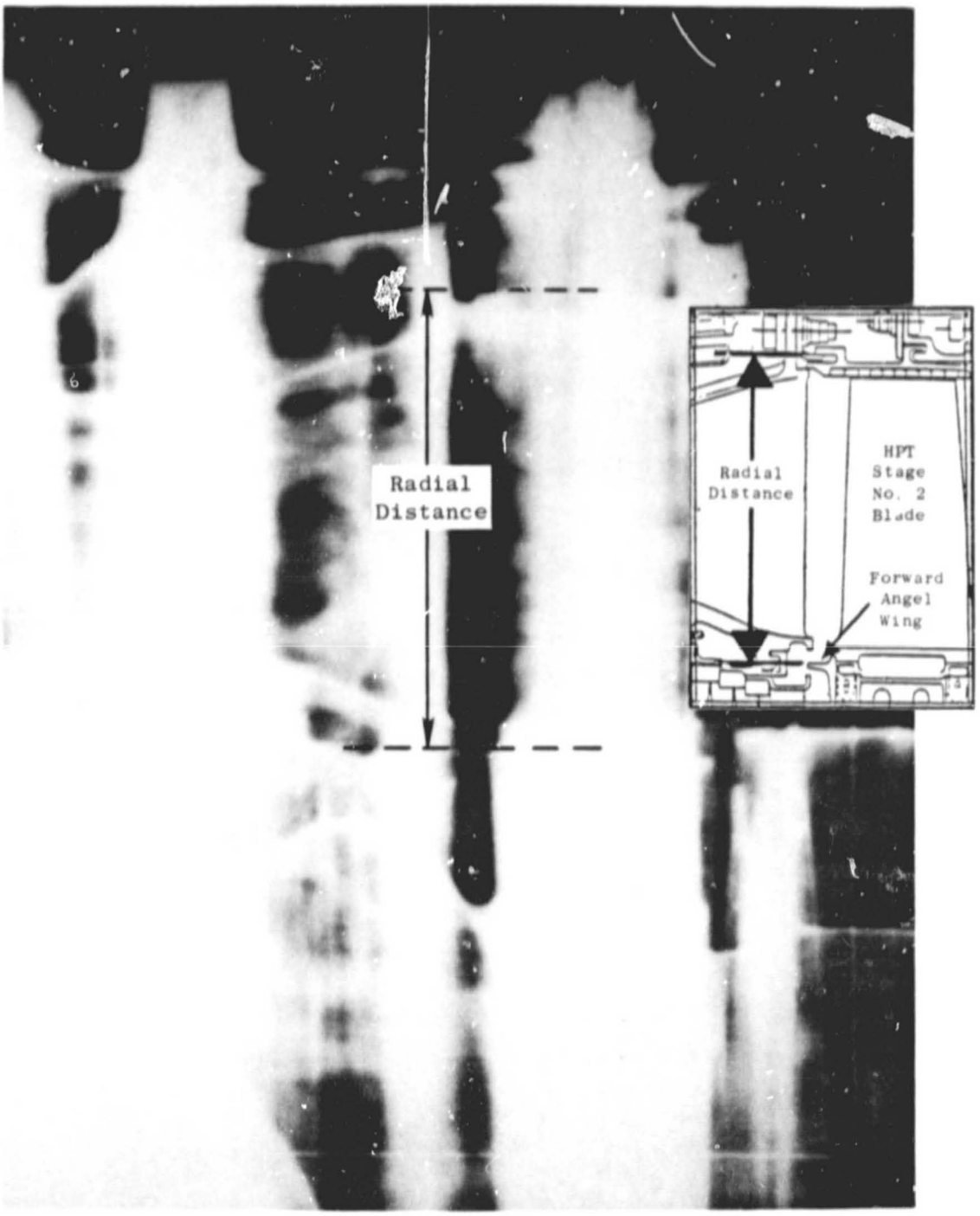

Figure 64. HEX Radiograph Stage 2 - Measurement.

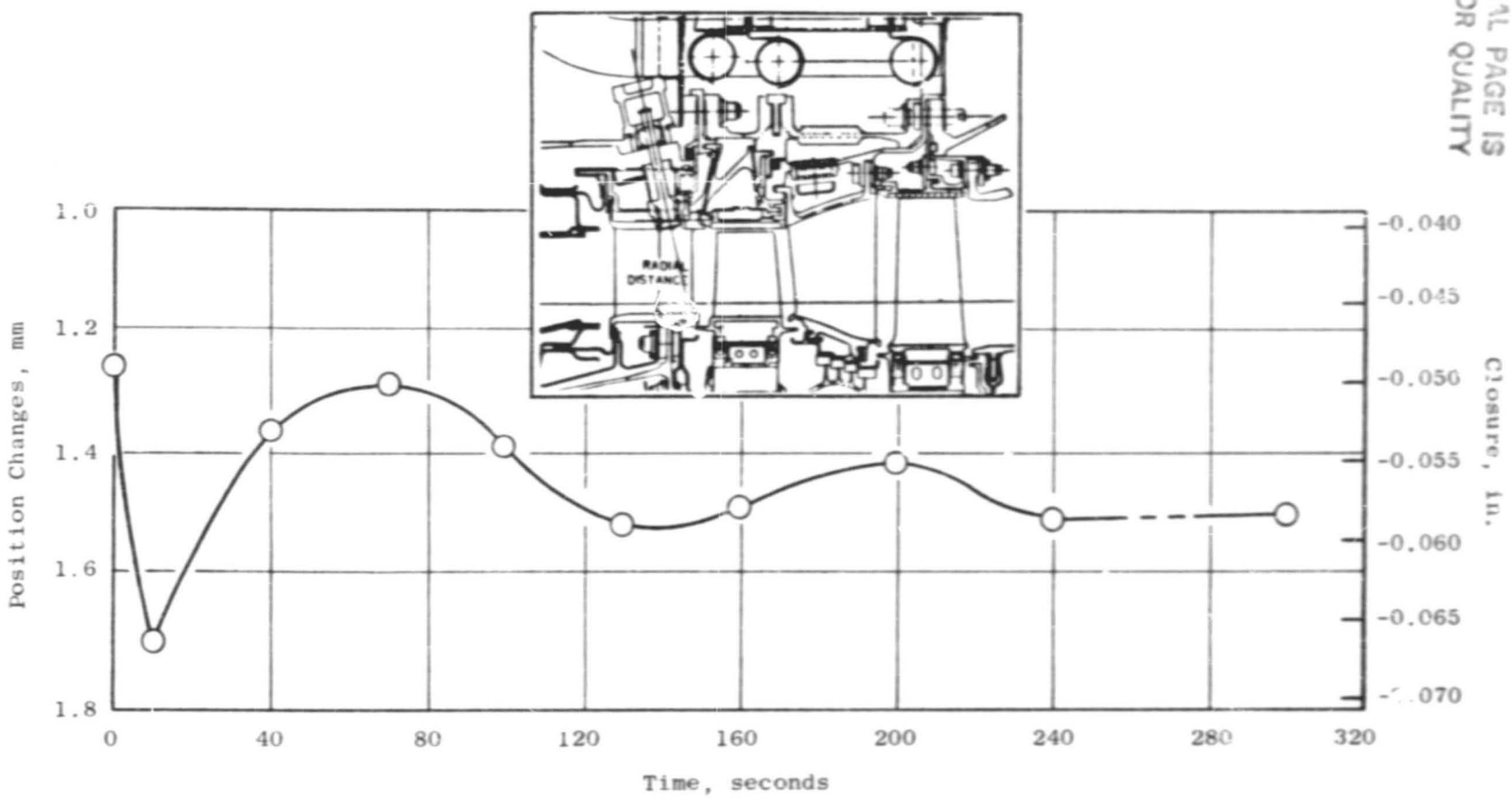

Figure 65. Stage 1 Position Change Following Throttle Burst from Ground Idle to Takeoff Power.

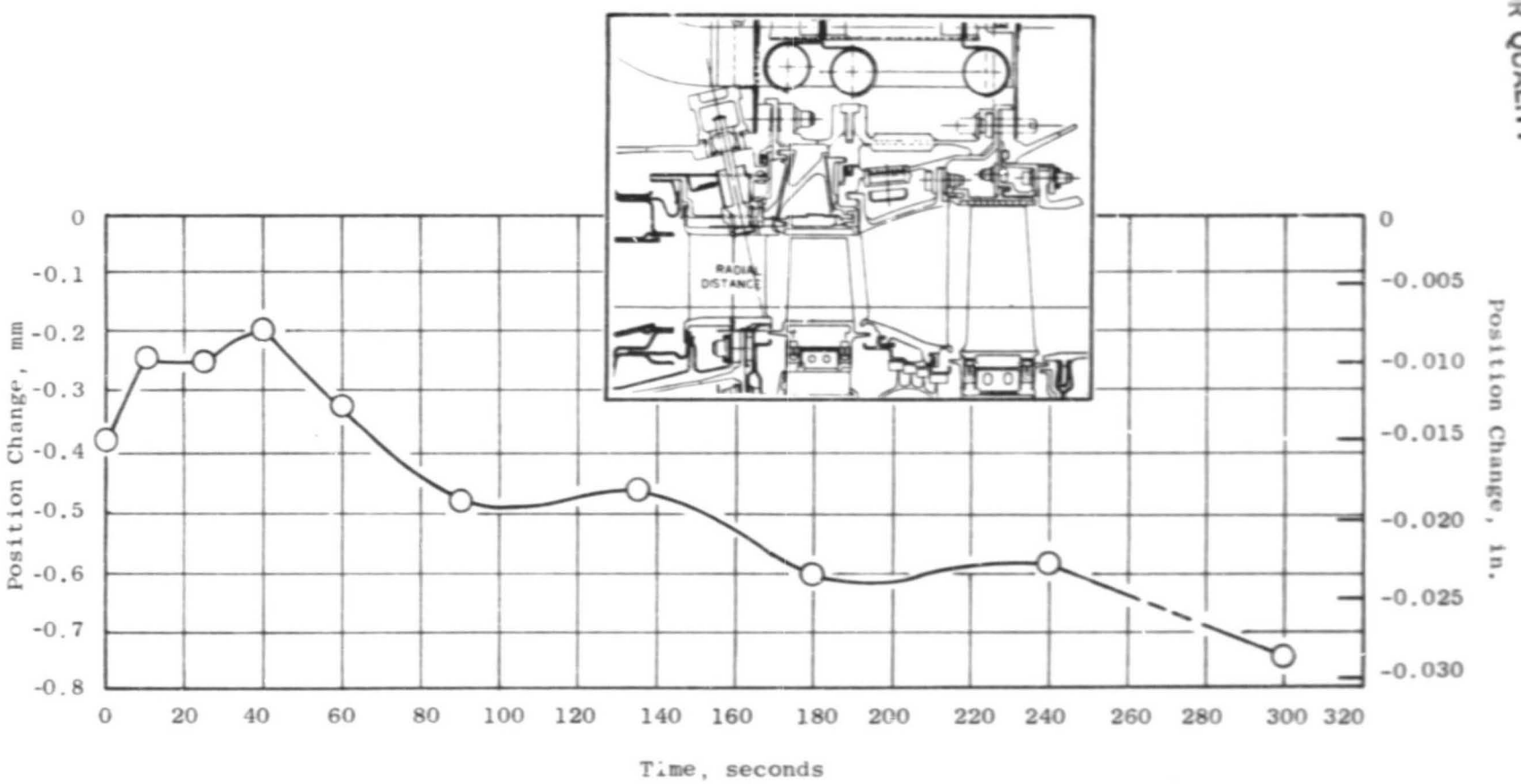

Figure 66. Stage 1 Position Change Following Hot Rotor Reburst to Maximum Climb After 70 Second Dwell at Flight Idle.

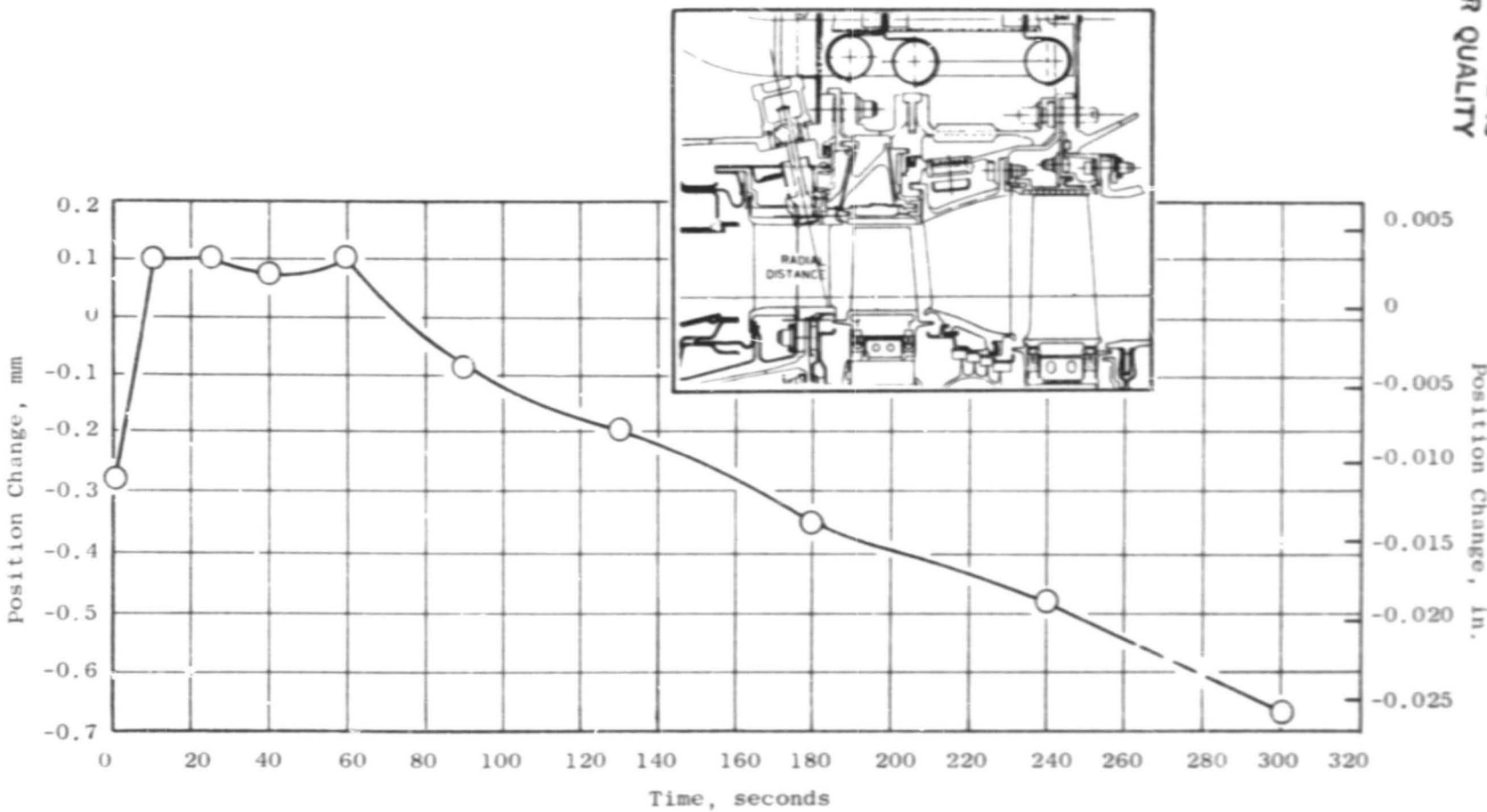

Figure 67. Stage 1 Position Change Following Hot Rotor Reburst to Maximum Climb After 130 Second Dwell at Flight Idle.

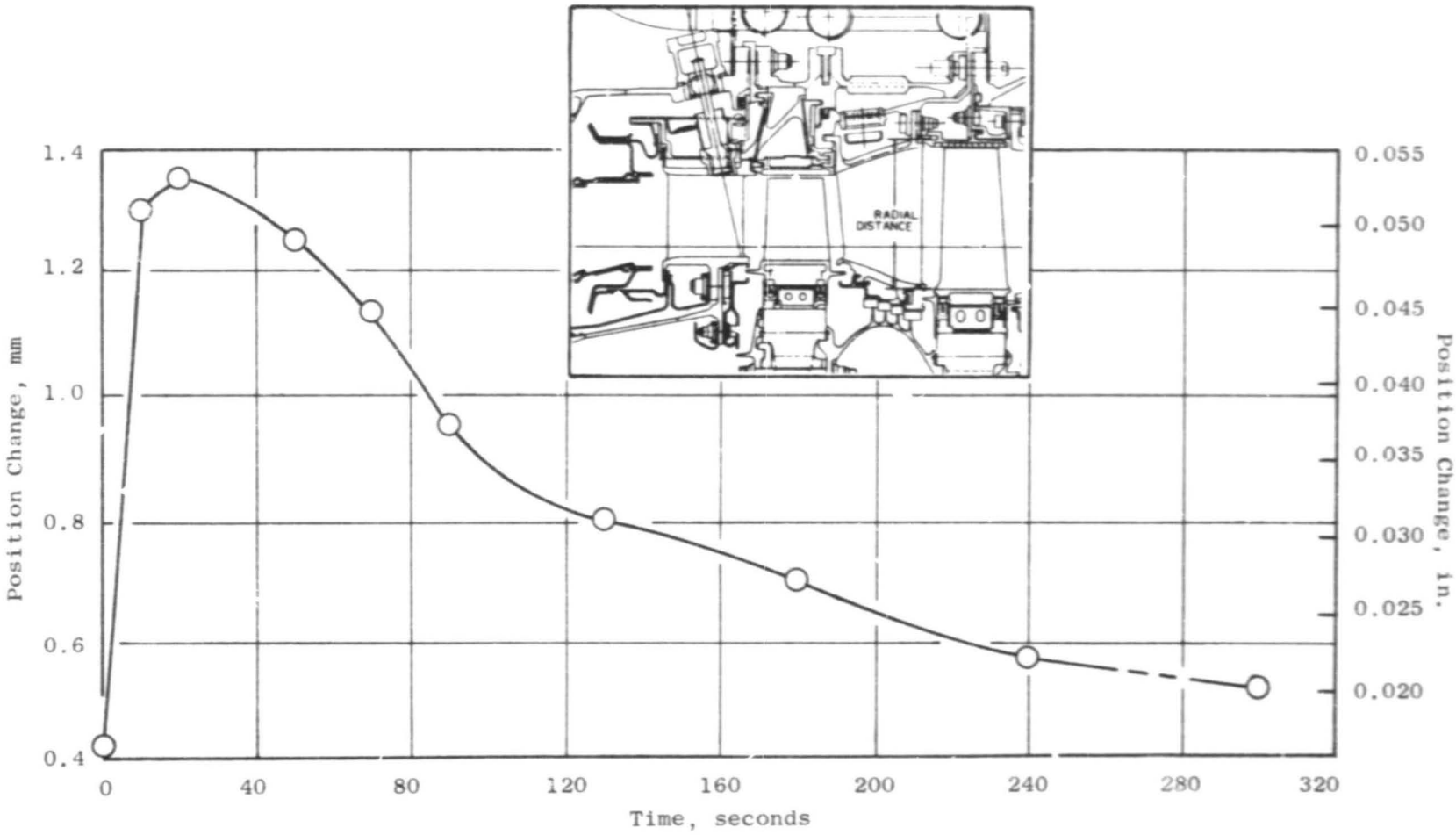

Figure 68. Stage 2 Position Change Following Throttle Burst from Ground Idle to Takeoff.

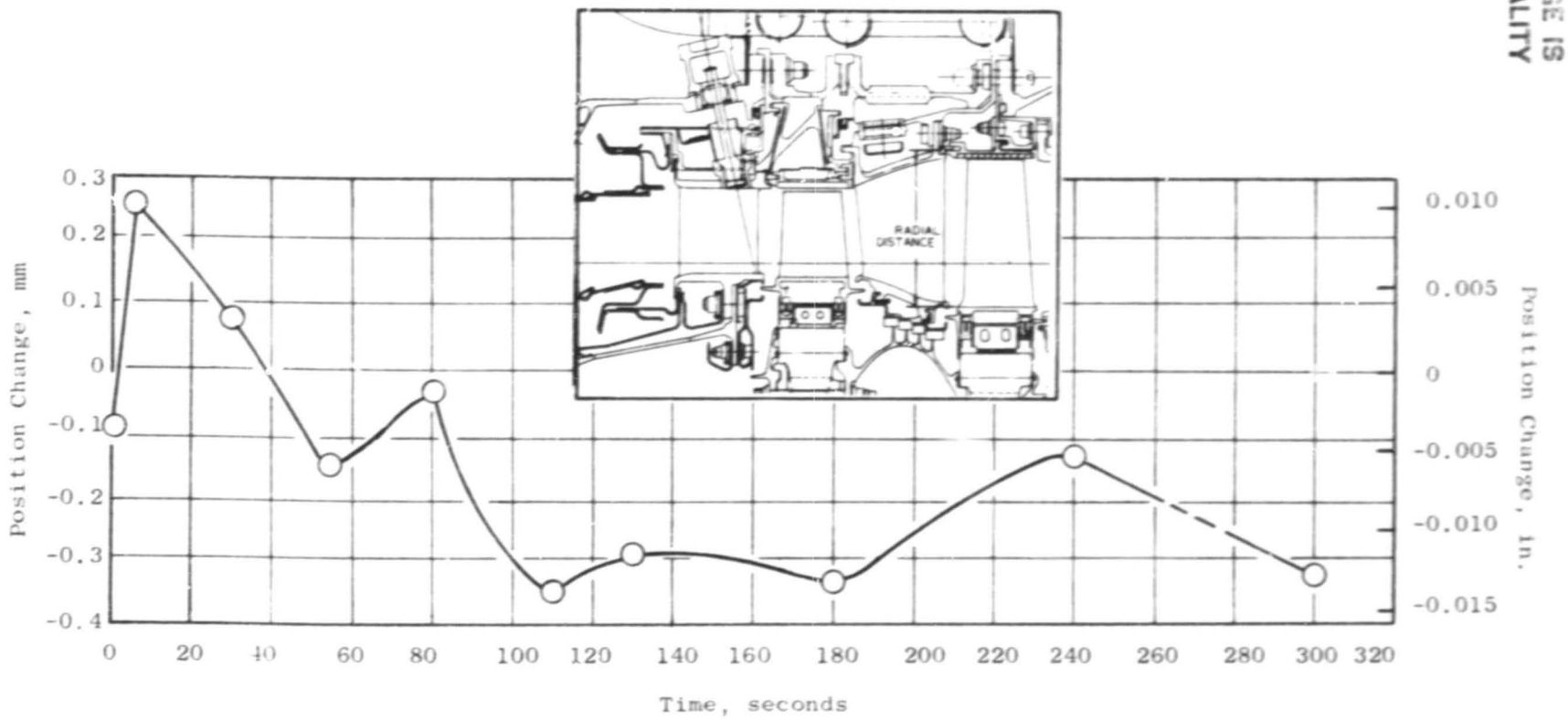

Figure 69. Stage 2 Position Change Following Throttle Chop from Takeoff to Ground Idle.

6.7 DATA COMPARISONS

This section of the report presents clearance comparisons between measured high energy X-Ray data and analytical results based on matching test cell temperatures. Results of transient and steady state testing are presented.

6.7.1 Transient Clearance Change

Figure 70 shows a comparison between measured HEX data and calculated turbine tip clearance. This figure depicts high pressure turbine tip clearance and includes the effect, on the HEX measurements, of blade growth.

6.7.2 Steady State Clearance Change

Figure 71 illustrates a comparison between the analytical closures and the measured HEX closures. As the figure shows, the measured closure on Stage 1 is 0.15 to 0.18 mm (.006 to .007 in.) less than the analytical closure based on matched temperature data. The correlation between the HEX and the performance measurements is discussed in Section 7.5.1, Sea Level Test Results. The reason for the difference may be attributed to archbinding of the Stage 1 shroud hangers when the casing was cooled sufficiently. It was noted at teardown inspection that archbinding did occur. This situation resulted in less actual closure than was calculated on the basis of measured temperature change. Archbinding could be readily alleviated for a production incorporation of this clearance control system by adjusting the circumferential gaps to be consistent with the minimum desired cooled shroud radius. For Stage 2 it can be seen that good correlation was obtained.

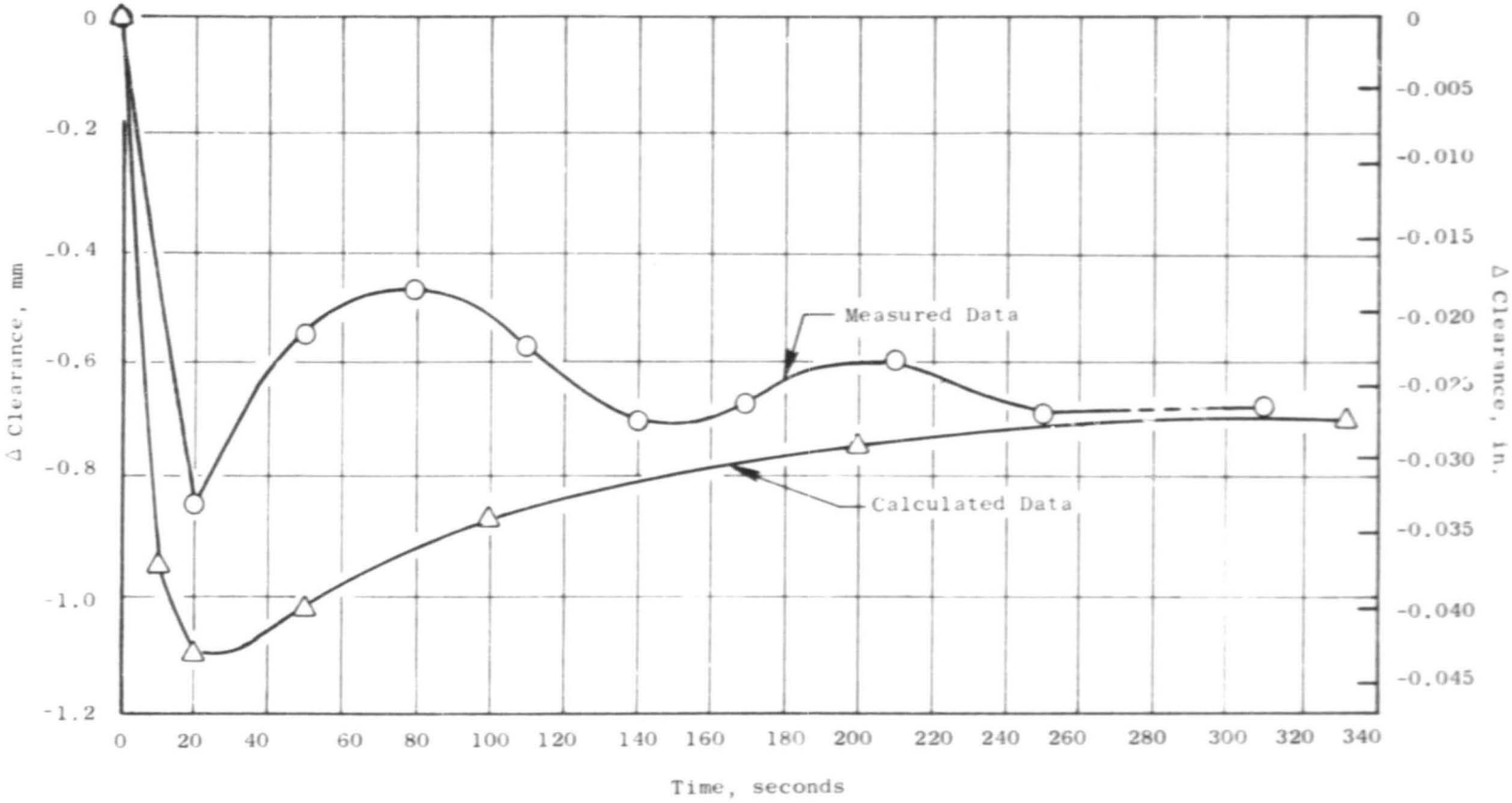

Figure 70. Stage 1 Change in Clearance Following Throttle Burst from Ground Idle to Takeoff Power.

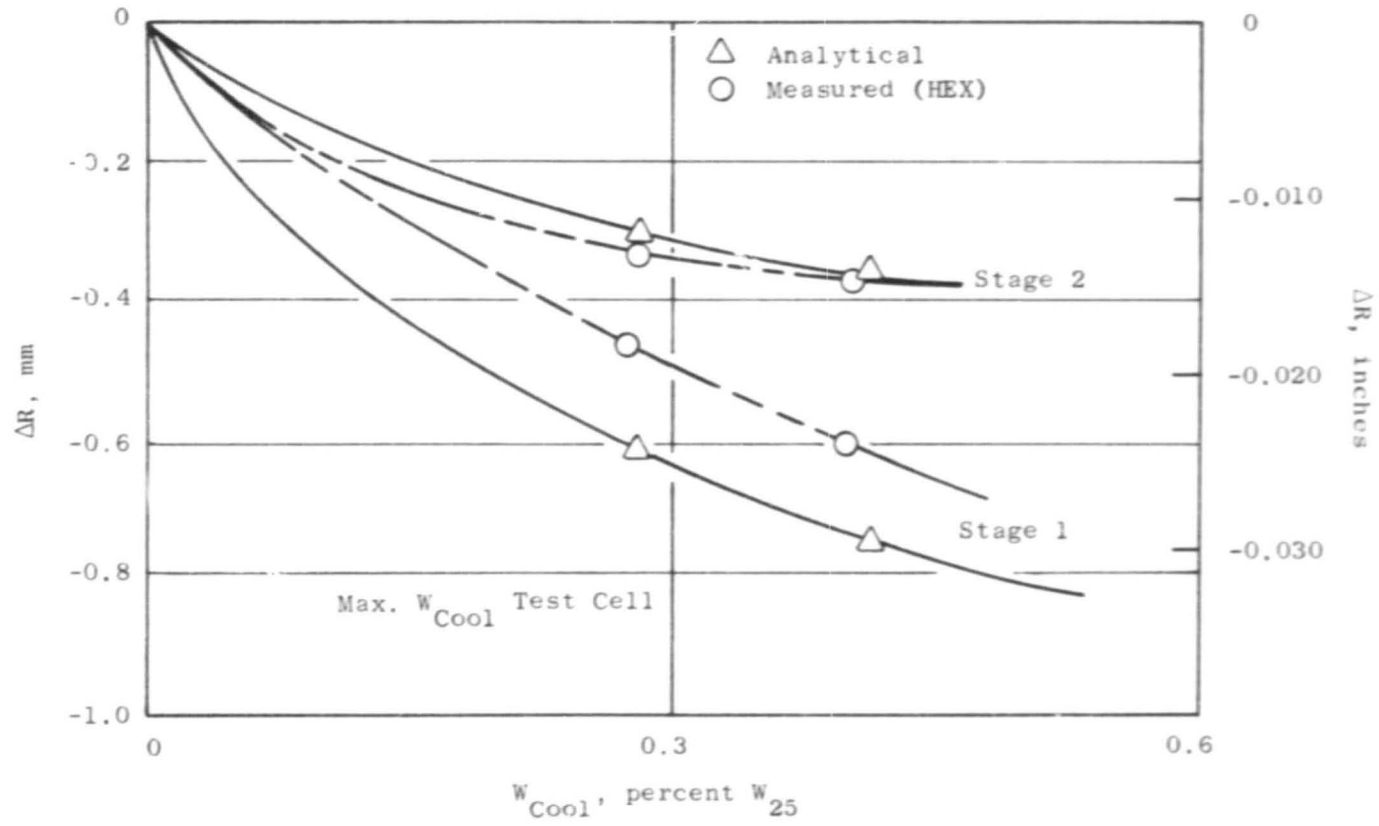

Fi re 71. Maximum Cruise Closure Versus Cooling Air.

7.0 PERFORMANCE TESTING

7.1 TEST OBJECTIVES

The test objectives of the Performance Testing were twofold. The first objective was to obtain performance improvement data as the fan cooling air was gradually introduced into the impingement system. The second objective was to operate the engine through a series of accels with gradually reduced compressor discharge air flow to the impingement system in order to determine the minimum amount of compressor discharge air required to prevent a turbine rub during an engine throttle burst.

7.2 TEST FACILITY

The testing was completed at the Evendale test facility. The modernized data acquisition and processing system used consisted of a Cell System and a Site System. The Cell System performed steady-state and transient data acquisition, conversion to engineering units, quick-look performance calculations, and short-term storage. Converted data was automatically transmitted to the Site System for further on-line processing, graphic display, and hard-copy output. The Site System utilized a data-base concept for efficient storage, retrieval, and reprocessing of current and historical data. In addition, data could be transmitted to the General Electric Evendale Time-Sharing Computer Center for further processing such as cycle deck analysis and comparison.

Data Channels Available

The following data channels are available:

1) 400 pressures

2) 400 temperatures

3) 10 frequencies

The steady-state system has the following capabilities:

1) Temperatures, position, thrust, transducers

   1.1) Acquisition time approx. 30 seconds

   1.2) Each parameter sampled 10 times over 30 second period.

1.3) Frequencies, 2.5 second average. Samples/average can be increased by calling for channel multiple times in config.

2) Pressures

2.1) Acquisition time approx. 48 seconds

2.2) Each parameter an average of 512 samples over a 16.7 M.S. period

3) Data Processing

3.1) Phase I and printer plots

3.2) On-line link to H6000 computer data bank

3.3) Limited output in test cell

The transient system has the following capabilities:

1) Any analog parameter (500 max.)

2) Scan rates - 200, 500, 1K, 2K, 10K channels per second

3) 14 on-line channels, engineering units only

4) Pressure required close coupled transducers, max. of 16

7.3 INSTRUMENTATION

In addition to the instrumentation as described in Section 6.4, Plane 2 performance rakes were installed.

7.4 PERFORMANCE TEST

The performance test consisted of maintaining the engine at a constant power level and varying the quantity of fan cooling air. The engine was allowed to stabilize 10 min. at each valve setting, and during the stabilization time, several Data Management System readings were taken. In order to reduce the scatter in the performance data, the engine was maintained at constant corrected thrust.

7.4.1 Sea Level Test Results

Figures 72 through 74 show the measured sfc improvement vs. cooling air for three engine power levels. Figure 75 shows a comparison between measured sfc and predicted sfc in the test cell at maximum cruise. The predicted sfc is based

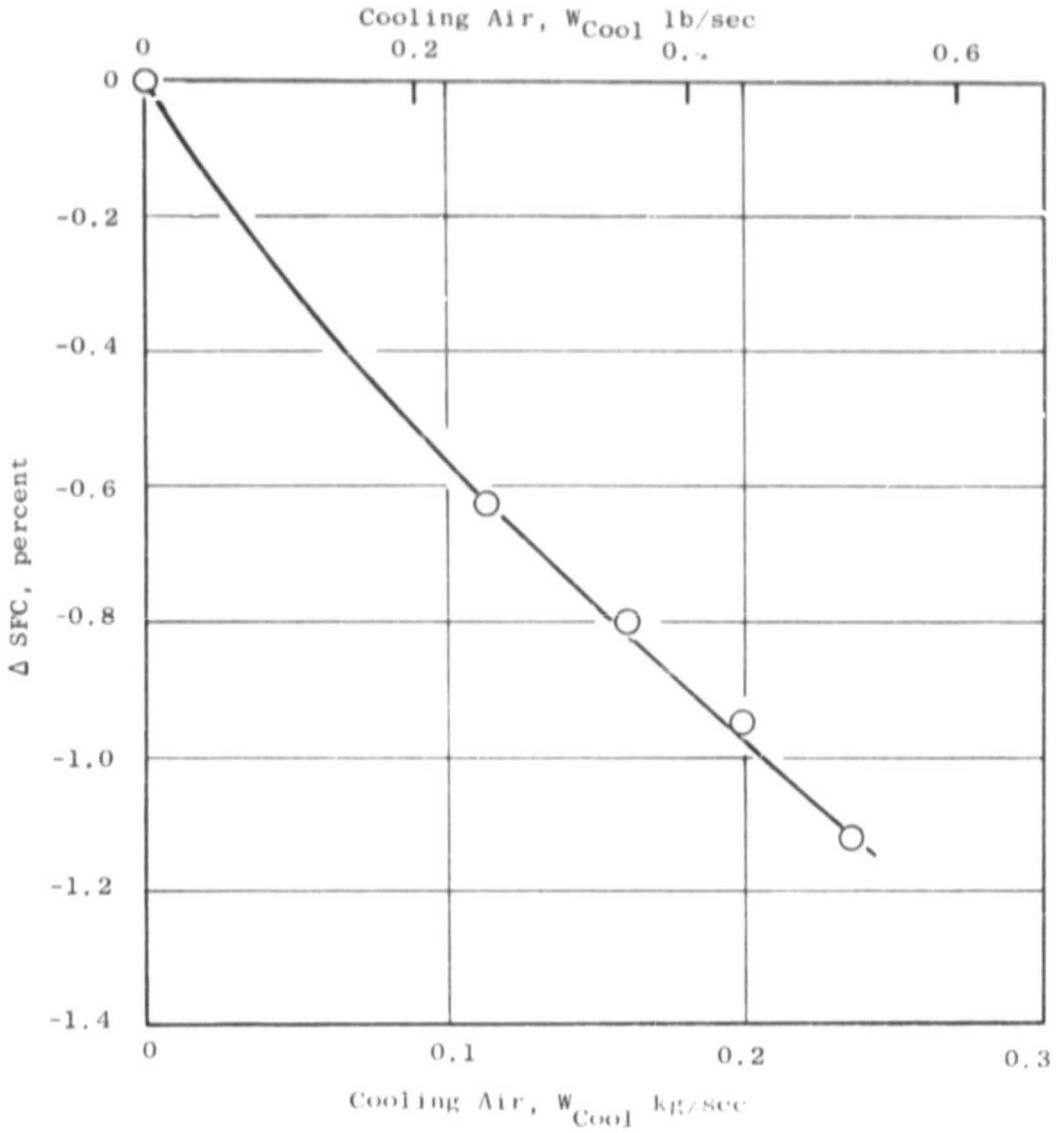

Figure 72. Measured SFC Improvement Versus W_{Cool} - Minimum Cruise.

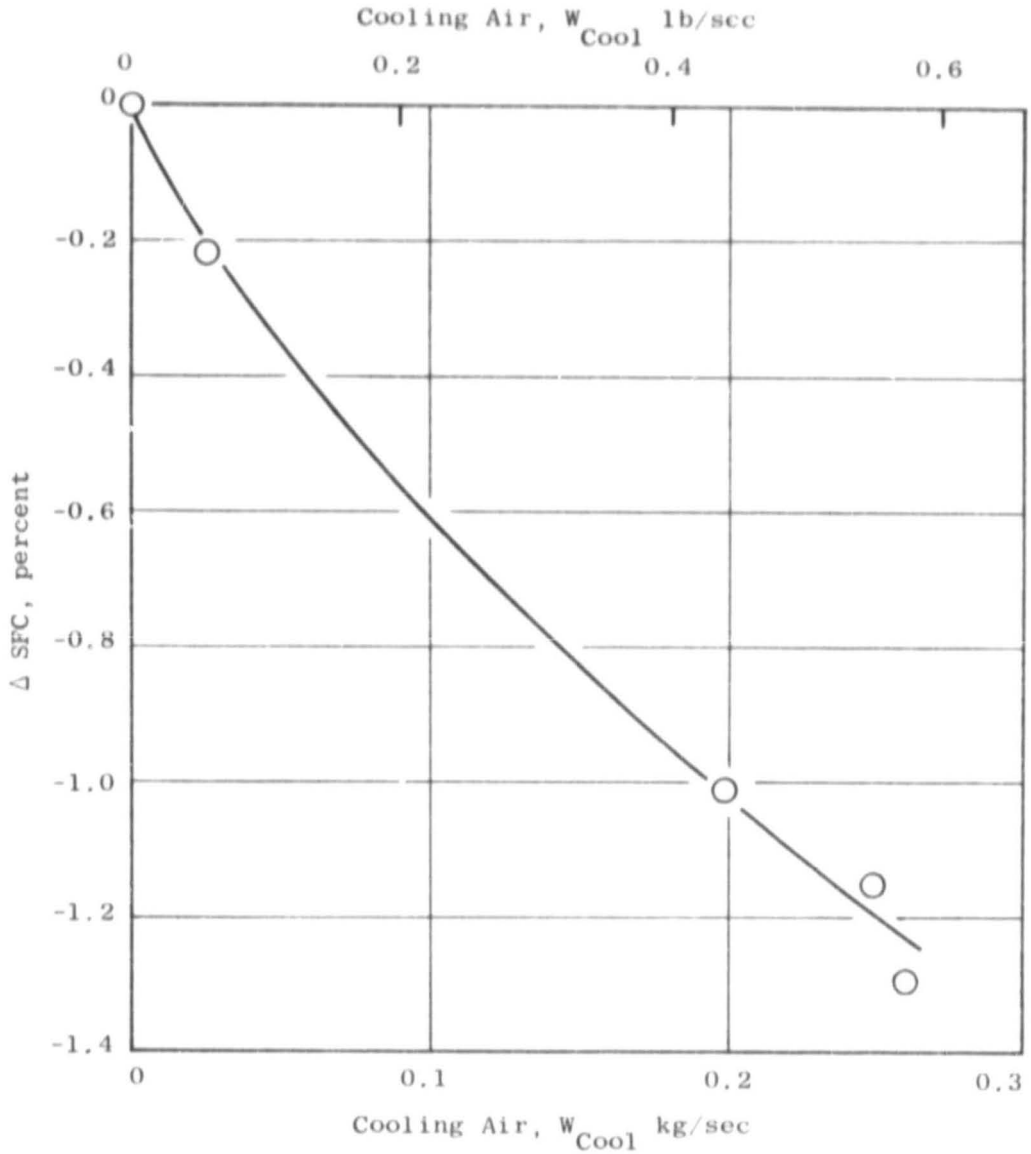

Figure 73. Measured SFC Improvement Versus W_{Cool} - Average Cruise.

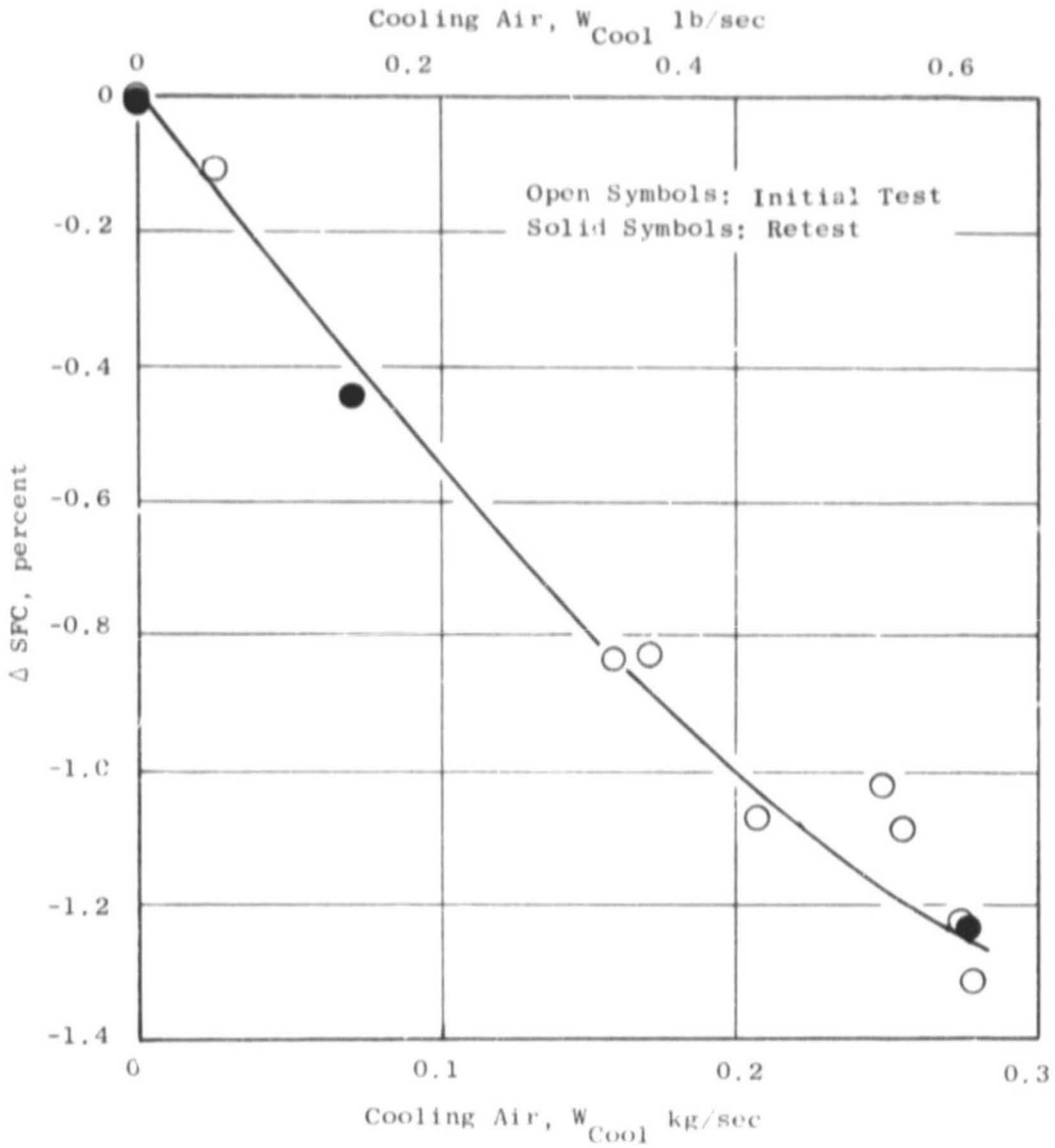

Figure 74. Measured SFC Improvement Versus W_{Cool} - Maximum Cruise.

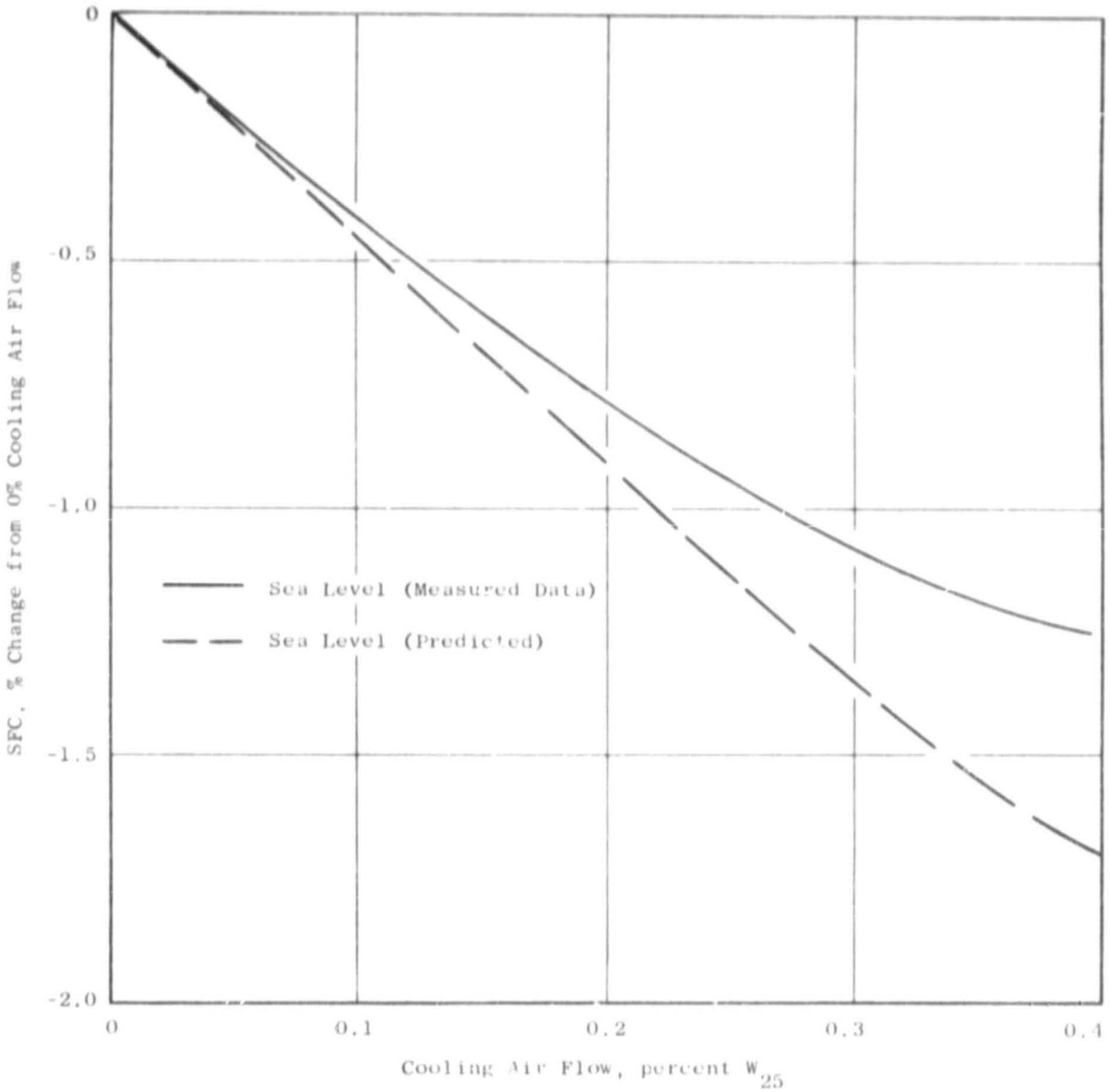

Figure 75. SFC Versus HPT ACC Cooling Flow, Engine 451-111/7 Sea Level Maximum Cruise.

on the matched cruise temperature data from the temperature survey testing (Peebles Test Facility). As shown, the measured performance improvement is smaller than the predicted performance improvement. (Reference Section 6.5.3.4 and 6.7 for additional information.) This difference can be attributed to the engine clearance reduction being less than analytically predicted and it can be shown that a decrease in clearance reduction of 0.15 mm (.006 in.) on Stage 1 and 0.10 mm (.004 in.) on Stage 2 would account for the difference between predicted and measured sfc values. There is evidence on the Stage 1 shroud hangers that some binding between shroud, "C" clip and hanger segments occurred and this probably accounts for some of the difference between the two results (See Figure 76). Also, HEX measurements, as pointed out in Section 6.7.2, show less closure than analytically predicted. Posttest inspection also revealed that the impingement air was not impinging consistently on the flanges in the axial locations which the analysis assumed. This probably accounts for the difference between predicted and measured values.

Figure 77 is a plot of turbine efficiency, η_T (total) vs. cooling air flow, W_{cool} in percent W_{25} based on matched test cell data.

7.4.2 Altitude Cruise Performance Estimates

The following method was used to estimate the sfc improvement at altitude cruise. A series of thermal analyses were completed using the engine altitude cycle conditions and the modified heat transfer coefficients determined from the temperature matching process. In completing these analyses, the assumptions were made that the heat transfer coefficient was a constant throughout the flight-regime. These temperatures were then imposed on the structural model, and a graph of Stage 1 and Stage 2 clearance reduction and turbine efficiency vs. cooling air was generated.

The turbine efficiency curve was used with the engine cycle analysis to generate the sfc improvement at altitude. Figures 78 thru 81 illustrate the results of the analyses. As is shown by Figure 81 the design intent of 0.6 percent reduction in altitude sfc was demonstrated.

It should be noted that Figures 78 and 79 are closures based on match temperature data, and Figures 80 and 81 are predictions based on these analyses. Included on Figures 80 and 81 are turbine efficiency and sfc improvements based

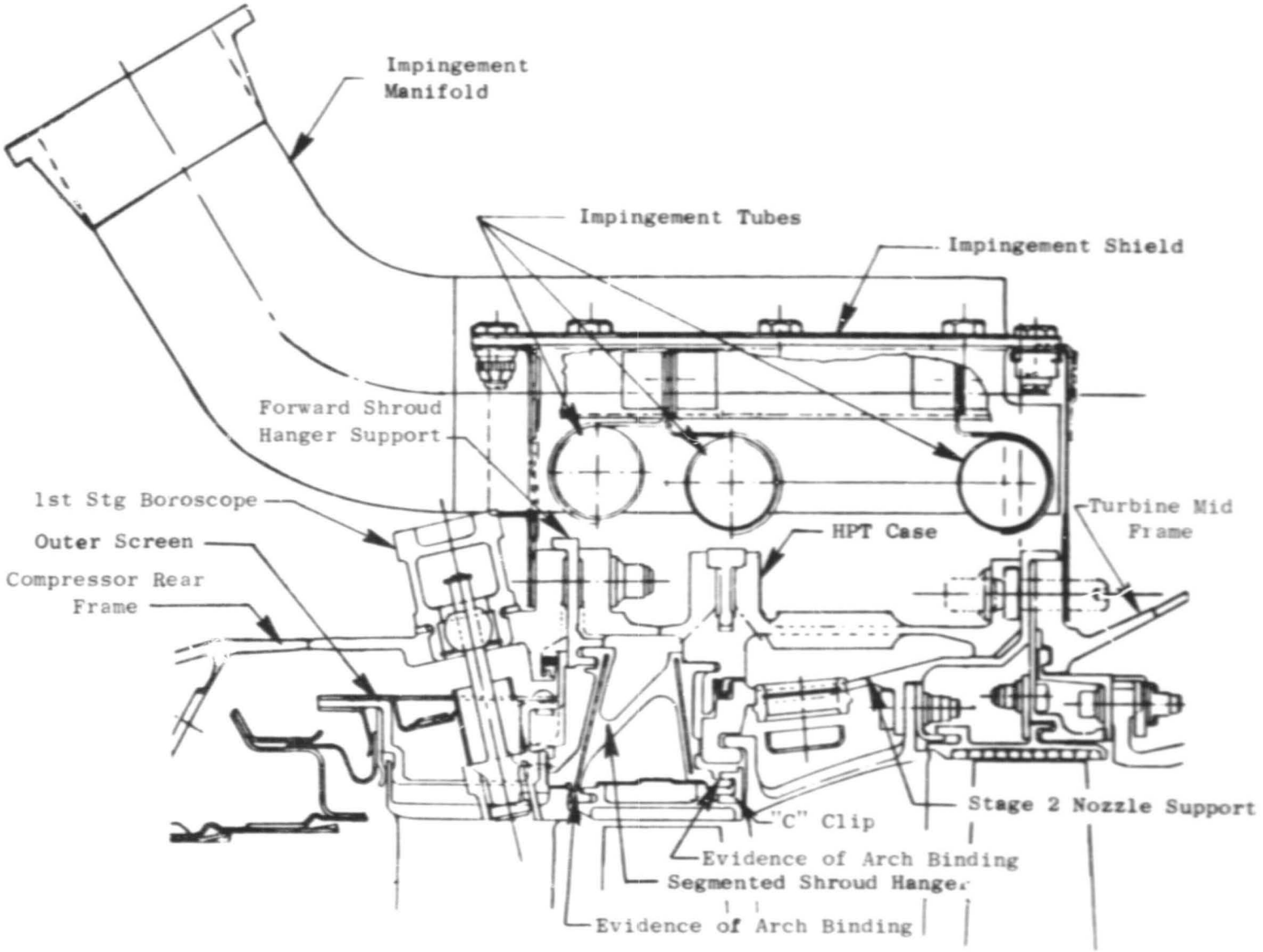

Figure 76. High Pressure Turbine Active Clearance Control.

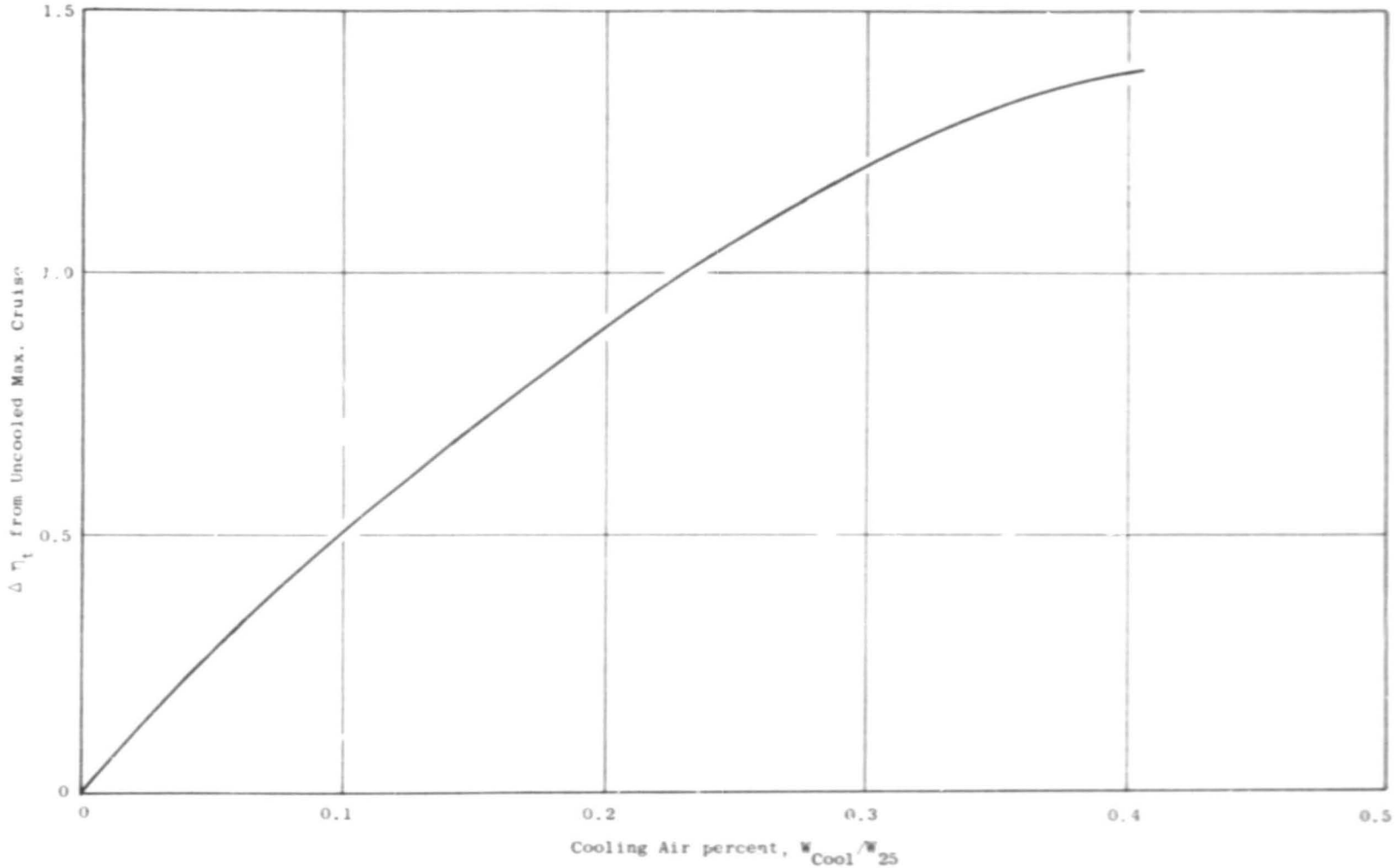

Figure 77. Δ Turbine Efficiency (η_t) Versus percent W_{cool} - Predicted.

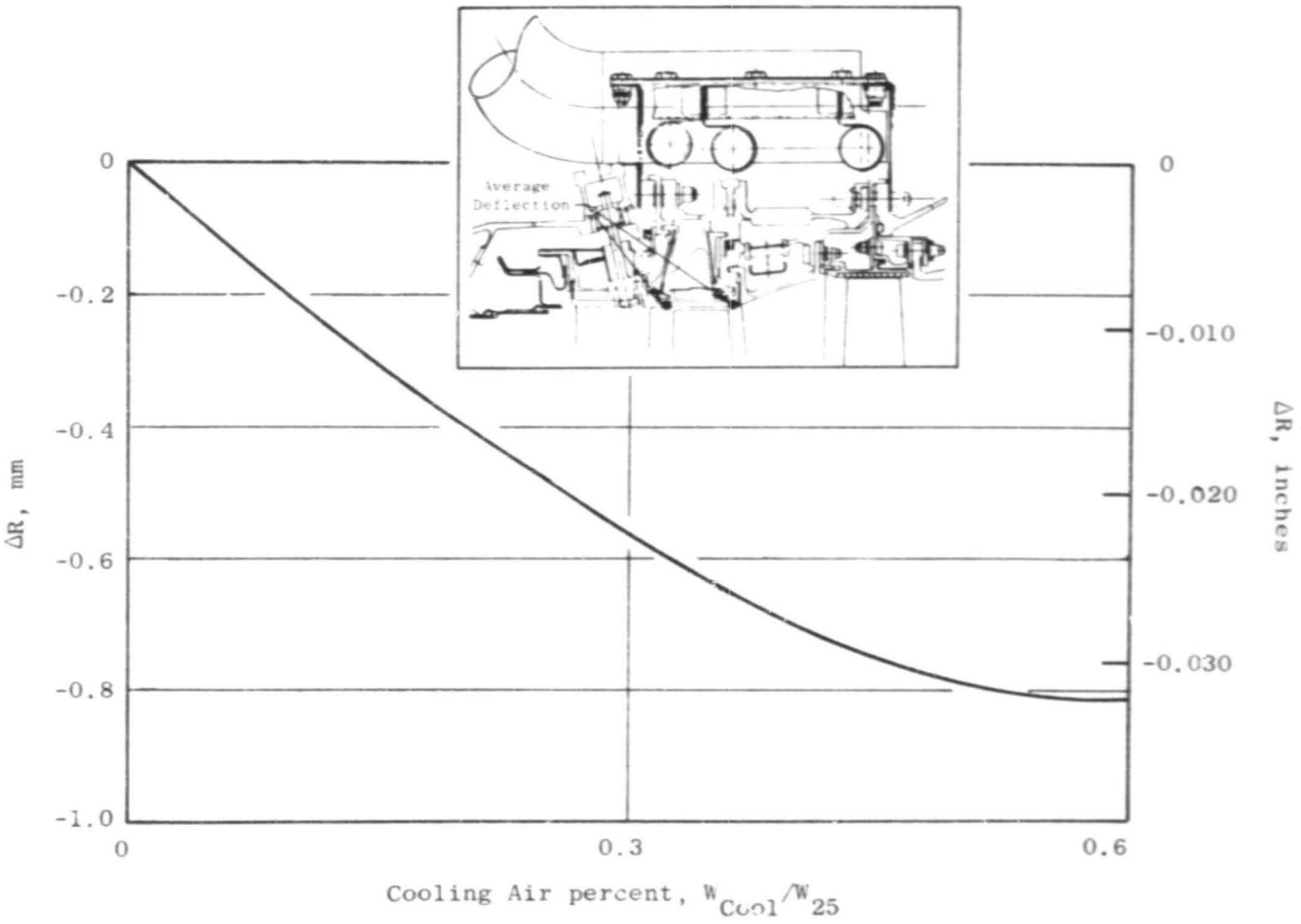

Figure 78. Stage 1 Closure at Altitude Cruise Versus W_{Cool}, Based on Matched Temperature Data.

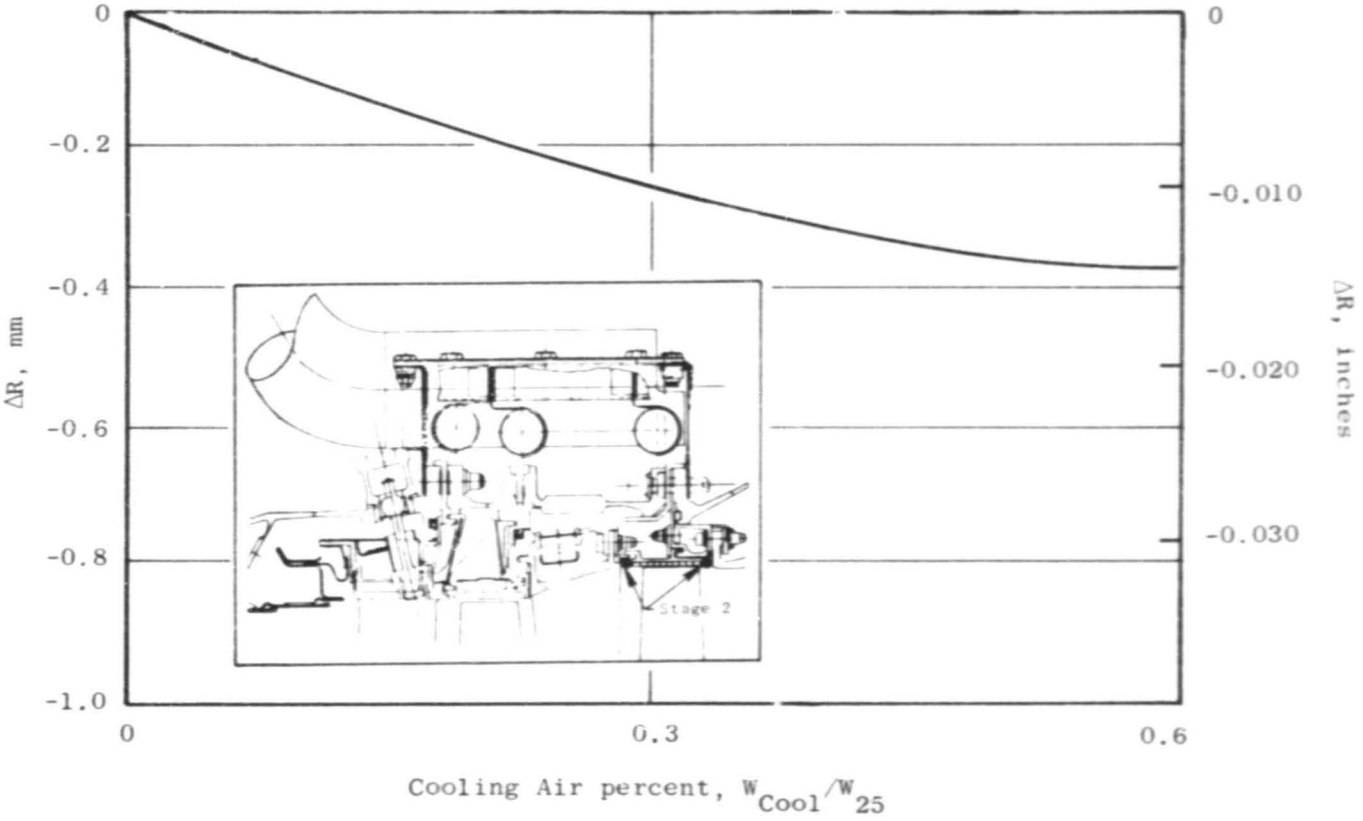

Figure 79. Stage 2 Closure Versus Percent W_{Cool}, Based on Matched Temperature Data.

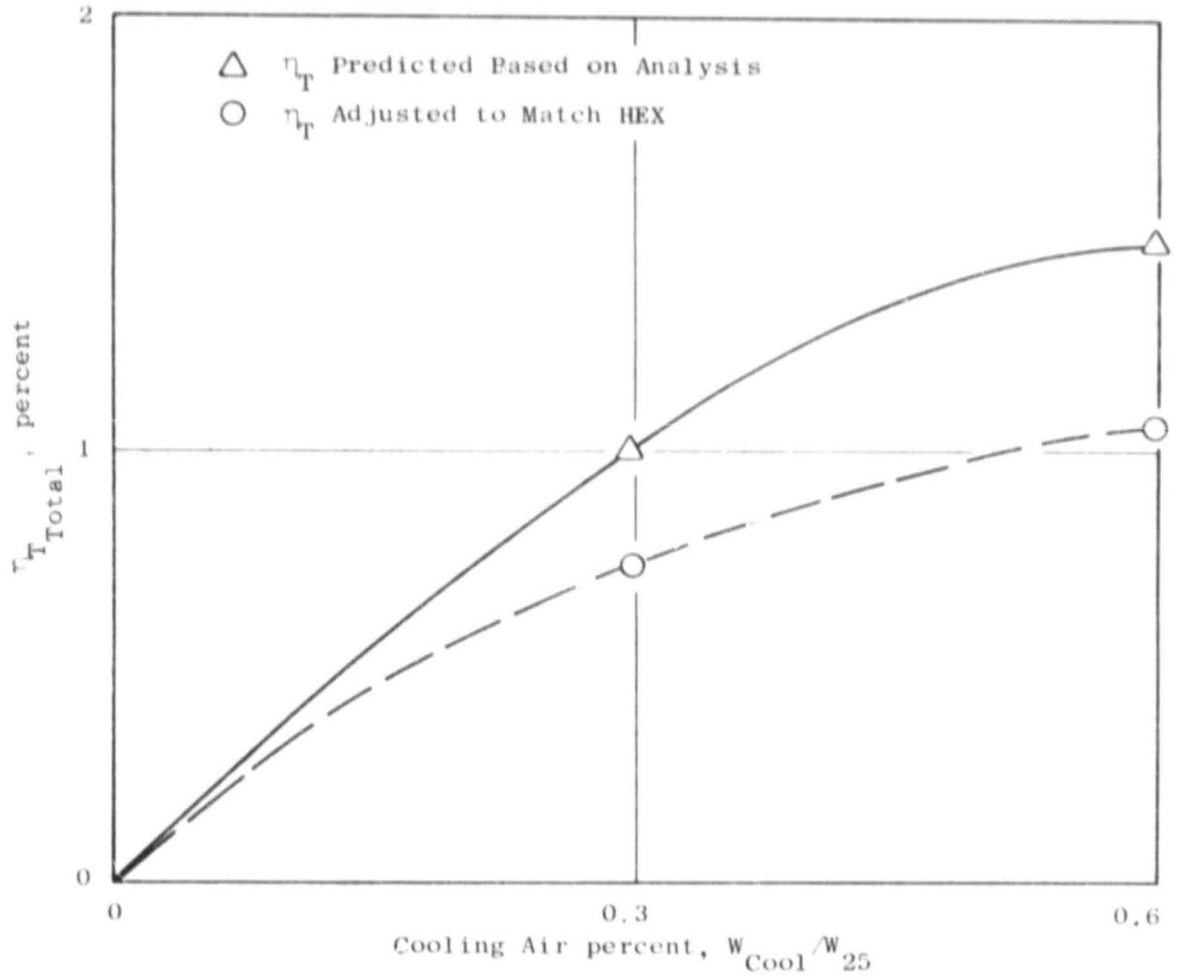

Figure 80. η_T Versus W_{Cool}.

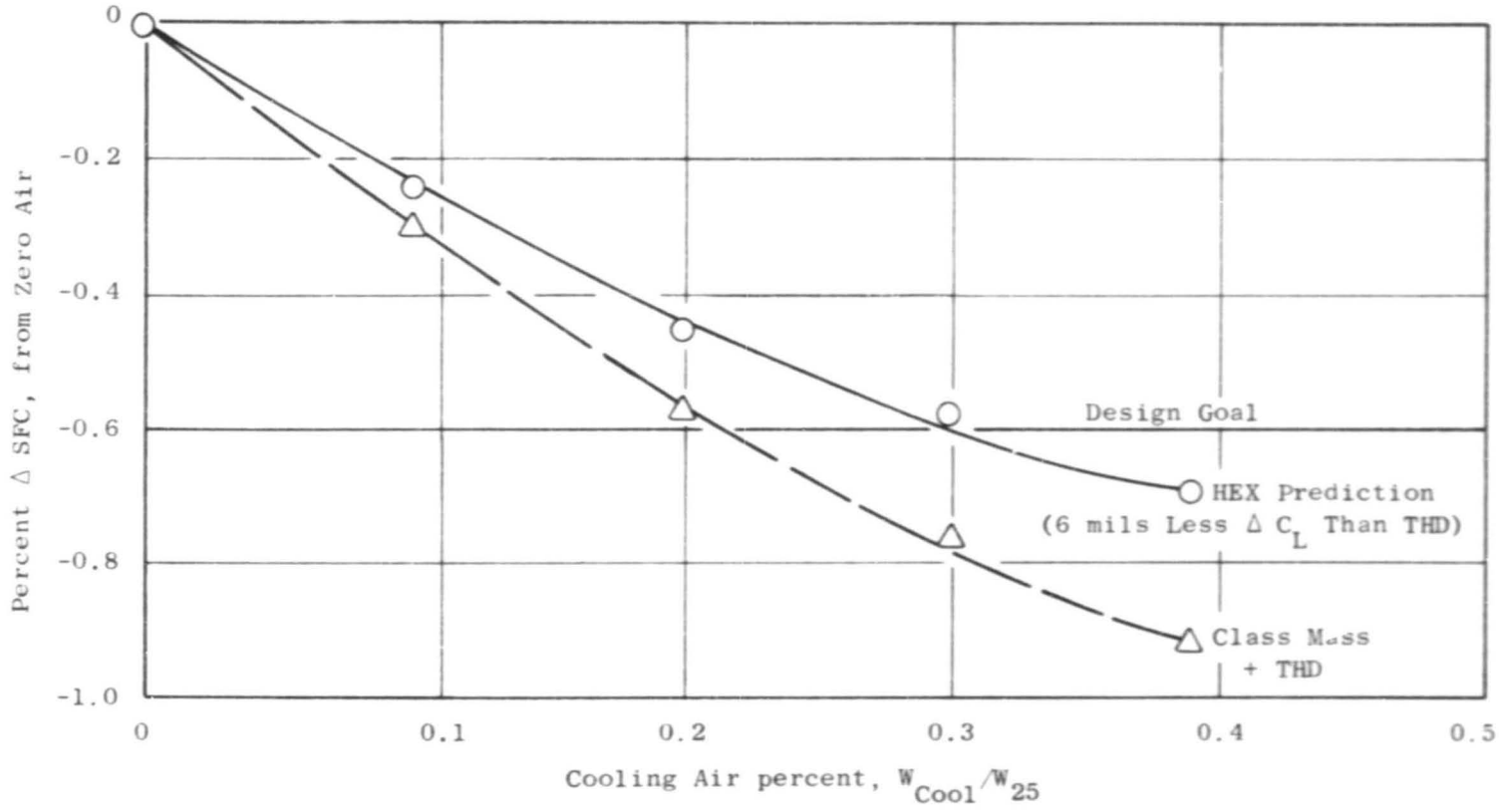

Figure 81. Engine Performance Improvement Versus Percent W_{Cool}.

on HEX closures. It is judged, based on test cell performance predictions, that the sfc improvement represented by the HEX prediction line is an accurate estimate of the altitude sfc and the improvement represented by the CLASS/MASS line is the maximum potential performance improvement obtainable providing that minor design modifications are carried out. The modification to be made would consist of eliminating archbinding during cooling and improving the axial consistency of air impingement on the turbine flanges.

7.5 ACCEL TESTING

The final phase of engine testing was a series of transients using varying amounts of CDP impingement air. The purpose of this testing was to determine the minimum amount of CDP air required to prevent a HPT rub during a takeoff throttle burst. The CDP impingement system was outfitted with an interchangeable metering orifice. After completing an engine throttle burst, borescope photos of the Stage 1 and Stage 2 HPT tip notches were taken and analyzed to determine the extent of the rub which may have occurred.

7.5.1 Test Results

Stage 1 and Stage 2 tip notch photos indicated that Stage 1 rubbed a total of 0.15 mm (0.006 in.) and Stage 2 did not rub. Power calibrations completed prior to the test sequence showed an increase in EGT of 5.6° C (10° F) which agrees with the measured rub. Both Stage 1 and Stage 2 rubs were less than anticipated, and indicate that the stator structure is substantiated by the HEX measurements which indicate that the Stage 1 and Stage 2 closure during a burst are less than predicted analytically. See Section 6.7 for additional details.

8.0 ECONOMIC ASSESSMENT

The HP Turbine Active Clearance Control Performance Improvement Concept was evaluated by Douglas for the DC-10-10 Aircraft, under the feasibility study of the program (Reference 1), for an estimated cruise SFC reduction of 0.6 percent. The results were updated for the 0.7 percent SFC reduction demonstrated in this program:

HP Turbine Active Clearance Control Block Fuel Savings
(Minimum Fuel Analysis)

Aircraft	Range (km)	Block Fuel Savings (kg)	(%)
DC-10-10	645	11	0.13
	1690	71	0.44
	3700	185	0.58

The estimated annual fuel savings for the above block fuel savings are shown below:

HP Turbine Active Clearance Control
Estimated Annual Fuel Savings Per Aircraft
(Minimum Fuel Analysis)

Aircraft	Range (km)	Annual Fuel Savings (Liters/AC/Year)
DC-10-10	645	30,200
	1690	132,600
	3700	184,000

Fuel prices used for the study (Reference 1) were dependent on the aircraft mission. The DC-10-10 generally operates over U.S. domestic routes, and, therefore, a medium fuel price of 11.9¢/liter (45¢/gal.) was assumed. The economic assessment based on this price is summarized in the following table:

Economic Assessment of HP Turbine Active Clearance Control Concept

(Medium Range, Medium Fuel Price, Minimum Fuel Analysis)

Aircraft	Payback (Year)	ROI (%)
DC-10-10	5.8	15

Because of the increase in the cost of fuel by over 100 percent since the conduction of the feasibility analysis (Ref. 1) in 1978, the payback and return on investment (ROI) of this concept are even more favorable now.

9.0 SUMMARY OF RESULTS

As part of the NASA sponsored Engine Component Improvement Project, an Active Clearance Control system has been developed for the CF6-6 HP Turbine which reduces fuel consumption.

The HP Turbine Active Clearance Control System demonstrated a repeatable SFC reduction, at sea level, of 1.3 percent with a potential SFC reduction of 1.75 percent. This is equivalent to a SFC reduction, at altitude, of 0.7-0.9 percent, respectively. The methods used to estimate the performance improvement have been shown to be accurate and valid. Therefore, based on the test results, it can be concluded that the system betters the program objective of 0.6 percent demonstrated reduction in altitude SFC, and that the performance improvement gained by an active clearance control system can be accurately predicted and measured. Also, it has been shown that only minor design modifications would be required to achieve the potential performance improvement of 0.9 percent SFC reduction at altitude.

The HP turbine active clearance control performance improvement offers an annual fuel savings per DC-10-10 aircraft of 30,200 to 184,000 liters (8000 to 48,600 gal.) depending on mission range.

APPENDIX A

QUALITY ASSURANCE

INTRODUCTION

The quality program applied to this contract is a documented system throughout the design, manufacture, repair, overhaul, and modification cycle for gas turbine aircraft engines. The quality system has been constructed to comply with military specifications MIL-Q-9858A, MIL-I-45208, and MIL-STD-45662 and Federal Aviation Regulations FAR-145 and applicable portion of FAR-21.

The quality system and its implementation are defined by a complete set of procedures which has been coordinated with the DOD and FAA and has their concurrence. In addition, the quality system as described in the quality programs meets the contractual requirements required by the NASA-Lewis Research Center. The following is a brief synopsis of the system.

QUALITY SYSTEM

The quality system is documented by operating procedures which coordinate the quality-related activities in the functional areas of Engineering, Manufacturing, Materials, Purchasing, and Engine Programs. The quality system is a single-standard system wherein all product lines are controlled by the common quality system. The actions and activities associated with determination of quality are recorded, and documentation is available for review.

Inherent in the system is the assurance of conformance to the quality requirements. This includes the performance of required inspections and tests. In addition, the system provides change control requirements which assure that design changes are incorporated into manufacturing, procurement and quality documentation, and into the products. Material used for parts is verified for conformance to applicable engineering specifications, utilizing appropriate physical and chemical testing procedures.

Measuring devices used for product acceptance and instrumentation used to control, record, monitor, or indicate results of readings during inspection and test are initially inspected and calibrated and periodically are reverified or recalibrated at a prescribed frequency. Such calibration is performed by technicians against standards which are traceable to the National Bureau of Standards. The gages are identified by a control number and are on a recall schedule for reverification and calibration. The calibration function maintains a record of the location of each gage and the date it requires recalibration. Instructions implement the provisions of MIL-STD-45662 and the appropriate FAR requirements.

Work sent to outside vendors is subject to quality plans which provide for control and appraisal to assure conformance to the technical requirements. Purchase orders issued to vendors contain a technical description of the work to be performed and instructions relative to quality requirements.

Engine parts are inspected to documented quality plans which define the characteristics to be inspected, the gages and tools to be used, the conditions under which the inspection is to be performed, the sampling plan, laboratory and special process testing, and the identification and record requirements.

Work instructions are issued for compliance by operators, inspectors, testers, and mechanics. Component part manufacture provides for laboratory overview of all special and critical processes, including qualifcation and certification of personnel, equipment and processes.

When work is performed in accordance with work instructions, the operator/inspector records that the work has been performed. This is accomplished by the operator/inspector stamping or signing the operation sequence sheet to signify that the operation has been performed.

Various designs of stamps are used to indicate the inspection of status of work in process and finished items. Performance or acceptance of special processes is indicated by distinctive stamps assigned specifically to personnel performing the process or inspection. Administration of the stamp system and the issuance of stamps are functions of the Quality Operation. The stamps are applied to the paperwork identifying or denoting the items requiring control. When stamping of hardware occurs, only laboratory approved ink is used to assure against damage.

The type and location of other part marking are specified by the design engineer on the drawing to assure effects do not compromise design requirements and part quality.

Control of part handling, storage and delivery is maintained through the entire cycle. Engines and assemblies are stored in special dollies and transportation carts. Finished assembled parts are stored so as to preclude damage and contamination, openings are covered, lines capped and protective covers applied as required.

Nonconforming hardware is controlled by a system of material review at the component source. Both a Quality representative and an Engineering representative provide the accept (use-as-is or repair) decisions. Nonconformances are documented, including the disposition and corrective action if applicable to prevent recurrence.

The system provides for storage, retention for specified periods, and retrieval of nonconformance documentation. Documentation for components is filed in the area where the component is manufactured/inspected.

APPENDIX B

NOMENCLATURE

ACC	Active Clearance Control
CDP	Compressor Discharge Pressure
CRF	Compressor Rear Frame
EGT	Exit Gas Temperature, °C (°F)
G/I	Ground Idle
HEX	High Energy X-Ray
HPT	High Pressure Turbine
LPT	Low Pressure Turbine
LVDT	Linear Variable Displacement Transducer
ROI	Return On Investment
SFC	Specific Fuel Consumption, $\frac{kg}{hr\text{-}daN}$, $\left(\frac{Lb}{1r\text{-}lb}\right)$
T/O	Take-Off
VSV	Variable Stator Vane
W25	Engine Flow kg/sec, (lb/sec)

APPENDIX C

REFERENCES

1. Fasching, W.A., "CF6 Jet Engine Performance Improvement Program, Task 1 - Feasibility Analysis," NASA CR-159450, March 1979.